

**CRUSTACEAN BEHAVIOR AND MORPHOLOGY IN LOW AND
INTERMEDIATE REYNOLDS NUMBER ENVIRONMENTS**

A Dissertation
Presented to
The Academic Faculty

By

Melissa Ruszczyk

In Partial Fulfillment
of the Requirements for the Degree
Doctor of Philosophy in the
School of Biological Sciences
Ocean Science and Engineering

Georgia Institute of Technology

May 2022

© Melissa Ruszczyk 2022

**CRUSTACEAN BEHAVIOR AND MORPHOLOGY IN LOW AND
INTERMEDIATE REYNOLDS NUMBER ENVIRONMENTS**

Thesis committee:

Dr. Jeannette Yen, Co-Advisor
School of Biological Sciences
Georgia Institute of Technology

Dr. Emanuele Di Lorenzo
School of Earth and Atmospheric Sci-
ences
Georgia Institute of Technology

Dr. Donald R. Webster, Co-Advisor
School of Civil and Environmental Engi-
neering
Georgia Institute of Technology

Dr. David W. Murphy
Department of Mechanical Engineering
University of South Florida

Dr. Marc Weissburg
School of Biological Sciences
Georgia Institute of Technology

Date approved: April 27, 2022

Occasionally achieving greatness

King of Pops

ACKNOWLEDGMENTS

Several people have helped with this monster of a project these past five years, and it would be remiss of me to not begin by thanking my advisors, Drs. Jeannette Yen and Donald Webster. Jeannette, I remember reading your articles as an undergraduate, and ever since I had the opportunity to work in your lab as an REU student, you have been an inspiration. Your enthusiasm for research is infectious, and I know that if I keep even a fraction of the passion you have going forward, I will be able to do next to anything. Don, thank you for being a pillar of stability in the chaotic world that is ecology. Animals are unpredictable, and I have learned how to balance flexibility in the lab with professionalism in the office by following your lead. I can only hope to be half as organized as you are going forward.

Thank you to my committee, Drs. David Murphy, Marc Weissburg, and Emanuele Di Lorenzo, for your thoughts, insights, and conversations about my research. David, your *Euphausia superba* research kicked off half of my dissertation, and I thank you for all the metachronal data you were able to share. Marc, thank you for your statistical guidance throughout this process. Manu, thank you for giving me the opportunity to do this research- it has been an honor to be a part of OSE's inaugural class.

Thank you to everyone outside of my committee who has helped with research. Thank you to Dr. Jennifer Fisher, for the collection of *Euphausia pacifica*, and to Dr. Eric Campos, for supplementary videos of *Odontodactylus havanensis* swimming. Thank you to Dr. Arvind Santhanakrishnan and Mitchell Ford for being the most approachable robotic engineers I have ever collaborated with. And finally, thank you to Dr. Dorsa Elmi, for your insights and preliminary code for the Burgers vortex analysis, and Angelica Connor for explaining all of fluid dynamics to me when I was too afraid to ask a professor.

Thank you to all the undergraduate researchers I have worked with- your assistance in digitizing the massive data sets I work with has been helpful beyond words. I would like

to specifically acknowledge Anikait Dhond, Juliette Goff, Ashley Jhun, Uma Patel, Ngoc Thuy An (Keira) Tran, and Tianyi Zuo for their assistance digitizing *Hesperodiaptomus shoshone*, and Anugraha Babuji, Enye Lee, Kevin Joseph, Agam Singh, and Emma Slater for their assistance digitizing *Euphausia pacifica*.

None of this research would have been possible without funding. I would like to acknowledge NSF OCE-1537284 for financial support for “A Freshwater Copepod’s Response to Turbulence”, and NSF CTS-1706007 for financial support for “Dual Phase-Shifted Ipsilateral Metachrony in *Americamysis bahia*” and “Trends in Stroke Kinematics, Reynolds Number, and Swimming Mode in Shrimp-Like Organisms.”

Thank you to my friends, who appear most frequently in the form of Dungeons and Dragons campaigns. To my Oregon group, Eli Wolff, Greg Knapp, Kelly Pohland, Kyle Bahnsen, and Marissa Masden: Thank you for taking a chance on an east coaster based only on Kelly’s word. You guys have been a great distraction during the COVID years, and I look forward to fighting many more 20ft shrimp (or other research manifestation) with you! To my Dragon Fruit Guild, Abbie Johnson, Alex Nolte, Alex Muscalus, Liz Ruszczuk, Nolan Barrett, Rachael Finigan, and Zach Wagner: It’s been an absolute delight to watch the blending of old friends and new. I look forward to all the dragons you may slay! To both groups: Each of you, individually, have helped me more than I have probably told you. Thank you for some of the most entertaining and meaningful downtime activities I could have ever asked for, in- and out-of-game!

I also could not have made it through my PhD without the Atlanta music scene. Thank you to Peachtree Symphonic Winds and Northwinds Symphonic Band for accepting an overworked scientist and under-practiced musician into your clarinet section. To Jess and John Charles Dougherty: Thank you for the at-home duets, the concerts, and letting me be a part of your lives during my time in Atlanta.

To my family: I did it. *We* did it. Thank you for believing in me, even when I did not. Your love and support always have, and always will, mean the world to me.

TABLE OF CONTENTS

Acknowledgments	iv
List of Tables	x
List of Figures	xi
List of Acronyms	xiii
Summary	xvi
Chapter 1: Introduction	1
Chapter 2: Literature Review	5
2.1 Conceptualizing Fluid Motion	5
2.1.1 Basic Terminology	5
2.1.2 Fluid Motion Varies with Length Scale	7
2.2 Turbulence Affects Copepods	8
2.2.1 What are Copepods?	8
2.2.2 Types of Turbulence	9
2.2.3 Meso- and Submesoscale Turbulence Affects Community Structure	10
2.2.4 Microscale Turbulence Affects Individual Interactions	11
2.3 Malacostracan Pleopods	13

2.3.1	What is Malacostraca?	13
2.3.2	Reproduction	14
2.3.3	Respiration	16
2.3.4	Locomotion	17
Chapter 3: A Freshwater Copepod's Response to Microscale Turbulence		18
3.1	Introduction	18
3.2	Methodology	22
3.2.1	Animal Collection and Maintenance	22
3.2.2	Burgers Vortex Apparatus	22
3.2.3	Experimentation	24
3.2.4	Image Analysis	25
3.2.5	Statistical Analysis	28
3.3	Results	30
3.4	Discussion	32
3.4.1	The Burgers Vortex does not Promote Aggregation in <i>H. shoshone</i>	33
3.4.2	Orientation versus Directionality	35
Chapter 4: Dual Phase-Shifted Ipsilateral Metachrony in <i>Americamysis bahia</i>		39
4.1	Introduction	39
4.2	Methodology	44
4.2.1	Animal Collection and Maintenance	44
4.2.2	Recording	44
4.2.3	Image Analysis	46

4.2.4	Statistical Analysis	47
4.3	Results	48
4.3.1	Thoracopod versus Pleopod Swimming	48
4.3.2	Pleopod Metachrony in <i>A. bahia</i>	49
4.3.3	Increasing Swimming Speed	53
4.4	Discussion	54
4.4.1	Consequences of Multiple Cycles	54
4.4.2	Nondimensional Characterization	59
4.4.3	When to Use Pleopods	62
Chapter 5: Trends in Stroke Kinematics, Reynolds Number, and Swimming Mode in Shrimp-like Organisms		64
5.1	Introduction	64
5.2	Methodology	67
5.2.1	Animal Collection and Maintenance	67
5.2.2	Recording	67
5.2.3	Image Analysis	68
5.2.4	Across-Species Data Formatting	70
5.2.5	Statistical Analysis	71
5.3	Results	72
5.3.1	<i>Euphausia pacifica</i> Kinematics	72
5.3.2	Metachrony in Caridoid Facies	75
5.4	Discussion	78
5.4.1	Metachrony in <i>E. pacifica</i>	78

5.4.2	Metachrony in Caridoid Facies	81
Chapter 6: Conclusions and Closing Remarks		88
6.1	A Freshwater Copepod’s Behavioral Response to Microscale Turbulence . .	88
6.1.1	Conclusions	88
6.1.2	Limitations and Future Directions	89
6.2	Trends in Shrimp-like Organisms’ Propulsive Design	90
6.2.1	Conclusions	91
6.2.2	Limitations and Future Directions	92
Appendices		95
	Appendix A: Supplementary Tables	96
References		98

LIST OF TABLES

3.1	Burgers vortex parameters	24
3.2	Number of passes for each level within a replicate	29
3.3	MANOVA results	30
3.4	Circular analysis results	31
4.1	Zero-order correlation and regression results for two models employed to predict swimming speed	54
4.2	Metachronal characterization of four crustaceans	63
5.1	Sample count and source of data included in the across-species comparison	71
5.2	<i>Euphausia pacifica</i> pleopod segment lengths	73
A.1	Correlation function of <i>A. bahia</i> pleopod stroke amplitude across pleopod combinations	96
A.2	Correlation function of <i>A. bahia</i> pleopod phase lag across pleopod-pair combinations	96
A.3	Tukey HSD p-values for <i>E. pacifica</i> pleopod length comparisons	96
A.4	Two-sample Watson-Williams p-values for <i>E. pacifica</i> FF stroke amplitude comparisons	97
A.5	Two-sample Watson-Williams p-values for <i>E. pacifica</i> stroke amplitude comparisons between swimming modes	97
A.6	Tukey HSD p-values for <i>E. pacifica</i> FF phase lag comparisons	97

LIST OF FIGURES

2.1	Couette flow	6
2.2	Laminar and turbulent flow	7
2.3	Malacostracan pleopods	14
3.1	Burgers vortex cartoon	21
3.2	Experimental apparatuses	23
3.3	Angles quantifying copepod motion in relation to a Burgers vortex.	28
3.4	<i>Hesperodiaptomus shoshone</i> variables dependent on one factor.	32
3.5	<i>Hesperodiaptomus shoshone</i> variables dependent on multiple factors	33
3.6	Cross-sectional trajectories for female and male <i>H. shoshone</i> across horizontal Burgers vortex intensity levels	38
4.1	<i>Americamysis bahia</i> morphology	42
4.2	<i>Americamysis bahia</i> digitization	47
4.3	Normalized swimming speeds for <i>A. bahia</i>	49
4.4	Time standardized pleopod angles for ipsilateral cycles during one complete metachronal stroke	50
4.5	Phase lag and amplitude in <i>A. bahia</i>	52
4.6	P5 stroke amplitude and normalized swimming speed for <i>A. bahia</i> and <i>E. superba</i>	56

4.7	Beat frequency and swimming speed for <i>A. bahia</i> , <i>E. superba</i> , and <i>G. ingens</i>	57
4.8	Sample swimming speed and power stroke synchrony	58
4.9	Strouhal number (St) decreases with normalized swimming speed for <i>A. bahia</i>	61
4.10	Normalized advance ratio (J_n) increases with normalized swimming speed for <i>A. bahia</i>	62
5.1	Digitization and angle definition for <i>E. pacifica</i>	69
5.2	Four-point logistic fit of <i>E. pacifica</i> kinematics to normalized swimming speed	73
5.3	Stroke angles for three swimming modes	74
5.4	Stroke amplitude for three swimming modes	75
5.5	Phase lag for three swimming modes	76
5.6	PCA of stroke kinematics in shrimp-like crustaceans	77
5.7	Metachronal stroke kinematics and Re_{BL} in swimming modes	78
5.8	Metachronal stroke kinematics and Re_{BL} in shrimp-like organisms	79
5.9	Re_{BL} response to stroke kinematics	84
5.10	Linear regression of frequency to BL	85
5.11	Phase lag across Re_{BL}	86

LIST OF ACRONYMS

- α angle between body and protopodite
- β angle between protopodite and exopodite
- δPRT change in proportional residence time
- $\delta\mathbf{x}$ horizontal fluid displacement
- ϵ dissipation rate
- η Kolmogorov length scale
- γ telson angle
- κ concentration parameter
- μ dynamic viscosity
- ν kinematic viscosity
- ω vorticity
- $\partial\mathbf{u}/\partial\mathbf{y}$ velocity gradient
- ρ density
- τ shear stress
- τ_η Kolmogorov time scale
- θ shear strain
- θ_{rad} stroke amplitude in radians
- A** cross-sectional area
- a** lower asymptote in a Gompertz function
- A_{pleo}** pleopod arc length
- b** upper asymptote in a Gompertz function
- BA** body angle with respect to the horizontal

BL body length

c growth rate in a Gompertz function

d inflection point in a Gompertz function

F force

f frequency

FF fast forward swimming mode

fps frames per second

G/L gap length between pleopods normalized by body length

h fluid depth

HOV hovering swimming mode

IR infrared

J advance ratio

J_n normalized advance ratio

KMO Kaiser-Meyer Olkin measure of sampling adequacy

KW Kruskal-Wallis test

L characteristic length scale

L_{pleo} pleopod length

m mass

n_{pad} number of paddles (pleopods)

NGDR net to gross displacement ratio

PC principal component

PCA principle component analysis

PRT proportional residence time

r_B characteristic vortex radius

Re Reynolds number

Re_{BL} whole-body Reynolds number

Re_{pleo} pleopod Reynolds number

SD standard deviation
SDAP Steel-Dwass all-pairs test
SE standard error
St Strouhal number
t time
U characteristic velocity
u flow velocity
 u_η Kolmogorov velocity scale
 U_{pleo} maximum pleopod tip speed
USD upside down swimming mode
V volume
 V_{BL} whole-body speed
VIF variance inflation factor

SUMMARY

An organism's physical environment can dramatically affect an organisms' behavior and morphological design. The Reynolds number represents the ratio between inertial and viscous forces in a fluid environment. This study is concerned with the challenges crustacean plankton face resulting from living in a low- and intermediate-Reynolds number aquatic environment.

In the first part of this study, the freshwater copepod *Hesperodiptomus shoshone* is exposed to a Burgers vortex- a flow feature meant to mimic turbulent eddies found in an organism's environment. Male and female copepods were exposed to four vortex intensity levels plus a negative control in either a horizontal or vertical orientation of the vortex axis. Trajectory analysis of *H. shoshone* swimming behavior shows that this copepod changes its swimming behavior in response to vortex orientation and not vortex level- a notable difference from marine copepods exposed to the same flow feature. These results may be linked to ecological and geographic differences between freshwater and marine copepods.

In the second part of this study, the pleopod synchrony in the mysid shrimp *Americamysis bahia* is quantified. Shrimp and krill beat their pleopods in an adlocomotory sequence, creating a metachronal wave. Usually, pleopod pairs on the same abdominal segment beat in tandem with each other, resulting in one 5-paddle stroke. *Americamysis bahia*'s pleopods on the same abdominal segment beat independently from each other, resulting in two 5-paddle metachronal cycles that run ipsilaterally along the body, 180° out of phase with each other. High-speed recordings of *A. bahia* stroke kinematics reveal how this mysid changes its stroke amplitude, beat frequency, and inter-appendage phase lag to achieve high speeds. Trends with Strouhal number and advance ratio suggest that the stroke kinematics of metachrony in *A. bahia* are tuned to achieve large normalized swimming speeds.

In the third part of this study, stroke kinematics in Pacific krill, *Euphausia pacifica*, are quantified for the first time. *Euphausia pacifica* (1-3cm body length) achieve similar

swimming modes as the larger *E. superba* (4-6cm body length) through a different set of stroke kinematics. To better understand the relationship between stroke kinematics, resulting swimming mode, and length scale, these data are used in tandem with previously published stroke kinematics of other 5-paddle metachronal swimmers, including mysid shrimp and stomatopods, to identify broad trends across species and length scale in metachrony. Principle component analysis (PCA) reveals trends in stroke kinematics, Reynolds number, and swimming mode as well as variation among taxonomic order. Additionally, uniform phase lag, i.e. when the timing between power strokes of all adjacent pleopods is equal, in 5-paddles systems is achieved at different Reynolds numbers for each swimming mode, which highlights the importance of taking into consideration stroke kinematics, length scale, and resulting swimming mode in bio-inspired design applications.

CHAPTER 1

INTRODUCTION

An organism's physical environment can affect an organism's behavior and morphological design, leaving it an often overlooked factor that can drive an organism's ecology. Physical challenges to sensory perception can drive the adaptation of different behaviors to overcome such obstacles. For example, many organisms rely on their sense of sight to interpret their environment, which is dependent on the amount of available light. The amount of light can change foraging patterns of hawkmoths (Stockl et al., 2017), navigational patterns of ants (Narendra et al., 2017), and vertical migration patterns in crustacean larvae (Epifanio and Cohen, 2016). In addition to changing behaviors, light levels can result in different morphological adaptations in similar species that experience different light levels. Species that rely on sight in dim conditions compared to bright conditions have more rods, which are sensitive to light level, than cones, which detect color, in their eye (Peichl, 2005; Landsberger et al., 2008).

This study seeks to relate features from an organisms' physical environment to resulting behaviors or morphological design in aquatic organisms by undertaking two unique projects. The first project investigates a freshwater copepod's behavioral response to microscale turbulence, and the second project seeks to understand trends in shrimp-like organisms' propulsive design. Each project has its own unique goal or set of goals.

Goal 1: Quantify a freshwater copepod's response to microscale turbulence

Turbulence exists across many different length scales. Organisms of all size are subject to fluid motion, including copepods, who are particularly subject to small-scale fluid motion. Turbulence at this length scale can affect several aspects of a copepod's life, including metabolic rates, predator-prey encounter rates, grazing rates, egg production, swimming behaviors, and population dynamics (Saiz and Alcaraz, 1992a; Saiz and Alcaraz, 1992b;

Saiz and Kiørboe, 1995; Fields and Yen, 1997). Here, the freshwater copepod *Hesperodiaptomus shoshone*'s behavioral response to a Burgers vortex – a flow feature meant to mimic turbulent eddies found in the organism's environment was investigated. Male and female *H. shoshone* were exposed to 4 different vortex intensity levels plus a stagnant negative control of a Burgers vortex in either a horizontal or vertical orientation of the vortex axis. Their swimming behavior was quantified using swimming speed, swimming path, angles in relation to the flow and the vortex, and time spent in the vortex to determine if a behavioral response was dependent on sex, turbulence intensity, or vortex orientation. *Hesperodiaptomus shoshone* behavior changes in response to the vortex orientation and not with turbulence intensity – a notable difference to the response of marine copepods exposed to the same flow feature. These results may be due to ecological and geographic differences between freshwater and marine copepods.

Goal 2: Quantify metachrony in a 10-paddle, shrimp-like system

Autonomous underwater vehicles have previously relied on a single propeller located at the back of the device as their primary means of propulsion. While this is an effective strategy, the device immediately runs the risk of becoming irretrievable if something were to happen to the propeller while out in the field. A multi-appendage design, in contrast, is more redundant. If something were to happen to one of the paddles, the remaining could still function, allowing the device to return to the surface. Engineers are looking to biology for inspiration for multi-appendage designs, specifically shrimp and krill, due to the diversity of approaches taken to achieve a similar means of propulsion- the adlocomotory beating of appendages resulting in a metachronal stroke (Byron et al., 2021a).

Previously documented metachrony in euphausiids focused on one, 5-paddle metachronal stroke where pleopods on the same abdominal segment beat in tandem with each other, propelling the animal forward. In contrast, the mysid shrimp *Americamysis bahia*'s pleopods on the same abdominal segment beat independently of each other, resulting in two, 5-paddle metachronal cycles running ipsilateral along the length of the body, 180° out of

phase. The morphology, kinematics, and nondimensional measurements of efficiency are compared primarily to the one-cycle *Euphausia superba* to determine how a two-cycle approach alters the design and kinematics of metachrony. Pleopodal swimming in *A. bahia* results in only fast forward swimming, with speeds ranging from 2-12BL/s (body lengths per second), through a combination of increasing stroke amplitude, beat frequency, and altering inter-limb phase lag. Trends with Strouhal number and advance ratio suggest that the kinematics of metachrony in *A. bahia* are beneficial to achieve large normalized swimming speeds.

Goal 3: Discover overarching kinematic trends in metachronal systems across different length scales and swimming modes

Metachronal propulsion is commonly seen in organisms with the caridoid facies body plan, i.e. shrimp-like organisms, as they beat their pleopods in an adlocomotory sequence. These organisms exist across length scales ranging several orders of Reynolds number magnitude, from 10 to 10^4 , during locomotion. Further, by altering their stroke kinematics, these organisms achieve three distinct swimming modes. To better understand the relationship between Reynolds number, stroke kinematics, and resulting swimming mode, *Euphausia pacifica* pleopod stroke kinematics were quantified using high-speed digital recordings and compared to the larger *E. superba*. *Euphausia pacifica* can achieve the same swimming modes as *E. superba* through a distinct set of stroke kinematics. *Euphausia pacifica* consistently operates with a greater beat frequency and smaller stroke amplitude than *E. superba*. These data are then used in combination with previously-published stroke kinematics from mysids and stomatopods to identify broad trends across species and length scale in metachrony. Principle component analysis (PCA) reveals trends in stroke kinematics and Reynolds number as well as the variation among taxonomic order. Overall, larger beat frequencies, stroke amplitudes, between-cycle phase lags, and Reynolds numbers are more representative of the fast forward swimming mode compared to the slower hovering mode. Additionally, each species has a unique combination of kinematics that

result in metachrony, indicating that there are other factors, perhaps morphological, which affect the overall metachronal characteristics of an organism. Finally, uniform phase lag, in which the timing between power strokes of all adjacent pleopods is equal, in 5-paddle systems is achieved at different Reynolds numbers for each swimming mode, highlighting the importance of taking into consideration stroke kinematics, length scale, and the resulting swimming mode.

To orient the reader to the thesis content, Chapter 2 is a literature review, featuring three sections. The first section is a conceptual understanding of fluid motion, which defines basic fluid dynamics terms and discusses water motion across length scales. The second section is a review on turbulence and its role in the daily life of copepods. In addition to introducing the reader to a copepod, this section discusses how macro- and microscale turbulence affects different aspects of a copepod's ecology from population structure to individual-level interactions. The final section gives an evolutionary overview of pleopods in malacostracan crustaceans. This section introduces the reader to the class Malacostraca and discusses the three primary functions pleopods may serve: locomotion, reproduction, and respiration. Chapters 3-5 present the research methodology, results, and discussion for one of each of the goals outlined above. Chapter 3 investigates the behavioral response of *H. shoshone* to a Burgers vortex, Chapter 4 quantifies the dual ipsilateral metachrony of *A. bahia*, and Chapter 5 quantifies metachrony in *E. pacifica* and discusses trends in stroke kinematics required to achieve similar swimming modes across different Reynolds numbers. Chapter 6 concludes with findings from the previous chapters, discusses limitations from the current study, and provides insights into future research projects.

CHAPTER 2

LITERATURE REVIEW

This study is interdisciplinary, spanning the fields of fluid dynamics, ecology, and functional morphology. Thus, the following literature review introduces terminology and concepts important for later chapters. Topics covered include a conceptualization of fluid motion, a review of the effects of turbulence on copepod ecology, and an introduction to pleopod morphology and function in Malacostraca.

2.1 Conceptualizing Fluid Motion

2.1.1 Basic Terminology

To understand the relationship between an organism and its physical environment, there are several basic physical terms to define before proceeding. Density (ρ) is the fluid mass (m) per unit volume (V). A fluid's viscosity represents its "stickiness". There are two versions of viscosity. Dynamic viscosity (μ) represents the amount of "friction" between two layers of fluid and how hard it would be to move those two layers of fluid relative to each other. Kinematic viscosity (ν) is calculated as

$$\nu = \frac{\mu}{\rho}. \quad (2.1)$$

and represents the diffusion rate of momentum in the flow.

For a basic conceptualization of fluid terms, it is useful to visualize two-dimensional Couette flow (Figure 2.1). Couette flow occurs between two parallel surfaces (plates) separated by a gap (h), filled with fluid. One of the surfaces is stationary (lower) while the other (upper) moves tangentially with respect to the stationary surface. In steady-state, a velocity gradient ($\partial u/\partial y$) occurs within the fluid, resulting in a greater velocity near the

moving plate and decreasing until the velocity reaches zero at the depth of the stationary plate. This phenomenon is known as shear: the deformation of a material in which parallel surfaces move at different rates relative to each other. Shear stress (τ) is the tangential force (F) per cross-sectional area (A) applied to create movement in the fluid,

$$\tau = \frac{F}{A} \quad (2.2)$$

and shear strain (θ) is the ratio of the horizontal fluid displacement (δx) over the depth of the fluid (h),

$$\theta = \frac{\delta x}{h}. \quad (2.3)$$

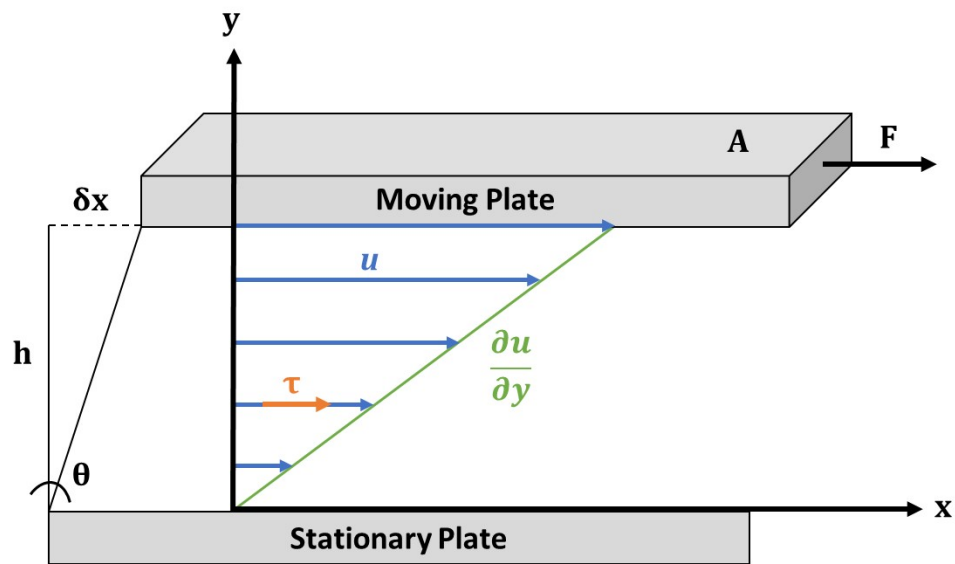


Figure 2.1: Couette flow. Schematic of Couette flow between a stationary plate and a moving plate separated by distance h . A tangential force, F , acts upon a plate with surface area A , causing it to move horizontally a displacement distance δx . This action induces the fluid movement with velocity, u , between the plates due to the viscosity of the fluid. One plate is moving and the other is not, resulting in a velocity gradient, $\partial u / \partial y$. The shear stress, τ , is the tangential force F per area A , and the shear strain, θ , is the horizontal displacement per gap width, which is defined as the ratio of δx to h .

The final fluid mechanics quantity to define from a biological perspective, is vorticity. Conceptually, vorticity (ω) is a measurement of the rotating motion of the fluid at a given

point. Mathematically, vorticity is calculated as the curl of the three-dimensional flow velocity (\vec{u}),

$$\omega = \nabla \times \vec{u}. \quad (2.4)$$

The magnitude of the vorticity vector indicates the strength of rotation, while the orientation of the vorticity vector defines the orientation of the axis of rotation. Further, vorticity is a field variable that has unique magnitude and orientation at every location in the flow domain, rather than a single global value.

2.1.2 Fluid Motion Varies with Length Scale

There are two main regimes of fluid flow – laminar and turbulent (Figure 2.2). In laminar flow, the fluid moves smoothly. Viscosity is dominant enough in laminar flows to discourage the formation of instability features such as eddies and vortices. In turbulent flow, the inertia of the moving fluid overcomes the viscous forces, and the fluid is subject to instability and random motions that take the form of swirling eddies.

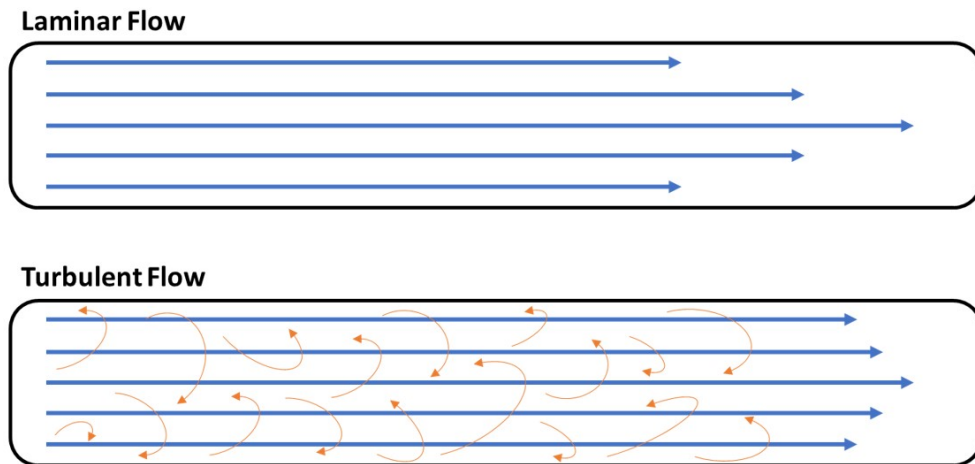


Figure 2.2: Laminar and turbulent flow. Schematic of simple laminar (upper) and turbulent (lower) flow in a pipe. Blue arrows represent the mean flow pattern in both laminar and turbulent flow. Orange arrows in turbulent flow highlight the instabilities and chaotic motion of the fluid.

The Reynolds number (Re) is a nondimensional parameter that represents the ratio of inertial to viscous forces and differentiates between laminar and turbulent flow. At low

Reynolds numbers the flow is considered laminar, and at greater Re the flow is considered turbulent, with a transitional regime falling between. The Reynolds number is calculated as

$$Re = \frac{\rho UL}{\mu} = \frac{UL}{\nu} \quad (2.5)$$

where L is the characteristic length scale for the flow (for example, the diameter of a pipe) and U represents the characteristic velocity (for example, the mean velocity of the fluid in a pipe).

Turbulent eddies have kinetic energy associated with their swirling fluid motion. Large eddies become unstable, due to the balance of inertial and viscous effects, and break into smaller eddies. This continues until eddies become so small that the kinetic energy is dissipated into heat by the fluid viscosity. The conceptualization of decreasing eddy size until it is lost to viscous dissipation is known as the turbulent energy cascade. The dissipation rate (ϵ) can be calculated for turbulent flows and represents the rate at which the kinetic energy is lost to viscous dissipation.

The smallest eddies that exist in a turbulent flow can be quantified using the Kolmogorov microscale. There are three main features of the Kolmogorov microscale. The Kolmogorov length scale (η) is the characteristic scale at which viscous dissipation occurs, the Kolmogorov time scale (τ_η) represents how long the smallest eddy can exist before being lost to viscous dissipation, and the Kolmogorov velocity scale (u_η) represents the velocity of the Kolmogorov-scale eddies.

2.2 Turbulence Affects Copepods

2.2.1 What are Copepods?

Copepods are small, crustaceous zooplankton found in nearly all bodies of water and make up a key link in aquatic food chains. They often exist at the same length scale as dissipative-scale eddies, i.e. at the Kolmogorov microscale. Copepods can detect chemical and hydro-

dynamic features in their environment by using setae, which are fine, hair-like structures located on their antennae. These setae may have chemoreceptors on them, allowing them to detect chemical cues in the water (Boxshall and Huys, 1998) or they may be more hydrodynamically receptive. Flow past setae causes them to bend, and the strength and direction of setal bending allows copepods to interpret different hydrodynamic cues (Yen and Nicoll, 1990; Yen and Strickler, 1996; Kiørboe et al., 1999; Doall et al., 2002).

2.2.2 Types of Turbulence

Turbulence is a random distribution of eddies constantly evolving in space and time, making fluid motion difficult to predict and analyze in a laboratory setting. To account for the different length scales of turbulence, it is easiest to envision turbulence as a means of dissipating energy. Energy in bodies of water is introduced into the water column as large-scale eddies, which as they become unstable, break down into smaller eddies until they are small enough to be dissipated into heat by viscosity (Kolmogorov, 1941). In the ocean eddies can reach diameters up to 100km, requiring differentiation of eddies by size. There are three different categories of turbulence based on eddy size – mesoscale, submesoscale, and microscale turbulence.

The largest eddies form mesoscale turbulence. Eddies at this scale have a diameter up to 100km and cores which extend up to 5km in depth (Rhines, 2015; Lutetaharms and Baker, 1980). These eddies allow for large-scale mixing and equalize energy built up as a result of heat gradients due to the uneven heating of bodies of water. Mesoscale eddies form when an instability in a larger current breaks off from the main current, deep-sea waves interact and propagate along the seafloor, or smaller eddies converge to form a larger eddy (Rhines, 2015).

Submesoscale turbulence is smaller than mesoscale turbulence, ranging from 0.1-10km in diameter and reaching depths up to 1km (McWilliams, 2016). Submesoscale eddies are usually fragments of mesoscale eddies. They are prominent in the surface layer and

mixed layer of the oceans, and further distribute heat gradients that form along the surface of the ocean. Eddies produced by wind stress are subject to Ekman pumping, where wind stress and the Coriolis effect work in tandem to create eddies that upwell deep, nutrient-rich waters to the surface (Eckman, 1905). Approximately 20-30% of all nitrogen flux is from submesoscale eddies, making them hot spots for primary production and biodiversity (Klein and Lapeyre, 2009).

Microscale turbulence is the smallest scale of turbulence. In the field of oceanography, microscale turbulence refers to eddies that have a diameter less than 0.1km. However, most of these eddies continue to serve similar functions as submesoscale turbulence. They are the continued dissipation of larger eddies that mix the ocean. Going forward, when referring to microscale turbulence, we will refer to special case of Kolmogorov microscale turbulence – the smallest eddies that are in equilibrium with their environment before being lost to viscous dissipation (Kolmogorov, 1941; Jimenez, 1997). Microscale turbulence can be visualized as a random distribution of vortex tubes that are constantly stretched and pulled in various directions (Jumars et al., 2009). Mesoscale, submesoscale, and microscale turbulence all affect copepod ecology.

2.2.3 Meso- and Submesoscale Turbulence Affects Community Structure

Copepods at first glance appear to be passive drifters in the ocean, subject to isolation from other communities and populations outside of their specific water mass. The inability to overcome the large-scale turbulent mixing of km-scale water masses can serve as a geographic barrier, blocking two different copepod populations from mixing, resulting in allopatric speciation (Hoskin et al., 2005). Allopatric speciation occurs when two populations of the same species can no longer interact, isolating gene pools and resulting in two distinct species over evolutionary time. This has been observed when comparing copepod populations between neighboring lakes that once were connected. The lakes each house a different species of copepod that once shared a common ancestor (Barrera-Moreno et al.,

2015). This phenomenon also has been observed when comparing copepod populations on different sides of an archipelago (Melo et al., 2014).

While these examples of allopatric speciation occur over large length scales with terrestrial barriers, these are extreme cases of population separation. On the length scale of different water masses, copepod patches that form within water masses are dominated by only one species, indicating that it is difficult for water masses to mix, which may serve as enough of a geographic barrier to allow speciation to occur (Tsuda et al., 2000). Population structure also varies between water masses which results in unpredictable and imbalanced sampling (Seridjii and Hafferssas, 2000; Labat et al., 2002). However, these separate populations can eventually be mixed, creating a new population if turbulent mixing is strong enough (Maar et al., 2003).

As eddies move across the ocean, they pick up different copepod populations, creating a unique community. As the geographic distance that an eddy travels increases, copepod abundance, biomass, and biodiversity within an eddy increases (Mackas et al., 2005; Huntley et al., 1995). The amount of biodiversity and species evenness between eddies also varies. In mesoscale and submesoscale turbulence, fluid volumes with greater turbulence have less biodiversity and species evenness than less turbulent volumes, resulting in a negative effect on biodiversity and ecosystem stability (Seridjii and Hafferssas, 2000).

2.2.4 Microscale Turbulence Affects Individual Interactions

Copepods face the challenge of living in a lower Reynolds number environment daily. At the Kolmogorov microscale, copepods interact with flow features that originate from other organisms, such as potential predators, prey, and mates, as well as with dissipative eddies that cascade down from mesoscale and submesoscale turbulent eddies. In contrast to mesoscale and submesoscale turbulence that affect copepod community and population structure, microscale turbulence affects copepods on a more individual level.

As turbulence increased to create a stressful environment, copepod metabolic, excre-

tion, and developmental rates also increase (Alcaraz 1997). Heart rate increases up to 93% (Alcaraz et al., 1994), nitrogen and phosphorus excretion rates increase up to 60% (Saiz and Alcaraz, 1992a), and growth rate decreases in more turbulent environments (Peters and Marrase, 2000).

Microscale turbulence also affects a copepod's ability to feed. Microscale turbulence increases encounter rates for organisms at this length scale (Kiørboe and Saiz, 1995b; MacKenzie and Kiørboe, 1995; Shimeta et al., 1995; Martinez et al., 2018; Michalec et al., 2020), resulting in feeding rates up to four times greater than in calm conditions (Saiz and Kiørboe, 1995; Caparroy et al., 1998). For ambush predators who actively forage for food, such as *Acartia tonsa*, there is a trade-off to the ideal turbulence level that increases foraging. Although increasing turbulence increases encounter rate, it also decreases the distance that *A. tonsa* can accurately detect prey. When turbulence levels are still relatively low, feeding in *A. tonsa* increases with turbulence, but a threshold arises where turbulence becomes too strong and the copepod can no longer detect prey (Saiz and Kiørboe, 1995).

These observations imply that there is an ideal turbulence level for a copepod which balances the advantages of an increased encounter rate with the disadvantages of a lower detection distance. Indeed, turbulence has the greatest effect on the number of prey encounters when the predator falls within the mm-cm body length scale, has limited or low motility, and has a long reaction distance – all traits characteristic of ambush-predator copepods, including *A. tonsa* (Kiørboe and Saiz, 1995a), *Centropages typicus* (Caparroy et al., 1998), and *Oithona davisae* (Saiz et al., 2003).

There are other competing factors as turbulence intensity increases. Increasing turbulence intensity increases the encounter rates with prey, which benefits the copepod when the copepod is a predator. However, copepods are common prey for organisms higher in the food chain, hence predation upon copepods may also increase with turbulence intensity. Copepod energy expenditure and mortality both increase with increased turbulence (Visser et al., 2009; Bickel et al., 2011). When the net energy gain from increased feed-

ing is weighed against increased energy expenditure and increased mortality rates, it may be more beneficial for an organism to function in an environment with lower turbulence (Visser et al., 2009).

Turbulence strength is quantified by different physical components. Several experiments have tried to correlate different behavioral responses to the physical components of turbulence, including shear (Kiørboe et al., 1999; True et al., 2015), vorticity (Kiørboe et al., 1999; Elmi et al., 2021), and acceleration (Kiørboe et al., 1999). These experiments show that species respond to hydrodynamic cues differently, and even within species, behavioral responses vary. Reliable experiments regarding copepods' response to turbulence requires simulated turbulence in a laboratory setting match similar dissipation rates to what occurs in an oceanic environment, which may not be as strong as previous experiments propose (Franks et al., 2022).

2.3 Malacostracan Pleopods

2.3.1 What is Malacostraca?

Malacostracan crustaceans comprise the largest class of crustaceans, including invertebrates such as lobsters, crabs, shrimp, amphipods, and isopods. These organisms range in size from isopods on the millimeter scale, to coconut crabs reaching just under 1m in length. While they all share similar morphologies, each is tailored to the physical environment it occupies.

Malacostraca have a chitinous exoskeleton comprised of three main body parts: the head, the thorax, and the abdomen. In some cases, the head and thorax have fused together over evolutionary time, forming the cephalothorax. If an organism has a cephalothorax, then the abdominal segment is referred to as the pleon. Malacostraca have two types of legs – thoracopods, located on the thoracic segment, and pleopods, located on the abdominal segment (Figure 2.3). In general, malacostracan abdominal segments features two pleopods that may be connected to each other via a retinaculum, or allowed to move inde-

pendently from each other. Pleopods consist of an upper segment, the protopodite, and a lower segment, the exopodite. The lower segment of the pleopod may be biramous, branching into two components- an exopodite and an endopodite. Through different adaptations, pleopods can be specialized to one of three main functions throughout the diversification of Malacostraca – reproduction, respiration, and most commonly, locomotion.

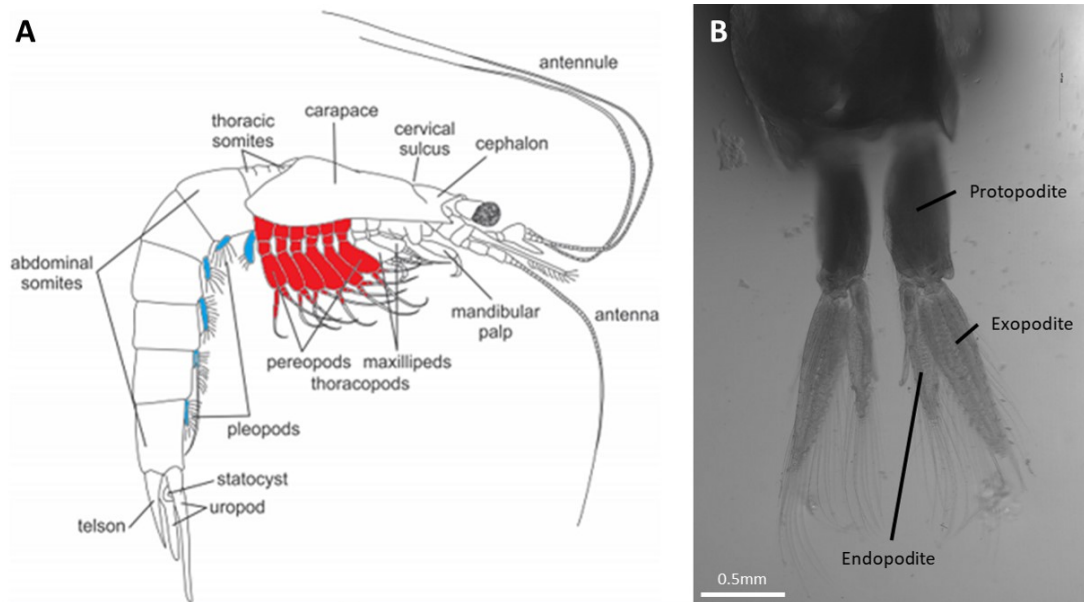


Figure 2.3: Malacostracan pleopods. (A) Pleopods (blue) and thoracopods (red) highlighted on a mysid shrimp. Image modified from Meland et al. (2015). (B) Image of the abdominal segment and pleopod pair of *Euphausia pacifica* with protopodite, exopodite, and endopodite identified.

2.3.2 Reproduction

In some Malacostraca, pleopods have assumed a reproductive purpose, becoming functionally gonopods. This is commonly observed in the Brachyura, or true crabs. True crabs have undergone an evolutionary process known as carcinization (reviewed by Keiler et al., 2017). Carcinization is the process where a lobster-shaped decapod evolves into a “crab-like habitus”. The head and thorax fuse into the cephalothorax, and the pleon will thin and ultimately fold under the cephalothorax, creating a pocket where the pleopods lay. While many organisms have this crab form, not all are considered true crabs. Instead of relying

on energy expenditure to hold the pleon in place, a true crab has a locking mechanism designed to hold the pleon in place, consisting of a “key” located on the fifth thoracic segment and a corresponding “lock” on the sixth abdominal segment (Kohnk et al., 2017).

Because the pleopods in true crabs are kept sequestered between the cephalothorax and the pleon, they are not used for locomotion. Instead, males have lost all but the first two pleopods, which have been modified into gonopods. Females have retained all of their pleopods, but instead, pleopods are used to attach and carry eggs during fertilization (Bliss, 1968; Kohnk et al., 2017). This increased carrying capacity within the space between the cephalothorax and the pleon creates some spatial limitations for female crabs, and often-times females are unable to fully institute a pleon-holding mechanism like the males in their species (Kohnk et al., 2018).

For males, pleopods are necessary for sex and have become reproductive organs for the crustacean. The first set of pleopods is fused together, forming a hollow tube which acts as a penis. The second pleopod pair, also fused together, becomes stiff and rigid. During copulation, both gonopods are inserted into the base of the female’s first pleopod. While the first gonopod releases sperm, the second acts as a piston, forcing sperm into the female. The female will then carry the sperm until she is ovigerous (Hartnoll, 1969).

It is important to note that gonopods are not restricted to the true crabs. Shrimp and lobsters also have modified pleopods that have a reproductive function. The loss of function in the first two pleopods of peppermint shrimp, *Lysmata wurdemanni*, prevents it from being able to successfully transfer sperm, indicating that this shrimp relies on pleopods for reproduction (Zhang and Lin, 2004). In *Homarus americanus*, the first set of pleopods is modified into gonopods in males and reduced in females so that egg attachment does not restrict the motion of the other four locomotory pleopods (Herrick, 1911; Comeau and Benhalima, 2018).

2.3.3 Respiration

In many isopods and amphipods, pleopods are specialized to assist in respiration. In aquatic species, amphipods and isopods have gills on their pleopods, serving as the site for gas and ion exchange. To amplify gas exchange, many species create a respiratory current to bring in water, increasing the amount of water the organism can filter and thus increasing the organism's oxygen levels (Friend and Richardson, 1986; Boudrias, 2002).

Functionality among an organisms pleopods can vary. The isopods *Idotea wosnessenskii* and *I. resecata* both have five pairs of pleopods. The two anterior-most pairs are used for locomotion, and the two posterior-most pairs are used for respiration, enhanced by the swimming current produced by the anterior pleopods. These pleopods have different physical properties that lend themselves to their functions. Pleopods used for locomotion are thicker and more rigid than pleopods used for respiration. The third pleopod pair, because it lies between the locomotory and respiratory pleopods, similarly has intermediate properties, allowing it to function as both a swimming leg and a respiratory leg, depending on where the need is greatest (Alexander et al., 1995).

Some amphipod and isopod species have transitioned recently over evolutionary time into terrestrial organisms, making them a unique case study for the challenges a terrestrial environment may impose upon an aquatic organism. Some of the most important challenges for an organism to face moving to a terrestrial environment include surviving desiccation and adapting a new respiratory system (Schmidt and Wagele, 2001). Amphipod pleopod length decreases as species transition from fully aquatic to littoral and terrestrial environments, highlighting the lessening pressure for pleopods that serve a respiratory purpose, as gills are no longer required. Coupling this, completely terrestrial amphipods no longer use their pleopods for locomotion and rely on their thoracopods instead, rendering pleopods rudimentary or completely vestigial in terrestrial species (Anagnostopoulou and Thomopoulos, 2013).

2.3.4 Locomotion

Many free-swimming crustaceans rely on a drag-based means of propulsion. Drag-based propulsion features an appendage, or set of appendages, undergoing a power stroke and a recovery stroke. During the power stroke, the appendage is fully extended, and during the recovery stroke, the appendage folds back on itself, either via a joint, or because the limb itself is flexible. This may be enhanced by the fanning and collapsing of setae to further increase the difference of drag between the power and recovery strokes (Cheer and Koehl, 1987). This asymmetry of the drag force throughout the entire stroke, in addition to suction thrust that arises from consecutive limbs, results in a net forward thrust that propels the organism (Kim and Gharib, 2011a; Colin et al., 2020).

Malacostracan pleopods beat in an asynchronous stroke to achieve drag-based propulsion. Pleopod pairs on the same abdominal segment will beat in tandem with each other and in a time-delayed manner relative to ipsilateral pairs, resulting in a metachronal stroke. Pleopod metachrony has been documented in anaspidacea (Grams and Richter, 2021), euphausiids (Kils, 1981; Murphy et al., 2011; Murphy et al., 2013), isopods (Alexander, 1988), mysid shrimp (Hessler, 1985; Quetin and Childress, 1980; Cowles et al., 1986; Wittmann, 2013), stomatopods (Campos et al., 2012; Garayev and Murphy, 2021; Ford et al., 2021), and lobsters, although pleopod metachrony in lobsters assists in walking, rather than free-swimming (Lim and DeMont, 2009).

It is important to note that while pleopods are often used for swimming, they may not be the primary propulsive appendage in some species of Malacostraca. Notably, several species of mysid shrimp rely on their thoracopods for swimming (Laverack et al., 1977; Schabes and Hamner, 1992; Sudo et al., 2009; Sudo et al., 2010). Because of the different appendages used for locomotion and the variations of pleopod metachrony in Malacostraca, pleopod functionality has been used to create phylogenetic trees and suggest evolutionary relationships within this order (Grams and Richter, 2021).

CHAPTER 3

A FRESHWATER COPEPOD'S RESPONSE TO MICROSCALE TURBULENCE

3.1 Introduction

Copepods are a diverse group of organisms found in nearly every body of water and are ecologically important, operating at the base of nearly every aquatic food chain. These organisms interact with their environment by interpreting chemical and hydrodynamic cues, which they detect using setae, thin, hair-like structures, on their antennae. Setal deformation as little as 10nm can elicit a behavioral response in a copepod (Lenz and Yen, 1993). Setae along the length of the antennae are subject to different flow patterns, with the section closest to the body experiencing faster flows than the more distal antennae tip (Fields and Yen, 1993; Lenz and Yen, 1993). To compensate for this velocity gradient, setae are specialized to respond to different hydrodynamic features (Lenz and Yen, 1993). One way setae may be specialized is by their length. Longer setae are more sensitive to lower frequency cues and shorter setae are more sensitive to higher frequency cues (Shen et al., 2020). The length and placement of setae allows for different patterns of bending, which a copepod can respond to and elicit a behavioral response appropriate to the source of the hydrodynamic feature (Yen et al., 1992).

Hydrodynamic features originate from predators, prey, and mates, and indeed, several studies directly investigate copepods' response to these ecological stimuli or flow fields meant to simulate these stimuli. Males in several species track females for mating through a combination of chemical and hydrodynamic features (*A. tonsa*: Bagøien and Kiørboe, 2005, *Eurytemora affinis*: Seuront, 2013, *T. longicornis*: Yen et al., 1998). Most commonly employed simulated flows are siphon flows, which produce a flow field that mimics a fish sucking in prey. The flow shear from siphon flow elicits escape responses in many species

(Gilbert and Buskey, 2005; Kiørboe et al., 1999; Fields and Yen, 1997; Fields, 2010; Yen et al., 2015). Additionally, the strength of the hydrodynamic feature can change the copepod's response. At low thresholds, copepods may interpret flow shear as a feeding cue and attack the source, whereas at larger thresholds, flow shear is interpreted as a predator and the copepod performs an escape response (Hwang and Strickler, 2001; Fields and Yen, 2002). Further, the threshold needed to elicit an escape response corresponds to the environment the copepod is from – copepods from a more energetic environment require a larger shear threshold before eliciting an escape response (Fields and Yen, 1997).

In addition to hydrodynamic features originating from other organisms, copepods contend with environmental flows, including turbulence. Large-scale eddies that form from biological sources, such as macroinvertebrates, or physical sources, such as wind-driven mixing, enter the water column and contribute to hydrodynamic features copepods interact with and interpret daily. Environmental turbulence has often been thought of as “background noise” to copepods; i.e., turbulence that does not have any direct meaning to the creature. Environmental turbulence can benefit copepods up to a certain level, before hindering them. For example, low levels of turbulence can increase copepod encounter rates with prey and conspecifics (Mariani et al., 2005; Michalec et al., 2015; Michalec et al., 2020). The optimal turbulence level for feeding in *Acartia sp.* does not occur in calm water, rather, it occurs at a level of turbulence that matches the organism's original environment (Saiz et al., 1992). In contrast, high turbulence levels decrease a copepod's perception distance (Gilbert and Buskey, 2005), feeding rate (Saiz et al., 1992), and swimming speed (Lee et al., 2011).

Studies investigating the influence of environmental turbulence usually expose copepods to tank-full disturbances and record the change in behavior of the copepods, without isolating a specific flow feature to determine what physical aspect of turbulence the copepod may be responding to. In other words, studies focus on broad trends in response to turbulence rather than the underlying mechanisms that evoke behavioral responses. Cope-

pods exist at the same scale as the Kolmogorov length scale, the physical scale at which viscosity is highly effective at dissipating kinetic energy into heat. Here, eddies stretch and intertwine, creating vortex tubes that organisms interact with (Jumars et al., 2009). To better understand how copepods respond to environmental turbulence, the challenge becomes isolating one of these vortex tubes in the laboratory. Flow features, including fluid velocity, vorticity, and strain then need to be quantified to determine what copepods are responding to.

It has been proposed that a steady-state Burgers vortex can serve as one of these vortex tubes at dissipative scales (Jumars et al., 2009). In a Burgers vortex, fluid rotates around the vortex axis while axial strain stretches the vortex along its axis. Vorticity is advected inward due to the radial flow, which balances the outward diffusion of vorticity, forming a steady vortex structure (Figure 3.1).

A steady-state Burgers vortex can be created in the lab by mounting two co-rotating paddles on hollow drive shafts to allow for flow between the two paddles (Webster and Young, 2015). By altering the spacing between the paddles, the flow rate between the paddles, and the rate at which the paddles rotate, Burgers vortices with different intensities corresponding to typical oceanic coastal turbulence levels can be created (Webster and Young, 2015). To date, two species have been exposed to a Burgers vortex; *Temora longicornis*, who in preliminary studies was exposed to two vortex intensity levels, and *Acartia tonsa*, who has been exposed to four vortex intensity levels (Webster et al., 2015; Elmi et al., 2021). *Acartia tonsa* changes its trajectories in response to the Burgers vortex to remain within the flow feature, indicating that a Burgers vortex may be an aggregation cue for this species (Elmi et al., 2021).

Hesperodiaptomus shoshone is a freshwater copepod found in seasonal, alpine lakes in Colorado, Utah, Wyoming, and southern Canada (Loria et al., 2020). Male *H. shoshone* exhibit mate tracking using chemical cues to find their mates (Yen et al., 2011). However, these experiments were conducted using dextran, a high molecular-weight sugar, to

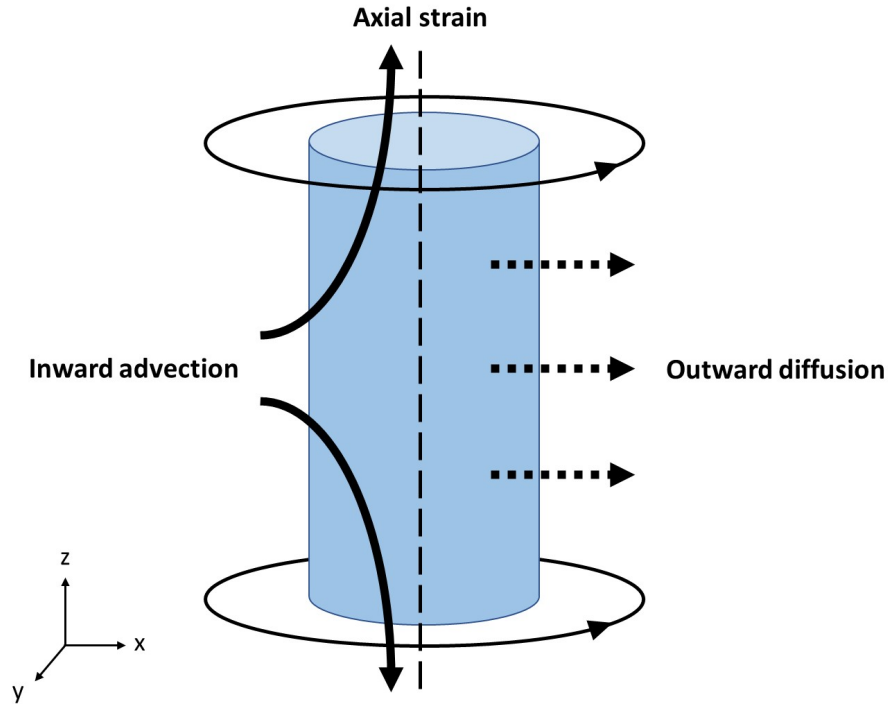


Figure 3.1: Burgers vortex cartoon. A cartoon diagram of a vertically-aligned Burgers vortex. The vortex axis is parallel to the z -axis and fluid rotation occurs about the axis. In addition to the swirling flow about the axis, there is a radially-inward flow and stretching flow in the axial direction. The radially-inward flow advects vorticity toward the axis, and inward advection is exactly balanced by outward diffusion of vorticity to create a steady vortex structure.

introduce a density gradient making trails visible to Schleioren optics. Further investigation into whether *H. shoshone* is responding to chemical exudates from conspecifics, dextran, or hydrodynamic features yields mixed results, making it unclear as to how this copepod senses its environment (Pender-Healy, 2014; Skipper, 2016). Although it is unclear if these organisms respond to hydrodynamic cues, *H. shoshone* are known aggregators (Marszalek, 2002; Salas, 2002), which primes them to respond to a Burgers vortex if a Burgers vortex is an aggregation cue.

To investigate the universality of a Burgers vortex as an aggregation cue, male and female *H. shoshone*, a freshwater copepod known to aggregate, were exposed to a Burgers vortex in two different orientations at four different vortex intensities as well as a negative control. Overall, *H. shoshone* will have a response similar to *A. tonsa*, as *H. shoshone* is a

known aggregator. *Hesperodiptomus shoshone* will change its trajectories with increasing turbulence level to maintain its position in the Burgers vortex, and the strength of this change will increase with increasing vortex strength. Males will have a different response to the Burgers vortex than females because males are sensitive to hydrodynamic features required for mating. Finally, the overall response to a horizontally-aligned vortex will be different than that of a vertically-aligned vortex.

3.2 Methodology

3.2.1 Animal Collection and Maintenance

Hesperodiptomus shoshone were collected from lakes along Beartooth Highway (MT, USA). Copepods were hand-collected using a 0.5m-33 μ m-mesh net. They were sorted by sex and stored in 1L Nalgene bottles at a density of approximately 50ind/L. Bottles were shipped overnight in a cooler filled with ice packs, to maintain a temperature of 14°C, to Georgia Institute of Technology (Atlanta, GA).

Upon arrival, bottles were transferred to a 12°C cold room, opened and allowed to aerate as bottle temperatures acclimated to the room's temperature. Once bottles reached 12°C, copepods were transferred to 36L housing buckets. Copepods were housed in EPA water at a density of 20-40ind/L, kept on a bubbler for aeration, and experienced a 12:12 light:dark photoperiod. Copepods were fed daily with *Artemia sp.* nauplii that were hatched in 20°C, 33ppt water. For feeding, *Artemia sp.* were collected by aggregating them to a light source and transferred via 1mm plastic pipette to a 35 μ m-mesh filter, where they were rinsed with EPA water before being given to *H. shoshone*.

3.2.2 Burgers Vortex Apparatus

Schematics from Webster and Young (2015), Webster et al. (2015), and Elmi et al. (2021) were followed to generate a Burgers vortex in the lab. In short, two hollow shafts, located 180° from each other, were mounted with paddles which rotated in the same direction

(Figure 3.2). This created a swirling flow between them. Each shaft also pulled water through it. This created a suction flow and stretched fluid to the poles of the vortex. The shafts were oriented either horizontally (along the x-axis) or vertically (along the z-axis) to create a Burgers vortex with a horizontal or vertical axis, respectively. Vortices of different intensities were generated by altering the flow rate of the paddles, the rotation rate of the paddles, and the spacing between the paddles.

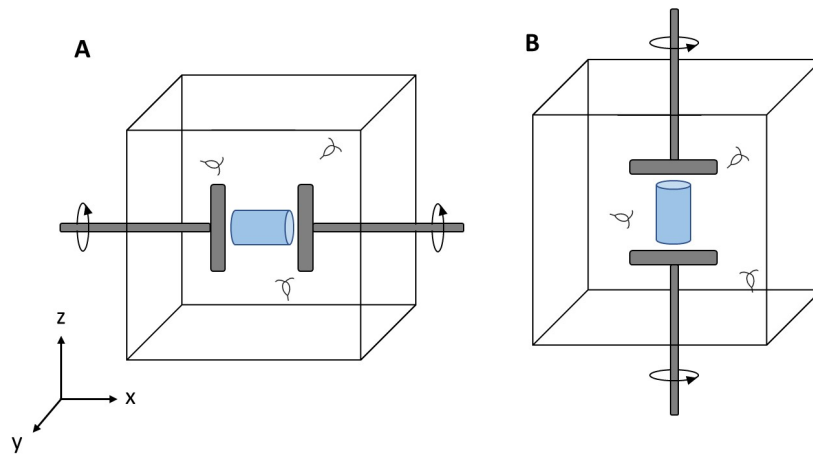


Figure 3.2: Experimental apparatuses. Schematic of Burgers vortex apparatuses. (A) Horizontal Burgers vortex. Two paddles mounted on hollow shafts rotate about the x-axis, creating a horizontally-aligned Burgers vortex. (B) Vertical Burgers vortex. Two paddles mounted on hollow shafts rotate about the z-axis, creating a vertically-aligned Burgers vortex.

The horizontal tank measured 20.6cm x 20.6cm x 27.3cm and the vertical tank measured 25.4cm x 25.4cm x 27.9cm. The disks (1.5cm radius) were located in the middle of each tank in either a horizontal or vertical orientation depending on the tank and were mounted on hollow stainless-steel shafts (inner diameter = 0.62cm). Rotation rates of the disks were controlled with a DC motor and flow rate through the shafts was controlled using a flowmeter valve connected via tubing to each shaft.

Spacing between paddles, flow rate, and paddle rotation rate were established by Elmi et al. (2021) to achieve four vortex intensity levels representative of typical turbulence in an oceanic environment (Webster et al., 2004). Target parameters for each vortex intensity

level are summarized in Table 3.1. Using these parameters allowed for the usage of flow data that has already been quantified for the corresponding vortices (Elmi et al., 2021).

Table 3.1: Burgers vortex parameters. Target parameters defined from Webster et al. (2004) and measured parameters obtained from Elmi et al. (2021).

		Vortex Level:	1	2	3	4
Target Parameters		Turbulent Dissipation Rate (cm^2s^{-3})	0.002	0.009	0.960	0.250
		Kolmogorov Length Scale (cm)	0.150	0.100	0.057	0.045
		Characteristic Radius (cm)	1.21	0.81	0.46	0.36
		Axial Strain Rate (s^{-1})	0.014	0.030	0.093	0.150
		Circulation (cm^2s^{-1})	0.84	1.41	2.15	2.13
Measured Parameters	Horizontal	Axial Strain Rate (s^{-1})	0.014	0.025	0.100	0.140
		Circulation (cm^2s^{-1})	0.92	1.71	2.52	2.45
	Vertical	Axial Strain Rate (s^{-1})	0.015	0.028	0.092	0.143
		Circulation (cm^2s^{-1})	0.89	1.43	2.58	2.39

3.2.3 Experimentation

Hesperodiaptomus shoshone's swimming behavior was quantified in response to three sets of independent variables; vortex intensity, vortex orientation, and sex. Vortex intensity had 4 levels, as defined in Table 3.1, plus a stagnant flow control and was quantified via the vortex axial strain rate; vortex orientation had 2 levels, horizontal or vertical; and sex had two levels, male or female. For an experiment, a group of 50 male or female copepods was transferred to either the horizontal or vertical experimental tank resulting in a density of 6.25ind/L. Males were visually differentiated from females via the asymmetric thickness of their antennae. One male antennae is thicker than the other, indicative of more musculature enabling the male to grasp and position the female during copulation. This experimental group was then exposed to all four vortex intensity levels plus the stagnant flow control in a random order. This comprised a single replicate for a given combination of vortex intensity level, vortex orientation, and sex. Three replicates for each experimental combination were run for male-horizontal, male-vertical, and female-horizontal. Only one replicate was run for female-vertical due to the limited number of individuals maintained in the lab culture over the 2mo experimentation period. Not enough females survived to run more than one vertical replicate.

Experiments took place in a dark, 12°C cold room to limit any phototactic response in the copepods. Recording took place via two orthogonally-mounted Flea3 MP Mono USB3 Vision (VITA 1300) cameras, each with a 50mm lens that recorded at 15fps. The tank was backlit with infrared lighting to further prevent a phototactic response. Cameras were connected to a computer where the experimenter watched live feeds of copepods swimming between the two paddles. Digital recordings were saved to an external drive for further analysis. Immediately after copepods were transferred to the experimental tank, a 1mm calibration plate was recorded in the field of view of both cameras to allow for image calibration. Copepods were then allowed a 60min acclimation period. If the first vortex intensity level copepods were exposed to contained a vortex, after 30min, the Burgers vortex with the appropriate intensity was generated, and the remaining time was allocated for the vortex to reach steady-state.

Recording for a vortex intensity level stopped when the experimenter noted 20-30 visually-identifiable passes between the two paddles on the live stream. Once this occurred, the vortex was changed to the next randomly-determined intensity, and copepods were allowed another 30min acclimation period as the vortex adjusted. An entire male replicate consisting of all five vortex intensity levels could be captured in approximately 8hrs, and an entire female replicate took approximately 16-24hrs.

3.2.4 Image Analysis

Copepod passes, whenever a copepod swam between the two paddles, were digitized using Hedrick's DLTdv5 software for MATLAB (Hedrick, 2008). The base of the copepod's antennae and base of the prosome were tracked in DLTdv5 five times for each pass, then averaged together for the mean coordinates to standardize tracking between several researchers who assisted in digitization. The mean, two-dimensional coordinates for each pass for each camera perspective were combined in an original MATLAB code to perform three-dimensional kinematic analysis. *Hesperodiptomus shoshone* three-dimensional tra-

jectories were then overlaid upon the known fluid velocity field of each vortex intensity level (courtesy of Elmi et al., 2021) to calculate kinematic variables.

Hesperodaptomus shoshone behavior was quantified using 6 kinematic variables: relative velocity, net-to-gross displacement ratio (NGDR), change in proportional residence time (δ PRT), the angle of the copepod's body relative to the local flow (i.e., body-flow alignment), the angle of the copepod's trajectory relative to the local fluid velocity (i.e., trajectory-flow alignment), and the angle of the copepod's body relative to the vortex axis (i.e., body-vortex alignment). Relative velocity was calculated by subtracting the local fluid velocity vector from the absolute velocity vector of the copepod and was averaged over the duration of the pass.

NGDR was calculated as the net distance travelled divided by the gross distance travelled to represent the curviness of the copepod's path. A high NGDR closer to 1 indicates a linear path, with the pathing becoming curvier as NGDR decreases. Since NGDR is a scale-dependent variable (Tiselius, 1992), it was calculated over 0.67s intervals for each pass before being averaged together within each pass.

Proportional residence time (PRT) is a standardized time measurement used to compare the time duration that the copepods spend in the Burgers vortex across vortex intensity levels (Elmi et al., 2021). PRT is calculated as the time spent in the vortex core (defined by the characteristic vortex radius, r_B) normalized by the time spent in a cylindrical volume centered on the core that encompasses three times the volume of the core (Figure 3.3). To account for different volumes across the vortex intensity levels, δ PRT was calculated as the difference between PRT for a given vortex intensity level and PRT in the control for that replicate in a volume with the same vortex parameters as the given level. If the copepods are spending more time in the vortex compared to the same physical region in the control, then δ PRT will be a positive value. If the copepods are spending less time in the vortex compared to the same physical region in the control, then δ PRT will be negative. If the vortex has no effect on *H. shoshone*'s spatial distribution, then δ PRT will be equal to zero.

The δ PRT in the control, therefore, equals zero.

Finally, three angles were calculated to quantify the copepod's alignment with various features of the Burgers vortex (Figure 3.3). Body-flow alignment is the angle that the copepod's body, represented as a vector that begins at the base of the prosome and extends through the base of the antennae, makes with the angle of the local flow at the copepod's midpoint (Figure 3.3A). The trajectory-flow alignment is the angle that the copepod's trajectory, calculated as the change in position of the copepod's midpoint between consecutive frames, makes with the angle of the local fluid velocity vector at the copepod's midpoint between consecutive frames estimated using the copepod's absolute velocity (Figure 3.3A). Body-vortex alignment is the acute angle that the copepod's body makes with the vortex axis (Figure 3.3B). Alignment angles less than 90° represent high alignment – that is the copepod's body aligns with the flow, the trajectory aligns with the flow, or body aligns parallel to the vortex axis. Alignment angles greater than 90° represent the copepod's body moving against the flow and the trajectory direction oriented against the flow. Alignment angles equal to 90° indicate that the copepod is swimming perpendicular to the local flow.

We hypothesize that if *H. shoshone* is using the Burgers vortex as an aggregation cue, then *H. shoshone* will (1) increase its relative velocity with turbulence level to remain within the vortex, (2) decrease NGDR in response to turbulence level indicative of curvier paths needed to remain within the vortex, (3) have a greater δ PRT in the presence of a vortex compared to a control, (4) change its body-flow alignment in the presence of a vortex compared to a control, (5) decrease its trajectory-flow alignment in the presence of the vortex indicating that it is using the flow to remain in the vortex, and (6) alter its body-vortex alignment in the presence of a vortex compared to a control. Males will have stronger responses for all 6 variables than females, and responses will vary with vortex orientation.

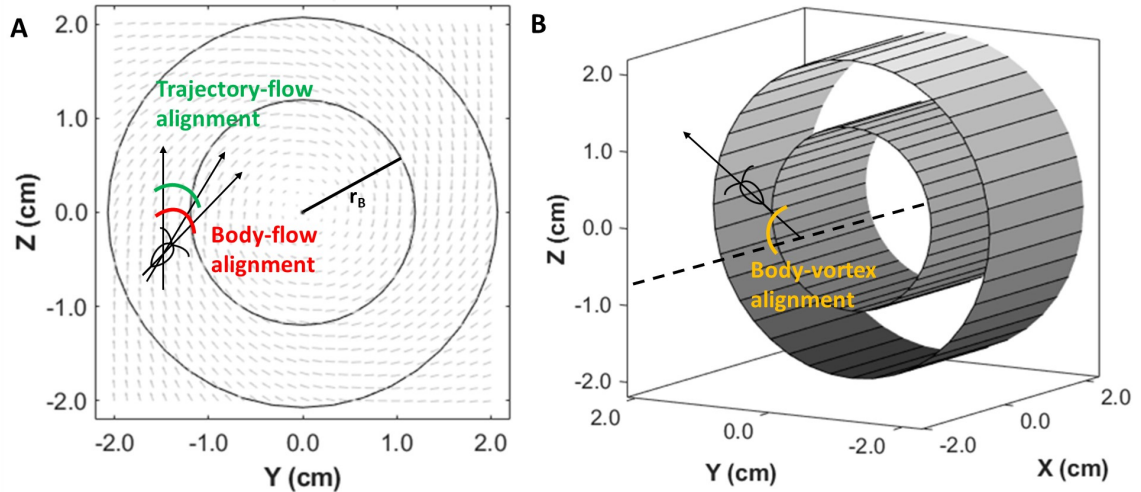


Figure 3.3: Angles quantifying copepod motion in relation to a Burgers vortex. (A) Alignment with flow. A cross-section of a level 1 velocity flow field and a copepod swimming in the Burgers vortex. The small circle encompasses the vortex core defined by the characteristic radius, r_B , and the larger circle encompasses a volume equal to three times that of the vortex core used to calculate PRT. Body-flow alignment (red) is calculated as the angle of the copepod's body axis, a vector from the base of the prosome to the base of the antennae, with the angle of the local flow at the midpoint of the copepod. Trajectory-flow alignment (green) is calculated as the angle of the copepod's trajectory, or physical displacement calculated at the midpoint between consecutive frames, with the angle of the local flow at the midpoint between those times, estimated using the copepod's absolute velocity. (B) Alignment with vortex. A three-dimensional representation of a copepod swimming in a Burgers vortex. The inner cylinder represents the vortex core, and the outer cylinder represents a cylinder with a volume three times that of the vortex core. Body-vortex alignment (yellow) is calculated as the acute angle that the copepod's body makes with the vortex axis.

3.2.5 Statistical Analysis

Fourteen to 64 passes were tracked for each level within a replicate (Table 3.2). Variables calculated for passes within a level in a replicate were averaged together, creating one representative data point for each level within a replicate. This resulted in three points for each experimental combination of vortex orientation, sex, and vortex intensity. There was only one data point for females in a vertically aligned Burgers vortex per level (Table 3.2).

Linear variables, including relative velocity, NGDR, and δ PRT, were analyzed using a 3-way factorial MANOVA to determine how *H. shoshone* altered its swimming behavior in response to vortex orientation, sex, and vortex intensity. Post-hoc analysis aggregated

Table 3.2: Number of passes for each level within a replicate.

Sex	Orientation	Replicate Number	Control	Level 1	Level 2	Level 3	Level 4
Male	Horizontal	1	24	34	49	31	37
		2	31	34	38	32	31
		3	26	38	36	37	39
	Vertical	1	29	32	38	43	21
		2	37	64	30	18	26
		3	31	45	44	46	30
Female	Horizontal	1	29	39	26	28	34
		2	44	27	28	27	21
		3	15	32	28	20	14
	Vertical	1	27	33	32	35	32

statistically similar data points and used t-tests to characterize significant responses to vortex orientation or sex. Variables significant in response to vortex intensity were regressed against axial strain rate.

Angular measurements, including body-vortex alignment, body-flow alignment, and trajectory-flow alignment, are subject to periodicity and require analysis via circular statistics, rather than linear statistics (Fisher, 1993). Data were first subject to a Watson goodness of fit test to verify that data followed a von Mises distribution. Concentration parameters (κ) were calculated and compared between groups to verify that κ s were greater than 1 and approximately equal between groups. These assumptions allowed for analysis via Watson-Williams test for homogeneity of means between groups. Sex and vortex orientation only had two factors, requiring no further posthoc analysis if a variable were significant in response to either of these independent variables. Angles that were significant in response to vortex intensity were regressed using circular-linear regression against axial strain rate.

Linear statistical analysis was performed in JMP Pro 16.0.0 (SAS Institute Inc., Cary, NC). Circular statistical analysis performed in R 4.1.1 and RStudio 1.4.1717 (RStudio Team, Boston, MA) using the package “circular” (Agostinelli and Lund, 2022). All data are presented as mean \pm standard error.

3.3 Results

Hesperodiptomus shoshone's response to a Burgers vortex changes in response to sex and vortex orientation, with multiple instances of confounding effects between sex and vortex orientation, and one instance of confounding effects between sex and axial strain rate, representing vortex intensity (Table 3.3, Table 3.4).

Table 3.3: MANOVA results. The factor “sex” has two levels, male or female. The factor “orientation” has two levels, horizontal or vertical alignment of the Burgers vortex axis. The factor “axial strain rate” has 5 levels corresponding to the four vortex treatments shown Table 3.1 and a negative control (i.e., stagnant flow). Significant values are bolded for $p < 0.05$.

		Whole Model	Relative Velocity	NGDR	δ PRT
Sex	DF(x,y)	(3,28)	(1,30)	(1,30)	(1,30)
	F	3.80	0.59	9.69	0.01
	p	0.02	0.45	<0.01	0.92
Orientation	DF(x,y)	(3,28)	(1,30)	(1,30)	(1,30)
	F	6.80	16.21	4.85	0.32
	p	< 0.01	< 0.001	0.04	0.57
Axial Strain Rate	DF(x,y)	(12,90)	(4,30)	(4,30)	(4,30)
	F	1.74	2.55	2.93	0.32
	p	0.07	0.06	0.04	0.86
Sex \times Orientation	DF(x,y)	(3,28)	(1,30)	(1,30)	(1,30)
	F	4.90	0.49	13.53	0.00
	p	< 0.01	0.49	< 0.001	0.97
Sex \times Axial Strain Rate	DF(x,y)	(12,90)	(4,30)	(4,30)	(4,30)
	F	1.27	1.26	3.16	0.27
	p	0.25	0.31	0.03	0.90
Orientation \times Axial Strain Rate	DF(x,y)	(12,90)	(4,30)	(4,30)	(4,30)
	F	0.63	1.07	0.33	0.30
	p	0.81	0.39	0.85	0.87
Sex \times Orientation \times Axial Strain Rate	DF(x,y)	(12,90)	(4,30)	(4,30)	(4,30)
	F	0.42	0.24	0.71	0.15
	p	0.95	0.91	0.59	0.96

Several variables were dependent on only one factor. *Hesperodiptomus shoshone* swim faster in a horizontally-aligned Burgers vortex than a vertically-aligned Burgers vortex [$t(48) = -3.56$, $p < 0.001$] (Figure 3.4A). Trajectory-flow alignment is greater in a horizontally-aligned Burgers vortex than a horizontally-aligned Burgers vortex (Figure 3.4B). Body-vortex alignment is lower in a horizontally-aligned Burgers vortex than a vertically-

Table 3.4: Circular analysis results. The factor “sex” has two levels, male or female. The factor “orientation” has two levels, horizontal or vertical alignment of the Burgers vortex axis. The factor “axial strain rate” has 5 levels corresponding to the four vortex treatments shown Table 3.1 and a negative control (i.e., stagnant flow). Significant values are bolded for $p < 0.05$.

		Body-Flow Alignment	Trajectory-Flow Alignment	Body-Vortex Alignment
Sex	DF(x,y)	(1,48)	(1,48)	(1,48)
	F	4.24	1.15	1.90
	p	0.04	0.29	0.17
Orientation	DF(x,y)	(1,48)	(1,48)	(1,48)
	F	3.20	8.23	69.70
	p	0.08	<0.01	<0.0001
Axial Strain Rate	DF(x,y)	(4,45)	(4,45)	(4,45)
	F	0.55	1.19	0.20
	p	0.70	0.33	0.94

aligned Burgers vortex (Figure 3.4C). Males have a greater body-flow alignment than females (Figure 3.4D).

NGDR varies with sex, vortex orientation, and axial strain rate (Table 3.3, Figure 3.5). When pooling data to look at trends in one set of independent variables, females have a greater NGDR than males [$t(48) = -3.84$, $p < 0.001$], and NGDR varies with axial strain rate [$R^2 = 0.16$, $F(1,48) = 9.04$, $p < 0.01$]. No immediate difference in NGDR in response to vortex orientation is apparent [$t(48) = -1.55$, $p = 0.13$]. However, the effect of vortex orientation matters differently to each sex (as noted by the significant interactive effect in Table 3.3). In a horizontally-aligned vortex, females have a significantly greater NGDR than males [$t(28) = -4.66$, $p < 0.001$]. There is no difference in NGDR between the sexes in a vertically-aligned vortex [$t(18) = 0.31$, $p = 0.76$]. NGDR for females is greater in a horizontally-aligned vortex than a vertically-aligned vortex [$t(18) = -3.85$, $p < 0.001$], while males do not change NGDR in response to vortex orientation [$t(28) = 0.94$, $p = 0.36$]. Additionally, each sex responds differently to vortex intensity as quantified by axial strain rate. As axial strain rate increases, males decrease NGDR [$R^2 = 0.53$, $F(1,28) = 31.86$, $p < 0.001$], while females do not change NGDR in response to axial strain rate [$R^2 = 0.00$, $F(1,18) = 0.00$, $p = 0.99$].

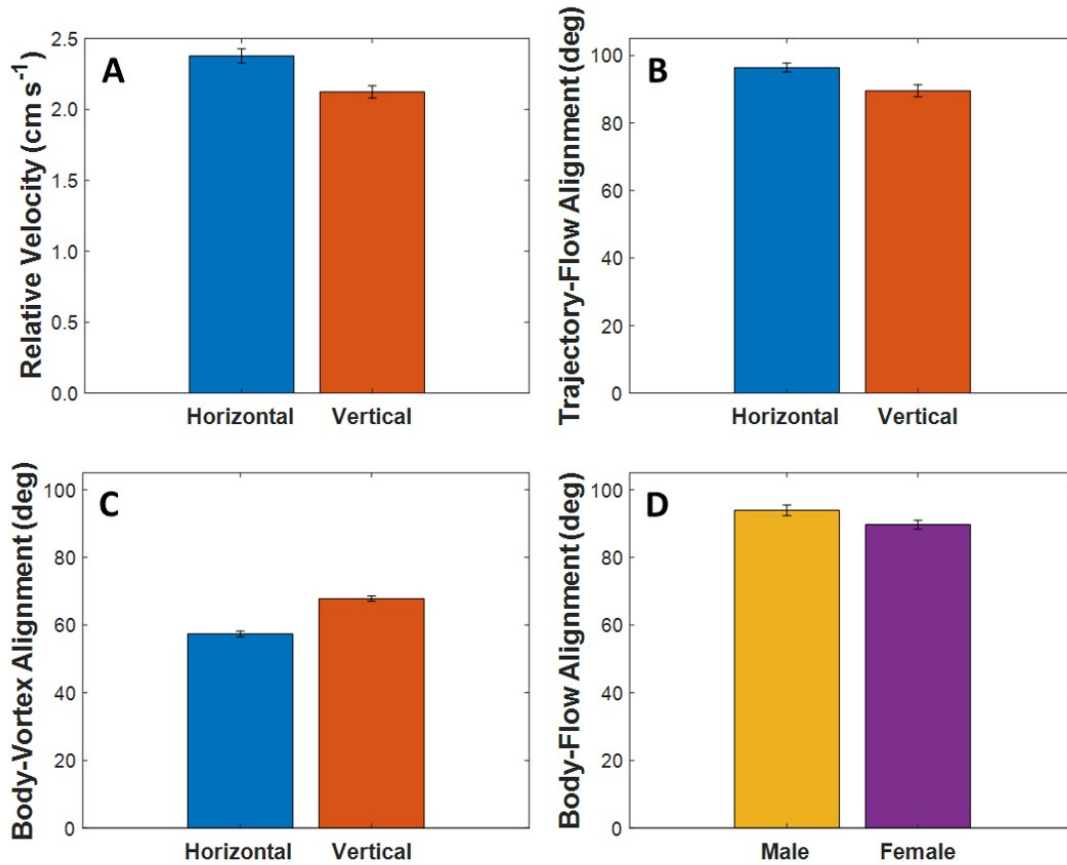


Figure 3.4: *Hesperodiaptomus shoshone* variables dependent on one factor (Mean \pm SE). (A) Relative velocity is greater in a horizontally-aligned than a vertically-aligned Burgers vortex. (B) Trajectory-flow alignment is greater in a horizontally-aligned than a vertically-aligned Burgers vortex. (C) Body-vortex alignment is lower in a horizontally-aligned than a vertically-aligned Burgers vortex. (D) Body-flow alignment is greater in males than in females.

3.4 Discussion

This experiment exposed the freshwater copepod, *H. shoshone* to different intensities of a Burgers vortex meant to mimic microscale turbulent eddies found in their environment. Unlike *A. tonsa*, *H. shoshone* show minimal response to vortex intensity, and instead alter their behavior in response to orientation. Males and females have subtle differences in their response to a Burgers vortex.

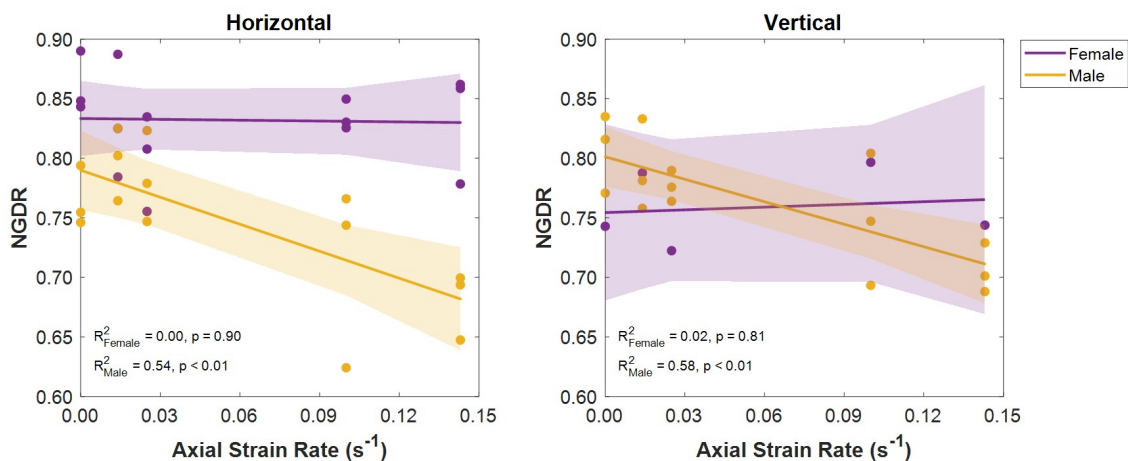


Figure 3.5: *Hesperodiaptomus shoshone* variables dependent on multiple factors. NGDR decreases with increasing vortex strength (i.e., axial strain rate) for males in both the horizontally-aligned and vertically-aligned Burgers vortex treatment. Although NDGR does not change with axial strain rate for females in either a horizontally-aligned or vertically-aligned Burgers vortex, it is significantly greater in a horizontally-aligned Burgers vortex than a vertically-aligned vortex.

3.4.1 The Burgers Vortex does not Promote Aggregation in *H. shoshone*

The Burgers vortex was used to represent microscale turbulent eddies at the dissipative length scale at the same scale as copepods (Jumars et al., 2009). Rather than studies that investigate an overarching species response to general isotropic turbulence (e.g., Yen et al., 2008; Michalec et al., 2015; Michalec et al., 2022), this study has the advantage of determining a copepod's response to a single isolated, steady vortex tube with quantified characteristics (Webster and Young, 2015). The Burgers vortex treatment has been used to determine how the marine species *T. longicornis* (Webster et al., 2015) and *A. tonsa* (Webster et al., 2015; Elmi et al., 2021) respond to a Burgers vortex. Behaviors between these two species differ, which is to be expected as copepod species often respond to turbulent features differently. In preliminary experiments, where both *A. tonsa* and *T. longicornis* were exposed only to Burgers vortex conditions equal to level 2 and level 3 in the present study, *T. longicornis* showed no change in response to the Burgers vortex, whereas *A. tonsa* increased its swim speed, trajectory with the vortex axis, and NGDR in level 3 compared

to level 2 (Webster et al., 2015). The non-responsiveness of *T. longicornis* was attributed to the limited range of vortex intensity tested, and the authors noted that this was expected to change if the parameter space was expanded to include greater vortex intensities.

The parameter space was later expanded, and Elmi et al. (2021) documented the behavioral response of *A. tonsa* to four vortex intensity levels in a Burgers vortex and a stagnant negative control in two orientations of the Burgers vortex. *Acartia tonsa* showed little behavioral change in response to the orientation of the vortex, and a strong change in behavior in response to the intensity of the vortex. At stronger vortex intensities, beginning at level 2 and continuing through levels 3 and 4, *A. tonsa* changed their pathing. Rather than swimming across the vortex in a random pattern, *A. tonsa* swam in spiral trajectories that followed the flow of the vortex. These trajectories were not a result of *A. tonsa* failing to be strong enough swimmers to escape the flow. *Acartia tonsa* performed hops across flow streamlines, allowing it to remain in the vortex and resulting in spiral trajectories about the vortex axis. These trajectories allowed *A. tonsa* to maintain its proximity to the vortex for a longer duration, potentially serving as an aggregation mechanism for *A. tonsa* to increase encounter rates between conspecifics (Elmi et al., 2021).

Hesperodiptomus shoshone does not appear to use the Burgers vortex as an aggregation cue, as it maintains relatively linear trajectories in all vortex intensity levels (Figure 3.6). Males adapt curvier paths than females in response to vortex intensity levels, but not to the extent that they follow spiral trajectory shapes like *A. tonsa*. Additionally, *H. shoshone*'s trajectory-flow alignment (horizontal: $96.5 \pm 1.3^\circ$, $n = 30$. vertical: $90.2 \pm 1.8^\circ$, $n = 20$) indicate that they are swimming roughly perpendicular to, if not slightly against, the flow. *Hesperodiptomus shoshone* may not evoke these spiral trajectories because it might not be under as much ecological pressure as *A. tonsa* to form aggregations.

Swimming in turbulence increases encounter rates for copepods, whether they are looking to encounter prey or conspecifics (Mariani et al., 2005; Michalec et al., 2015; Michalec et al., 2020). One key difference between *A. tonsa* and *H. shoshone* is that *A. tonsa* are

prey for many organisms including jellyfish (Suchman and Sullivan, 1998), ctenophores (Fininko et al., 2006), and fish (Hjelmeland et al., 1988), while *H. shoshone* live in relatively fishless lakes with few natural predators (Sprules, 1972; Williams, 2012). Because of this, *H. shoshone* do not feel pressure from predation to ensure mating as strongly as *A. tonsa* and may not aggregate as consistently.

3.4.2 Orientation versus Directionality

Several parameters included in this analysis, including relative swimming velocity, body-vortex alignment, and trajectory-flow alignment showed variation in response to orientation, but not to vortex strength. Rather than analyze *H. shoshone*'s response to vortex orientation, as the presence of a vortex had no effect on these variables, *H. shoshone*'s swimming behavior may be linked to the directional the copepod was swimming, which was influenced by the experimental apparatus.

The design of the Burgers vortex apparatuses consists of two rotating paddles spaced 2.5-3cm apart depending on the vortex intensity level. These paddles are aligned in either a horizontal or a vertical orientation depending on the orientation of the vortex. The placement of these paddles naturally restricts the motion of the copepods, making it so that they cannot swim in a fully unconfined space. When the paddles are placed for a horizontally-aligned vortex, the copepods are encouraged to have trajectories with a greater vertical component to swim through the region of interest. When the paddles are placed in a vertically-aligned vortex, the copepods are encouraged to have a more horizontal trajectory to swim through the region of interest.

This effect can be seen in the body-vortex alignment between these two treatments. In a horizontally-aligned vortex, because body-vortex alignment was calculated as the body angle with respect to a horizontal axis, the average angle was $57.4 \pm 0.9^\circ$, indicating that copepods swam diagonally through the vortex region. In the vertically-aligned vortex, body-vortex alignment was calculated with respect to the vertical axis, resulting in an av-

erage angle of $67.8 \pm 0.8^\circ$. This translates to a mean angle with the horizontal of approximately 22° . When *H. shoshone* was exposed to the horizontally-aligned vortex treatment, trajectories with horizontal orientation were restricted, resulting in a greater body angle with respect to the horizontal. When *H. shoshone* was exposed to the vertically-aligned vortex treatment and vertically-oriented trajectories were restricted, resulting trajectories naturally aligned with the horizontal.

Although *H. shoshone* do not have a strong response to a vortex per se in these experimental configurations, because the Burgers vortex apparatus confined their movement, effectively functioning as a tube for copepods to swim through, it is possible to investigate how vertical motion (observed in the horizontal Burgers vortex configuration) differs from horizontal motion (observed in the vertical Burgers vortex configuration). *Hesperodiaptomus shoshone* swim faster and more linear in the horizontal apparatus, when performing more vertical trajectories, than in the vertical apparatus, when performing more horizontal trajectories. With no apparent ecological trigger that would typically promote vertical movement, such as escaping from a predator or a phototactic cue for vertical migration, *H. shoshone* may be swimming faster and more linearly when swimming vertically in response to gravity. *Hesperodiaptomus shoshone* are negatively buoyant, and will sink in the water column. It is plausible for them to reach greater velocities while sinking than when they actively swim, particularly if they are not swimming at their top speeds. Additionally, sinking in a tank with no flow stimulus would lead to a linear trajectory. The positioning of the paddles to generate a horizontal Burgers vortex allows *H. shoshone* to passively sink in the water column through both paddles, capturing this as a behavior.

It is important to comment on why the changes in response to vortex orientation were prominent in *H. shoshone* and absent in *A. tonsa*. As mentioned, *A. tonsa* will align with the flow of a Burgers vortex and actively remain within it. This change in behavior is strong enough to overshadow any effects of the apparatus itself limiting motion in the copepod, as the copepod actively remains between the paddles (Elmi et al., 2021). *Hesperodiaptomus*

shoshone does not increase the time spent between the paddles across vortex intensity levels, resulting in many trajectories where the copepod swims directly across the vortex flow, effectively, excepting male NGDR, resulting in a negative response to the Burgers vortex across all kinematic parameters.

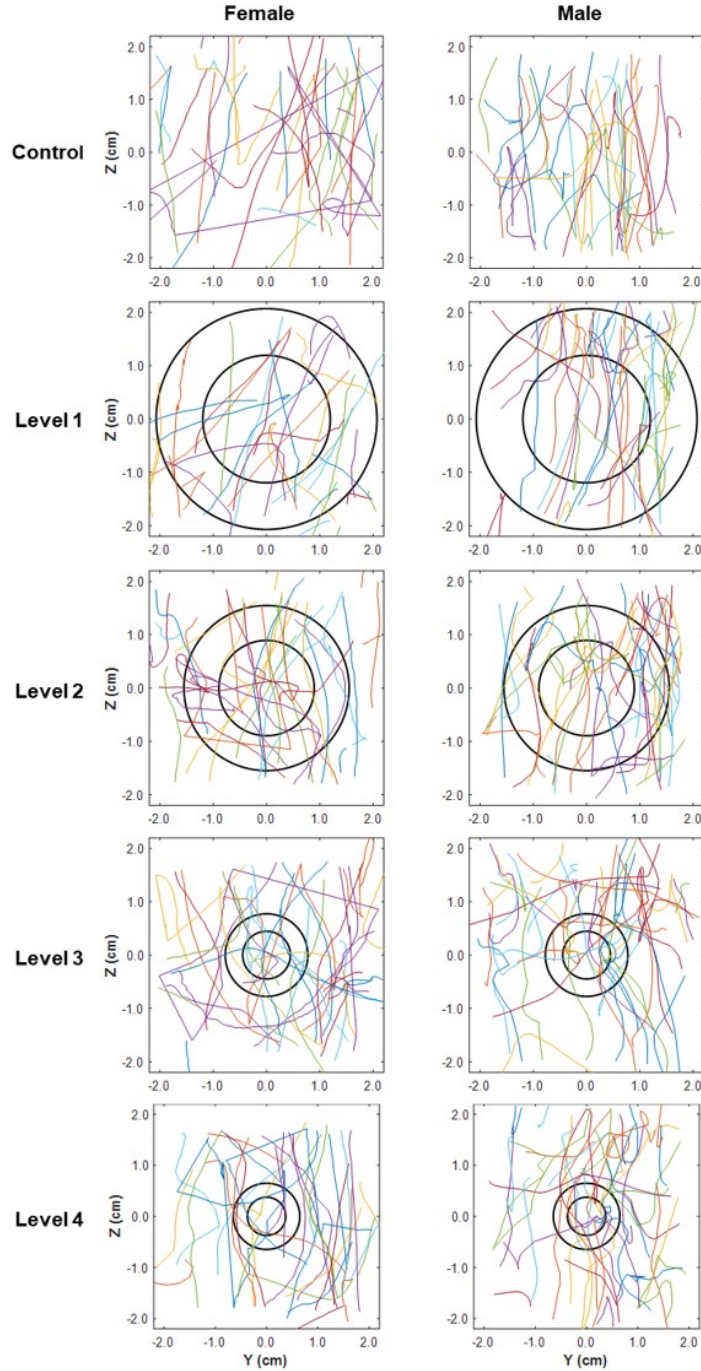


Figure 3.6: Cross-sectional trajectories for female and male *H. shoshone* across horizontal Burgers vortex intensity levels. Two-dimensional cross-sectional trajectories for female (left) and male (right) *H. shoshone* in a negative control and four levels of vortex intensity for a horizontally-aligned Burgers vortex. In each panel, the smaller black circle represents the core of the vortex (defined by the characteristic radius, r_B), and the larger black circle represents a cylinder with a volume three times that of the vortex core. Both sexes follow fairly linear cross-sectional trajectories across all five vortex intensity levels, with male trajectories becoming curvier, indicating a greater NGDR, at higher vortex intensity levels.

CHAPTER 4

DUAL PHASE-SHIFTED IPSILATERAL METACHRONY IN *AMERICAMYSIS*

BAHIA

4.1 Introduction

One aspect of an organism's physical environment that plays a role in their propulsive design is the relative importance of viscous effects compared to inertial effects. The Reynolds number (Re), calculated as

$$Re = \frac{\rho UL}{\mu} = \frac{UL}{\nu} \quad (4.1)$$

where ρ is the fluid density, U is the characteristic velocity, L is the characteristic length scale, μ is the dynamic viscosity of the fluid, and ν is the kinematic viscosity, is a nondimensional parameter that characterizes the balance between viscous and inertial forces. At high Reynolds numbers ($Re \gg 1000$), inertial forces dominate, and at lower Reynolds numbers ($Re \ll 1$), viscous forces dominate. Contending with different force balances results in different approaches to propulsion in organisms (Yen, 2000), which is perhaps best observed in aquatic environments.

At high Reynolds numbers ($Re \gg 1000$), aquatic propulsion occurs as the result of flapping via appendages, such as flippers or fins, or undulating motions, like rays, in a plane perpendicular to the direction of movement, generating thrust through vortex shedding (Vogel, 2013). Fish, rays, and aquatic mammals such as whales, dolphins, and porpoises utilize lift-based propulsion to swim (Drucker and Jensen, 1996; Fish and Lauder, 2006; Fulton et al., 2013; Ayancik et al., 2020).

At lower Reynolds numbers ($Re \ll 1000$), there are two distinct approaches to propulsion. In jetting, organisms, such as jellyfish (DeMont and Gosline, 1998), siphonophores (Costello et al., 2015), and squids (Anderson and Grosenbaugh, 2005) contract and expel a

jet of fluid in the direction opposite of motion. In drag-based propulsion, appendage motion occurs in a plane parallel to the direction of motion, like a paddle. It consists of a power stroke in which the appendage is fully extended, and a recovery stroke in which the appendage contracts. Bristles or hairs may fan out during the power stroke and retract on the recovery stroke, causing the limb to function as a “leaky rake” in parts of the stroke (Cheer and Koehl, 1987). This causes the surface area to vary throughout the stroke, resulting in greater drag during the power stroke than the recovery stroke and ultimately, a net forward thrust force (Kim and Gharib, 2011a). The pressure distribution around the appendage also plays a key role in determining the thrust generated (Colin et al., 2020).

Crustaceans have different approaches to drag-based propulsion, making them an ideal group to investigate overarching design elements for these propulsive systems. The first design element to consider in drag-based propulsion is the number of paddles used in the stroke. This number is highly variable within crustaceans, ranging from 2 in the daphniid *Daphnia magna* (Skipper et al., 2019), to 38 in the remipede *Speleonectes lucayensis* (Kohlhage and Yager, 2011). A second design element is paddle orientation. Paddles may be positioned in a monoplanar arrangement (euphausiid pleopods: Murphy et al., 2011) or in two parallel planes that vary during the power and recovery strokes to minimize appendage congestion (remipede legs: Kohlhage and Yager, 2011; mysid thoracopods: Laverack et al., 1977). A third design element to consider is paddle synchrony. Adjacent appendages may beat independently of each other or at the same time. In euphausiids, contralateral – left and right – pleopods beat at the same time. Although they have 10 total appendages, this results in a 5-paddle stroke. Additionally, paddles may undergo their power and recovery strokes at the same time resulting in a synchronous stroke, or beat with a phase difference among paddles. When the paddles stroke in an adlocomotory, time-delayed manner, the stroke is metachronal. A complete stroke, consisting of both the power and recovery stroke, may be completely synchronous (daphniids: Skipper et al., 2019), completely metachronal (euphausiids: Alben et al., 2010; Murphy et al.,

2011), or a combination of synchronous and metachronal (*Odontodactylus havenensis* escape response: Campos et al., 2012). There is also variability between each paddle. By changing parameters such as stroke amplitude, beat frequency, and time delay between adjacent power strokes, *E. superba* achieves a variety of different swimming styles (Murphy et al., 2011; Murphy et al., 2013). Further, morphological parameters, including the distance between paddles and the paddle shape, add more variables to the design space.

Data from these observational studies have been applied in models and experimental systems to determine the optimal parameters of a metachronal stroke and how parameters vary with Reynolds number. By altering the time delay between power strokes of adjacent paddles, studies have shown that perfect metachrony – having the same phase delay between all adjacent paddles – results in the greatest body speeds (Alben et al., 2010; Ford and Santhanakrishnan, 2021b) and greatest efficiency measured by fluid flux per stroke (Zhang et al., 2014; Granzier-Nakajima et al., 2020). Models also predict that the number of paddles needed to maximize distance travelled per unit energy varies with Reynolds number (Granzier-Nakajima et al., 2020). However, these models only account for the organism having one metachronal cycle occurring at a time. How would these parameters change if an organism were to have multiple concurrent metachronal cycles?

Mysid shrimp (superorder Paracarida) are malacostracan crustaceans with a similar, shrimp-like body plan to euphausiids, known as the caridoid facies. Mysids are distinguishable from other malacostracans by the presence in females of a brood pouch, or marsupium, on the base of their thoracic appendages, thoracopods, where they keep fertilized eggs until they hatch (Figure 4.1A). In contrast, many euphausiids, including *E. superba* and *E. pacifica* are broadcast spawners and release gametes into the water, thus lacking a marsupium (Ross and Quetin, 2000). Additionally, euphausiids and decapods, which use their pleopods to swim, have a structure called a retinaculum on their pleopods that functions as a set of hooks, linking the pleopods on the same abdominal segment together and ensuring that they beat in tandem. Mysid shrimp do not have a retinaculum, allowing

pleopods on the same abdominal segment to move independently of each other, doubling the number of paddles the mysid uses in its metachronal stroke (Grams and Richter, 2021).

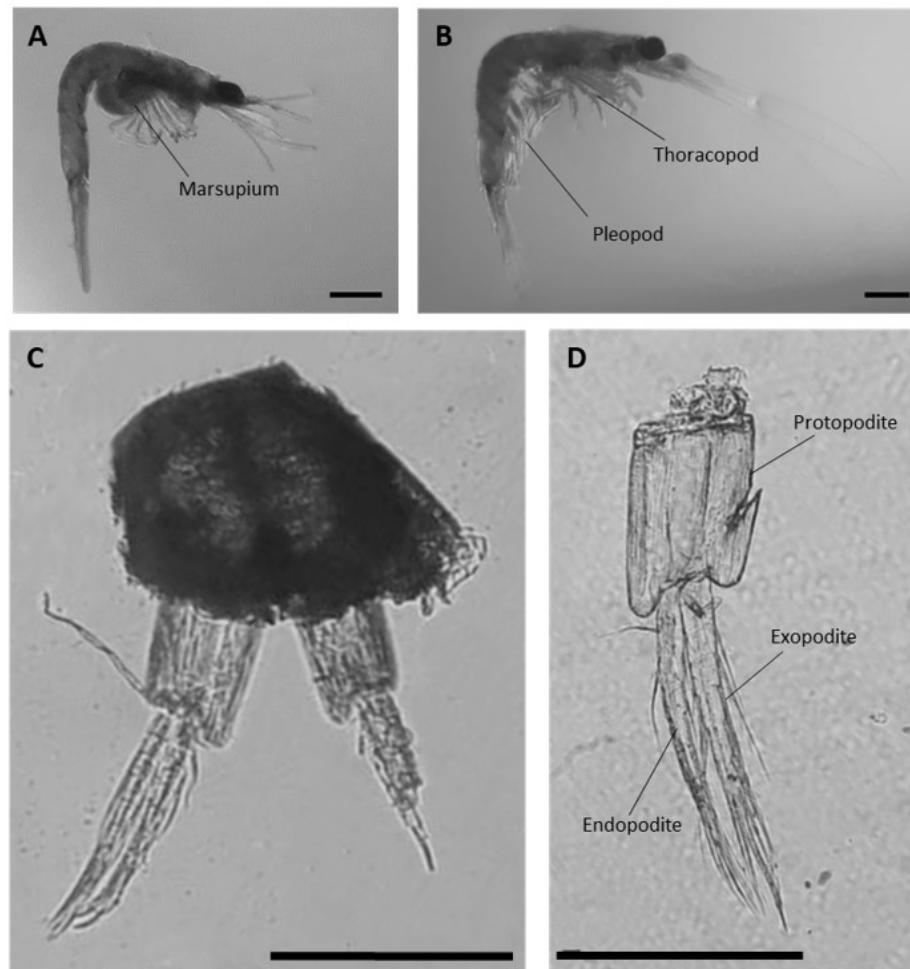


Figure 4.1: *Americamysis bahia* morphology. Scale bars are 1mm. (A) Adult female with marsupium. (B) Adult male with thoracopods and pleopods identified. (C) Transverse plane of the adult, male first abdominal segment with attached pleopods. The left pleopod is intact and the right pleopod has been damaged. (D) Adult, male pleopod from the third abdominal segment with protopodite, exopodite, and endopodite identified. Specimens were preserved in 37% by weight aqueous formaldehyde and photographed under a Wild M5A stereomicroscope.

Pleopod morphology and the resulting propulsive approach differs among the three orders of mysid shrimp. Stygiomysida pleopods are reduced, and these mysids rely solely on their thoracopods for swimming (Meland et al., 2015). In contrast, Lophogastrida, such as *Gnathopausia ingens*, have 5 fully-developed pleopod pairs that beat with 8 thoraco-

pod pairs in a metachronal stroke comprised of 2 antiphase cycles (Hessler, 1985; Quetin and Childress, 1980). Mysida propulsion is less well-defined. Early sources claim that Mysida pleopods are small, rudimentary, and not used for swimming (Tattersall and Tattersall, 1951), though more recent sources claim that, depending on the species, male Mysida have fully-developed, biramous pleopods that are used for swimming (Meland et al., 2015). However, kinematic analyses of Mysida species reveal that these species rely on their thoracopods for swimming, which beat in a rostro-caudal ellipse on their cephalothorax (Laverack et al., 1977; Schabes and Hamner, 1992). Even though Mysida may have pleopods, they rely on their thoracic appendages for swimming.

Americamysis bahia is an unusual Mysida because it uses its pleopods to swim, albeit occasionally. It is a hyperbenthic, subtropical species, primarily found in the Gulf of Mexico (Molenock, 1969; Lussier et al., 1988). It is easy to culture in the laboratory and highly sensitive to toxins in the water column, making it a model organism for toxicity experiments (Lussier et al., 1988; Lussier et al., 1999). *Americamysis bahia* have five pairs of pleopods on their abdomen that beat independently of each other, resulting in two ipsilateral metachronal cycles – one running along the left side, another running along the right side of the body. Further, *A. bahia* show pleopod sexual dimorphism within the species. Male pleopods are fully developed and female pleopods are reduced (Figure 4.1). Males and females rely primarily on their thoracopods for propulsion, but males occasionally swim using their pleopods in addition to their thoracopods.

While previous studies have focused on system design and optimization for organisms using only one metachronal cycle, this study will address how having two metachronal cycles comprising a metachronal stroke will alter swimming performance. In this study when referring to metachrony in *A. bahia*, a metachronal cycle refers to the 5-paddle beat pattern on one side of the body and a metachronal stroke refers to the complete 10-paddle beat pattern of left and right cycles together. The metachronal gait and resulting swimming behavior in *A. bahia* is quantified to test the hypothesis that pleopod utilization results in

different swimming behavior than thoracopod utilization. Two-cycle metachronal swimming in *A. bahia* is compared to 1-cycle metachronal swimming in *E. superba* to test the hypotheses that multiple cycles (1) require different pleopod morphology, (2) maintain steadier swimming speeds, and (3) achieve similar nondimensional measurements of efficiency compared to a single-cycle design.

4.2 Methodology

4.2.1 Animal Collection and Maintenance

Experiments took place during the summers of 2018 and 2020. *Americamysis bahia* were ordered from Sachs System Aquaculture (St. Augustine, FL), and mailed via 2-day shipping to Georgia Institute of Technology (Atlanta, GA). Upon arrival, mysids were allowed to acclimate to room temperature before being transferred to a 36L, 28ppt, aerated, saltwater aquarium. Mysids were fed 36hr *Artemia spp.* nauplii twice daily, with bi-weekly 30% water changes. The tank was cleaned once per week. Under these conditions, healthy *A. bahia* cultures were maintained for up to three months.

4.2.2 Recording

For all experiments, 10 mysids were haphazardly selected from their housing tank and transferred to a 1L, cubic, experimental tank. For thoracopod swimming experiments (2018), organisms were transferred directly from their housing tank to the experimental tank. For pleopod swimming experiments (2020), mysids were first transferred to a 3 × 3 pyrex spot plate and pleopod presence was verified underneath a Wild M5A stereomicroscope (Wild Heerbrugg, Switzerland) before being transferred to the experimental tank. The tank contained 28ppt saltwater filtered through a Pall A/E glass fiber filter (1 μ -pore size). Animals were allowed a 30min acclimation period in the experimental tank before recording began.

Unprovoked, free swimming mysid behavior was recorded by two

orthogonally-positioned high-speed cameras (AOS PRI-X and AOS PRI-S; AOS Technologies AG, Braden-Daettwil, Switzerland), each with an AF Micro-Nikkor 60mm f/2.8D lens at 500fps, focused on the center of the tank, away from the walls to prevent boundary interactions. Cameras captured an active volume of 9.5mL (2.3cm × 2.3cm × 1.8cm). Each camera was backlit with an 850nm dual voltage IR light (Super Circuits, Austin, TX) to prevent any phototactic response. The cameras were connected to a computer, where the experimenter watched live feeds. The cameras were manually triggered when an animal swam in the field of view, capturing the previous 1000 frames and recording the next 1000 frames. Recordings were saved for further analysis. Organisms were observed for 2hr periods before being switched for fresh animals, to ensure independent sampling. Digital calibration was accomplished by filming a 1mm calibration wand in the active volume before each 30min acclimation period began.

In 2018, experiments took place over 8 days, with a total of fourteen 2hr blocks. All mysid passes in front of both cameras were recorded regardless of the appendages used for swimming. One random pass from each block was selected for thoracopod swimming analysis, resulting in $n = 14$ instances of thoracopod swimming. In 2020, experiments took place over 4 days, with a total of seven 2hr blocks. These experiments differed from those in 2018 because mysids were pre-sorted to have pleopods and the recordings captured only pleopod swimming. One instance of pleopod swimming was randomly selected from each block. In tandem with 6 pleopod swimming instances recorded in 2018, there were $n = 13$ instances of pleopod swimming in *A. bahia*. The analyzed pleopod recordings featured at least one complete metachronal stroke that was in focus on one of the two cameras, with the organism being present in the view of the second camera, to allow for 3D reconstruction of appendage location.

4.2.3 Image Analysis

Recordings were digitized using the DLTdv5 software (Hedrick, 2008) for MATLAB. For thoracopod swimming analysis, the mysid's head and base of the telson were tracked on both cameras to extrapolate 3-dimensional kinematics. For pleopod swimming analysis, in addition to the head and the base of the telson, the 6th abdominal segment was tracked on both cameras, to determine if the telson angle (γ) affected swimming performance in *A. bahia*. Body length (BL) was measured as the distance from the organism's head to the base of the telson (Figure 4.2).

On the camera that had the best lateral view of the organism, points where the pleopod met the body, midjoints between the protopodite and exopodite, and pleopod tips were located in the digital image. Pleopod marker points were rotated into a 3-dimensional position based on the 3-dimensional position of the head, 6th abdominal segment, and telson points, resulting in a 28-point digitization of the mysid. The angle the pleopod makes with its body (α) and angle between the protopod and the exopodite (β) were calculated from this data set (Figure 4.2).

Instantaneous swimming speed was calculated by following the 3-dimensional position of the head throughout the entire recording. Mean swimming speed was calculated from these points for the duration of the entire recording.

Recordings varied in the number of sequential metachronal strokes performed by the mysid, ranging from 1-6. For instances where there were multiple metachronal strokes within one recording, separate strokes were identified by the initiation of the first P5 power stroke captured on camera. This pleopod, whether on the left or the right side of the body, became the pleopod that differentiated between consecutive strokes, with one complete stroke lasting the duration between consecutive power strokes of this specific appendage. Stroke amplitude curves were calculated following the method of Murphy et al. (2011). Stroke amplitude data for each pleopod cycle were centered to begin at $t = 0s$ and standardized to the mean cycle period. Cubic spline functions were fit to each pleopod stroke,

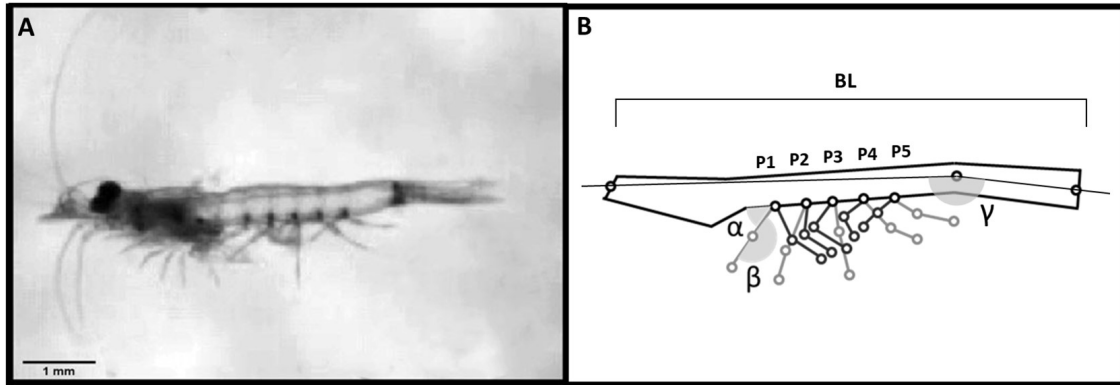


Figure 4.2: *Americamysis bahia* digitization. (A) Image of a free swimming mysid with pleopods. (B) Digitization of a similarly positioned mysid, showing the points tracked, body length (BL), angle between the protopodite and the body (α), angle between the protopodite and the exopodite (β), and telson angle (γ). Pleopods are numbered such that P1 is the anterior-most and P5 is the posterior-most. Shading indicates ipsilateral members of the same metachronal cycle. P1-P5 in light grey, are in various stages of their power stroke, and P1-P5 in dark grey, are in various stages of their recovery stroke. Angles α and β are depicted on the P1 pleopod in its power stroke.

and 100 equally spaced points were calculated based on the fitted function. The individual curves were ensemble averaged to create the mean pleopod α and β curves. Phase lag, stroke period, and cycle period were calculated from these curves.

4.2.4 Statistical Analysis

Statistical analysis was performed in JMP Pro 15.0.0 (SAS Institute Inc., Cary, NC). Parametric comparisons were made when variables were each normally distributed (tested via Anderson-Darling test) and had equal variance (tested via Levene's test) otherwise, non-parametric analysis between variables was performed. Data are reported as mean \pm standard error. Further, a first-order multivariate regression was performed to determine how *A. bahia* swimming speed depends on pleopod stroke amplitude, beat frequency, and phase lag.

4.3 Results

4.3.1 Thoracopod versus Pleopod Swimming

Americamysis bahia constantly beats its thoracopods to swim. Occasionally, the thoracopods are assisted by a brief series of metachronal strokes from its pleopods – the pleopods are never the sole propulsive appendage. Pleopod usage appeared random, and could not be associated with any stimulus. In 2018, when all instances of the mysid swimming in front of the cameras were recorded regardless of whether *A. bahia* used its pleopods or not, there were only 6 instances of *A. bahia* using its pleopods to swim out of 61 total passes. Based on these data, *A. bahia* use their pleopods approximately 10% of the time.

When using its pleopods, *A. bahia* achieves significantly greater swimming speeds (7.56 ± 0.74 BL/s, $n = 13$) compared to solely using its thoracopods (3.72 ± 0.61 BL/s, $n = 14$) (thoracopod swimming speeds not normally distributed, $p = 0.05$; 2-Sample Wilcoxon Rank, $p = 0.001$) (Figure 4.3). When using its thoracopods, the organism maintains a more stationary position in the water column by hovering in place, though it may also propel itself forward. In contrast, pleopods are utilized occasionally and only result in forward propulsion.

The angle the mysid made with the horizontal plane was quantified as body angle. A positive angle occurred when the organism's head was higher in the water column than its telson, and the organism was ascending, and a negative angle occurred when the organism was swimming deeper into the water column. There is no significant difference between the mean body angle the mysid has while swimming using its thoracopods ($21.4 \pm 6.0^\circ$, $n = 14$) compared to while swimming with its pleopods ($9.5 \pm 7.8^\circ$, $n = 13$) (thoracopod body angle not normally distributed, $p < 0.01$; 2-Sample Wilcoxon Rank, $p = 0.17$). Though the mean body angle is positive for both propulsive approaches, the pleopod body angle data are skewed such that the mysid favors its pleopods over its thoracopods when diving.

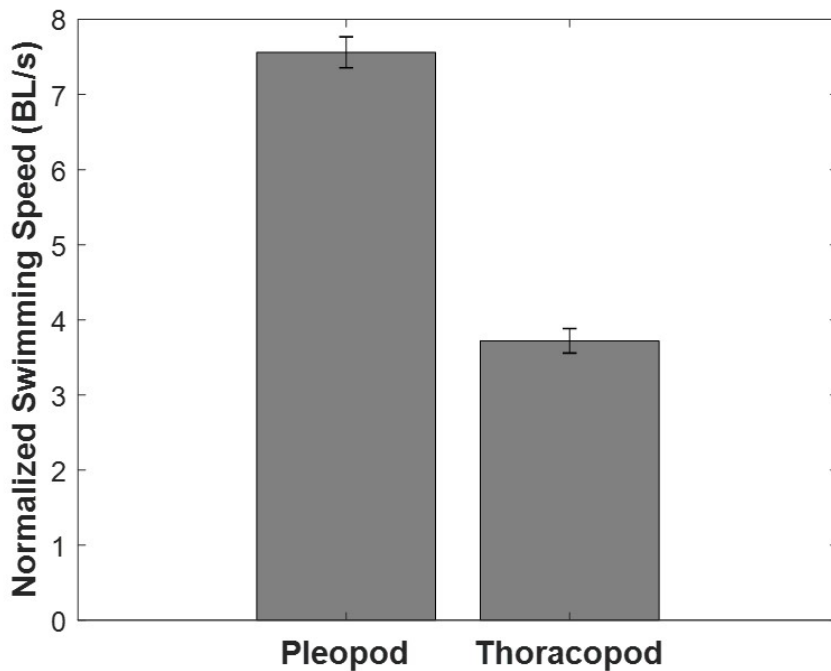


Figure 4.3: Normalized swimming speeds for *A. bahia*. Mean normalized swimming speed and SE achieved when the mysid uses its pleopods (n = 13) or thoracopods (n = 14) to swim.

4.3.2 Pleopod Metachrony in *A. bahia*

Figure 4.4 depicts α and β for one complete ideal stroke of the left and right cycles for *A. bahia*, beginning with the P5 power stroke in the left cycle. Left and right cycles are 180° out of phase with each other ($175.1 \pm 8.4^\circ$, n = 13; one-sample t-test, p = 0.58). The pleopods beat at 13.8 ± 0.6 Hz (n = 26 cycles) in an adlocomotory fashion moving posteriorly to anteriorly within ipsilateral cycles. During the interval between consecutive P1-P5 power strokes in the same cycle, the opposite cycle initiates all five of its power strokes. The telson angle throughout the stroke is $162.7 \pm 5.2^\circ$ (n = 13).

Phase lag was used to determine whether metachrony in *A. bahia* should be analyzed as one continuous 10-paddle stroke, or two concurrent ipsilateral 5-paddle cycles. The time between initiations of power strokes between ipsilateral pleopods can be normalized by the duration of the entire stroke, resulting in a dimensionless parameter – phase lag (simplified for one ipsilateral cycle in Figure 4.5A). Perfect metachrony occurs when phase lag is equal

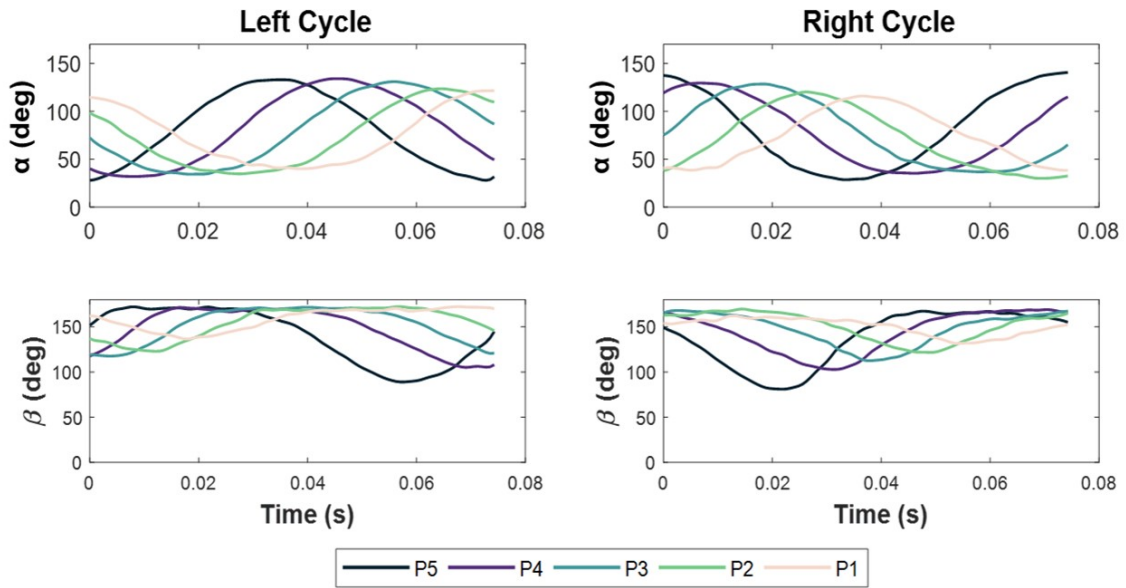


Figure 4.4: Time standardized pleopod angles for ipsilateral cycles during one complete metachronal stroke. Angles for $n = 13$ cases were combined for each pleopod (following method in Murphy et al. (2011)), represented in a different color, and time standardized to represent one ideal metachronal stroke.

for each ipsilateral pair combination. For a 10-paddle cycle, each phase lag is expected to take up one-tenth of the entire cycle's duration, resulting in an expected phase lag of 0.1. For a 5-paddle cycle, each phase lag would last one-fifth of the cycle, for an expected phase lag of 0.2. To analyze the stroke as a continuous 10-paddle cycle, the stroke duration was calculated as the duration between two consecutive power strokes from the same P5 and the P1-P5 lag was calculated using power strokes from contralateral cycles. The mean phase lag was then calculated, pooling each ipsilateral pair combination for all 13 replicates, resulting in $n = 130$. The mean phase lag for *A. bahia* when analyzed as a 10-paddle stroke (0.16 ± 0.01 , $n = 130$) is greater than the expected lag of 0.1 ($n = 130$, one-sample t-test, $p < 0.0001$). To analyze the stroke as two concurrent ipsilateral 5-paddle cycles, left and right cycles were analyzed separately with P1-P5 phase lag calculated from the same cycle. Again, each ipsilateral pair combination was pooled for the mean calculation, resulting in n

= 130. The mean phase lag for each ipsilateral pair spacing when the stroke is analyzed as two concurrent 5-paddle cycles (0.21 ± 0.01 , $n = 130$) closely agrees to the ideal 0.2 phase lag expected from a 5-paddle metachronal stroke ($n = 130$, one-sample t-test, $p = 0.71$). Therefore, metachrony in *A. bahia* was analyzed as though the organism's complete stroke is comprised of two concurrent ipsilateral 5-paddle cycles.

To determine how to best pool data, pleopod-specific variables, including pleopod tip speed, stroke amplitude, beat frequency, and phase lag were compared between corresponding contralateral appendages using a random complete block ANOVA, with the individual serving as a block. Pleopod length was assumed to be the same for left and right pleopods on the same abdominal segment. Pleopod tip speed ($p = 0.11$), stroke amplitude ($p = 0.06$), and β amplitude ($p = 0.24$) could be pooled per abdominal segment, resulting in $n = 26$ observations for these variables. Phase lag between ipsilateral pleopods varied between cycles ($p < 0.0001$), but was assumed to be a consequence of turning and pooled for mean calculations. Cycle beat period was calculated based on the time between consecutive P5 power strokes in the same ipsilateral cycle, resulting in two frequencies, one per cycle. For each pass, there was no significant difference between cycle frequencies for the left and right sides ($p = 0.34$), and cycle frequencies were combined for each pass, resulting in $n = 26$ beat frequencies.

Although the mean phase lag of all ipsilateral pairs is 0.21, there is variation between phase lags from different ipsilateral pairs. The P2-P1 (0.23 ± 0.02 , $n = 26$) and P1-P5 (0.42 ± 0.02 , $n = 26$) lags are greater than 0.2 ($p_{P2-P1} = 0.05$, $n = 26$; $p_{P1-P5} < 0.0001$, $n = 26$), while P3-P2 (0.12 ± 0.01 , $n = 26$) and P5-P4 (0.10 ± 0.01 , $n = 26$) are less than 0.2 ($p_{P3-P2} < 0.0001$, $n = 26$; $p_{P5-P4} < 0.0001$, $n = 26$). Only the P4-P3 lag is not significantly different from 0.2 (0.17 ± 0.02 , $p = 0.2$, $n = 26$). The greatest inter-limb phase lag occurs between P1 and the initiation of the next cycle in the following P5 power stroke, corresponding to the time when the opposite cycle is in its set of power strokes. (Figure 4.5B).

Stroke amplitude, calculated from α , varied between pleopods ($F = 3.8$, $p < 0.01$)

(Figure 4.5C). The only significant difference between stroke amplitudes occurred between P5 ($122.9 \pm 3.2^\circ$, $n = 26$) and P1 ($105.2 \pm 4.4^\circ$, $n = 26$) (Tukey-Kramer HSD, $p < 0.01$). The amplitudes for P2 ($109.4 \pm 4.1^\circ$, $n = 26$), P3 ($117.0 \pm 3.3^\circ$, $n = 26$), and P4 ($118.9 \pm 3.5^\circ$, $n = 26$) were not different compared to those for any other pleopod.

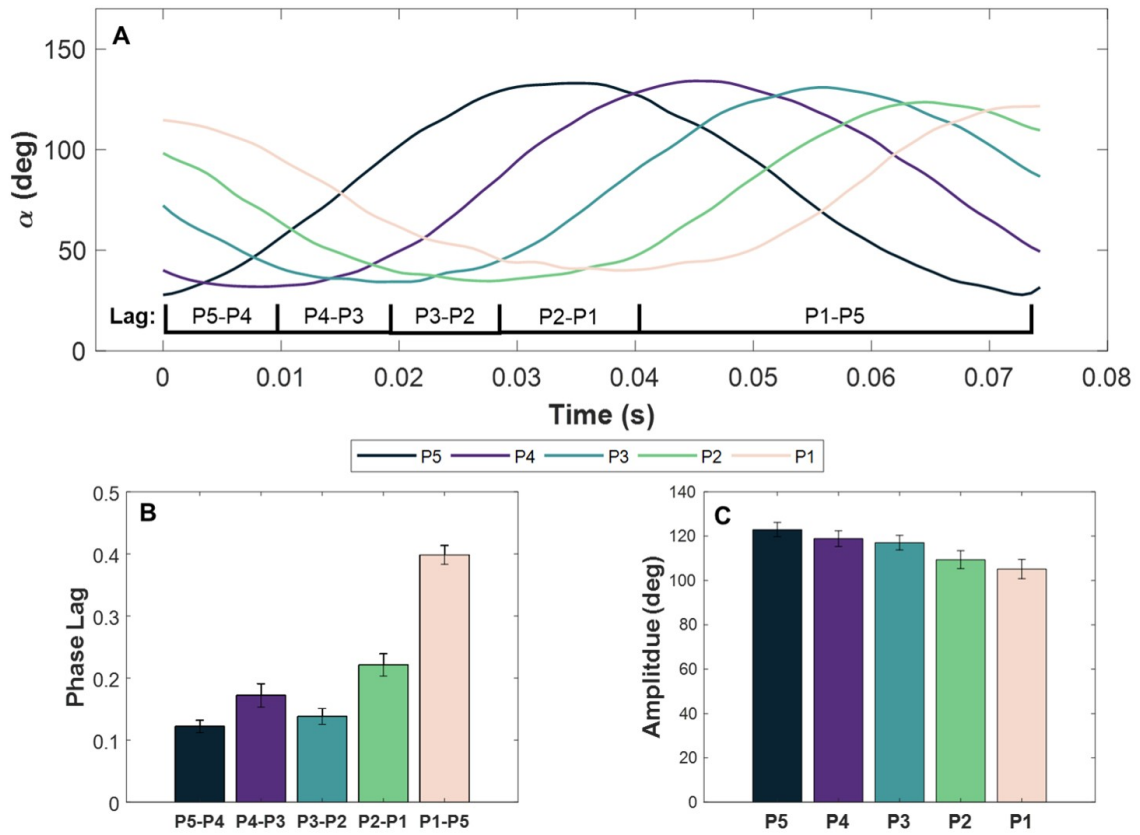


Figure 4.5: Phase lag and amplitude in *A. bahia*. (A) Angle α for one ipsilateral cycle of *A. bahia* with individual brackets indicating the duration between adjacent pleopod power strokes. The entire bracket encloses the duration of the complete stroke. (B) The mean phase lag between adjacent pleopods, defined as the fraction of a full cycle between initiation of power strokes of adjacent pleopods. Phase lag data for pleopods on the same abdominal segment were combined to calculate mean \pm SE ($n = 26$). (C) Stroke amplitude for pleopods on the same abdominal segment were combined to calculate mean \pm SE stroke amplitude for each pleopod ($n = 26$).

Americamysis bahia pleopods have significantly different lengths in relation to their position on their body ($F = 3.58$, $p < 0.01$). P1 is 0.66 ± 0.02 mm, P2 is 0.69 ± 0.02 mm, P3 is 0.70 ± 0.02 mm, P4 is 0.68 ± 0.02 mm, and P5 is 0.61 ± 0.02 mm in length ($n_{P1} = n_{P2} = n_{P3} =$

$n_{P4} = n_{P5} = 26$). P5 is significantly shorter than both P2 and P3 (Tukey-Kramer HSD, $p_{P5-P2} = 0.02$, $p_{P5-P3} = 0.01$). The rest of the pleopods are similar in length. The spacing between appendages can be calculated as the distance between adjacent appendages (G) normalized by the appendage length (L). The mean G/L ratio between pleopods is 0.46 ± 0.01 .

4.3.3 Increasing Swimming Speed

A multivariate regression was used to determine how stroke amplitude, beat frequency, and phase lag affect swimming speed. Stroke amplitude data were combined into one variable, mean stroke amplitude, for analysis due to high correlation of amplitude among appendages (Table A.1) to prevent collinearity in the final model. Phase lag data were not as highly correlated as stroke amplitude data and were analyzed independently in the model (Table A.2). Multiple correlations were analyzed to verify significant relationships between model inputs and normalized swimming speed, and only parameters with significant relationships were included in the final model.

Two models were analyzed to determine how stroke amplitude, beat frequency, and various phase lags contribute to swimming speed in *A. bahia*. The first model includes all variables that had a significant linear relationship with normalized swimming speed. Though this model shows a significant relationship between the input terms and swimming speed ($R^2 = 0.75$, $R_{adj}^2 = 0.58$, $F = 4.30$, $p = 0.04$), the variance inflation factor (VIF) is greater than 5 for P5-P4 lag in this calculation, suggesting collinearity is present in the model. The second model removes P5-P4 lag and the collinearity decreases. This model accounts for 62% of the overall variance ($R^2 = 0.75$, $R_{adj}^2 = 0.62$, $F = 5.98$, $p = 0.02$). Stroke amplitude is the only parameter to significantly contribute to this model ($p = 0.05$). The results of both models, as well as their zero-order relations with swimming speed are summarized in Table 4.1.

Table 4.1: Zero-order correlation and regression results for two models employed to predict swimming speed

Term	Zero-order		Model 1			Model 2		
	r	p	Standardized Coefficient	p	VIF	Standardized Coefficient	p	VIF
Intercept	-	-	0.00	0.31	-	0.00	0.24	-
Amplitude	0.63	0.02	0.57	0.21	4.72	0.43	0.05	1.17
Frequency	0.64	0.02	0.20	0.44	1.74	0.23	0.32	1.53
P5-P4 Lag	-0.68	0.01	0.18	0.74	6.58	-	-	-
P4-P3 Lag	-0.45	0.12	-	-	-	-	-	-
P3-P2 Lag	-0.61	0.03	-0.35	0.34	3.46	-0.26	0.30	1.75
P2-P1 Lag	0.64	0.01	0.28	0.31	1.83	0.26	0.30	1.80
P1-P5 Lag	0.48	0.10	-	-	-	-	-	-

Significant relationships with swimming speed are bolded

4.4 Discussion

4.4.1 Consequences of Multiple Cycles

Morphology

The most defining feature of metachrony in *A. bahia* is the number of paddles used in one stroke. Euphausiids' and decapods' contralateral pleopods are connected with a retinaculum ensuring they beat at the same time in a metachronal stroke with 3-5 paddles. Mysid shrimp lack a retinaculum, allowing their pleopods to beat independently (Grams and Richter, 2021). *Americamysis bahia* employs two simultaneous, 5-paddle metachronal cycles- one running along the left side, the other along the right side of the body- effectively using 10 total paddles in its metachronal stroke instead of 5. Having more paddles in a metachronal stroke at this Reynolds number is beneficial to *A. bahia* (mean $Re = 170 \pm 20$). At Reynolds numbers of 100, efficiency, measured as time-averaged fluid flux to time-averaged power supplied to the fluid, increases with the number of paddles, only operating at 90% efficiency with 4 paddles, and reaching maximum efficiency at 8 paddles and beyond (Granzier-Nakajima et al., 2020).

Pleopod structure differs between *A. bahia* and *E. superba*. In *A. bahia*, the protopodite is $48 \pm 2\%$ the length of the entire pleopod, whereas in *E. superba*, the protopodite is $41 \pm 2\%$ the length of the entire pleopod. In *A. bahia*, the protopodite, as the upper section

of the pleopod that connects the appendage to the body, houses more appendage musculature than the more distal exopodite and endopodite, which may be where *A. bahia* derive the power for their stroke (Hessler, 1985). *Euphausia superba* fan their exopodite and endopodite on their pleopods at an angle of 80° to increase the surface area of their paddles and increase drag (Murphy et al., 2011). In this study, though the distal segment of the pleopods has an exopodite and endopodite, they were not observed to fan out.

Gait Kinematics

Although pleopod usage is infrequent, due to our inability to associate pleopod usage with any specific stimuli, pleopod swimming in *A. bahia* appears to be a general swimming behavior. It is assumed to be a sustained swimming behavior rather than an escape response even though it is only observed for short periods of time, and as such, warrants comparisons to other organisms with a similar body plan that use their pleopods to swim - primarily *E. superba* and *Gnathophausia ingens*.

An important question for *A. bahia* is whether swimming speed is related to stroke amplitude and frequency, especially as these parameters are strong predictors for *E. superba* swimming speed (Murphy et al., 2011). A first-order multivariate regression was employed for *A. bahia* swimming kinematics to determine which stroke parameter is most responsible for dictating swimming speed. Most parameters expected to predict swimming speed showed similar, low levels of correlation with swimming speed in *A. bahia*. Stroke amplitude, beat frequency, P5-P4 phase lag, P3-P2 phase lag, and P2-P1 phase lag were all significant zero-order predictors. Of these, P5-P4 phase lag was highly correlated with the other predictors and could be encapsulated in those variables. Of the final parameters used in the first-order multivariate regression, stroke amplitude was the only significant predictor in the model, suggesting that stroke amplitude has the strongest effect on swimming speed in *A. bahia* (Table 4.1). In the final model, increasing frequency, decreasing P3-P2 lag, and increasing P2-P1 lag all have similar weights on swimming speed, reflected in similar

standardized coefficients.

When using their pleopods, *A. bahia* swim in a horizontal orientation (mean body angle = $9.5 \pm 7.8^\circ$, $n = 13$) at speeds greater than 2BL/s, which matches the qualifications for fast forward swimming defined in Murphy et al. (2011). *Euphausia superba*, in contrast, have much more variability in their metachrony, evident in the different swimming behaviors they can achieve. They can hover, swim fast forward, or swim upside down, differentiable by the organism's swimming speed and orientation (Murphy et al., 2011).

Americamysis bahia have less variability in stroke amplitude compared to *E. superba* and can achieve greater normalized swimming speeds (Figure 4.6). The primary reason for the difference is the swimming styles of these organisms. *Euphausia superba* swims only using its pleopods and achieves speeds less than 2BL/s by decreasing its stroke amplitude. In contrast, *A. bahia* never swims less than 2BL/s when using its pleopods – it achieves these slower swimming speeds when using its thoracopods.

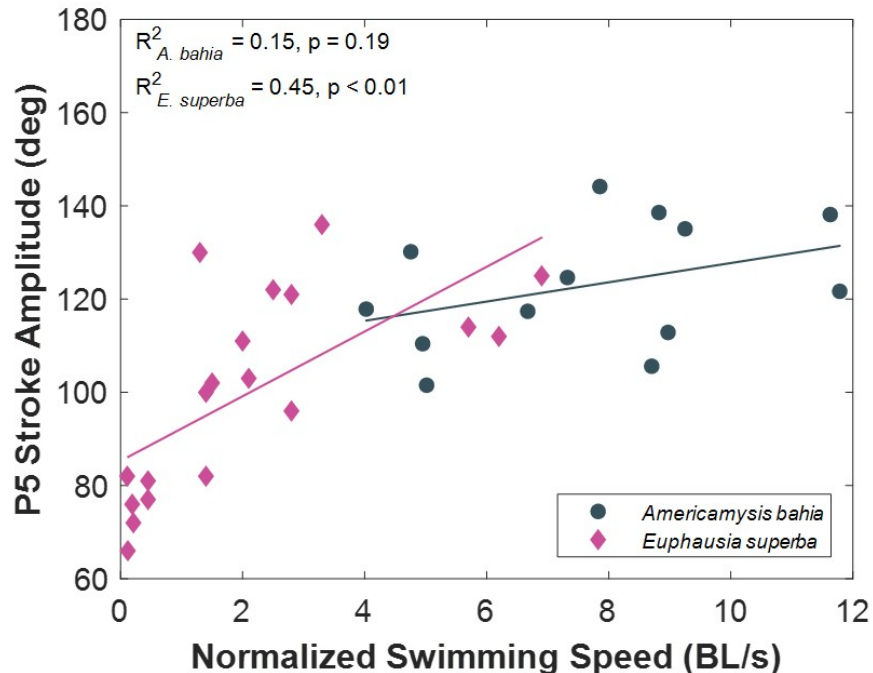


Figure 4.6: P5 stroke amplitude and normalized swimming speed for *A. bahia* and *E. superba* (Murphy et al., 2011).

Above the 2BL/s threshold, *E. superba* transitions to increasing its speed by increasing

beat frequency, rather than stroke amplitude (Murphy et al., 2011). *Americamysis bahia* also increase beat frequency to swim faster, though this relationship is not as strong as it is in *E. superba* (Figure 4.7A). The hyperbenthic mysid *Gnathopausia ingens*, which also uses two ipsilateral metachronal cycles, never swims faster than 2BL/s (Cowles et al., 1986). While this variability in attainable speeds may be attributed to differences in experimental conditions between the three studies, if a logistic growth curve is fit to these data, a maximum beat frequency for attainable speeds using metachrony occurs at approximately 15Hz ($R^2 = 0.88$), indicating an upper limit to stroke frequency in metachrony. Even though these three species swim with their pleopods at vastly different normalized speeds, come from different environments, and exist at different Reynolds numbers, they all achieve similar absolute speeds, between 0 and 5 cm/s, indicating a practical range of absolute speeds in which sustained metachrony is an effective approach to aquatic locomotion (Figure 4.7B).

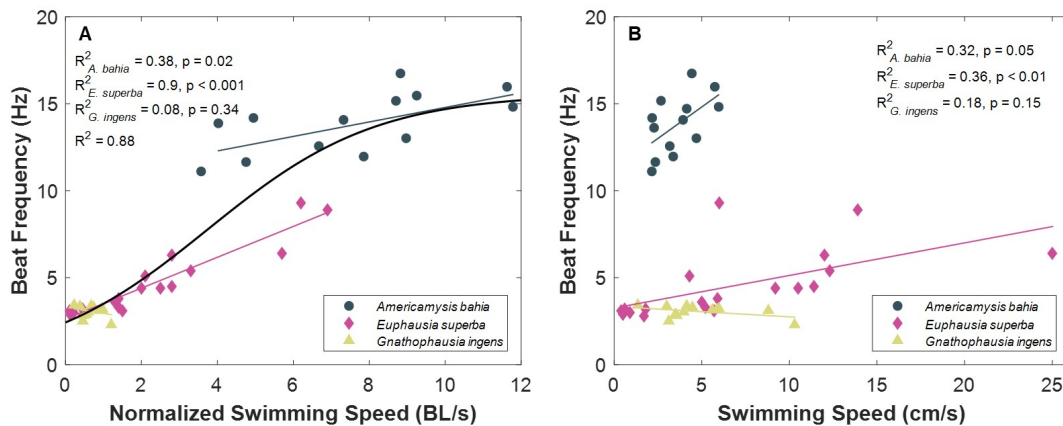


Figure 4.7: Beat frequency and swimming speed for *A. bahia*, *E. superba* (Murphy et al., 2011), and *G. ingens* (Cowles et al., 1986). (A) Frequency plotted against normalized swimming speed. (B) Frequency plotted against swimming speed.

Smoothness of Swimming

Swimming speeds in *A. bahia*, while they may fluctuate over the duration of an entire stroke, show no periodic increases that have been associated with specific power strokes in other organisms (Figure 4.8). When *E. superba* hover, their speed shows periodic increases

corresponding to their P3 power stroke, which is their longest paddle (Murphy et al., 2013). Remipedes also show periodic speeds, with increased speeds corresponding to their longest paddles (Kohlhage and Yager, 2011). *Americamysis bahia* have no significantly long appendage. Even though P3 is the longest pleopod, there is no spike in speed correlated to a P3 power stroke in *A. bahia*.

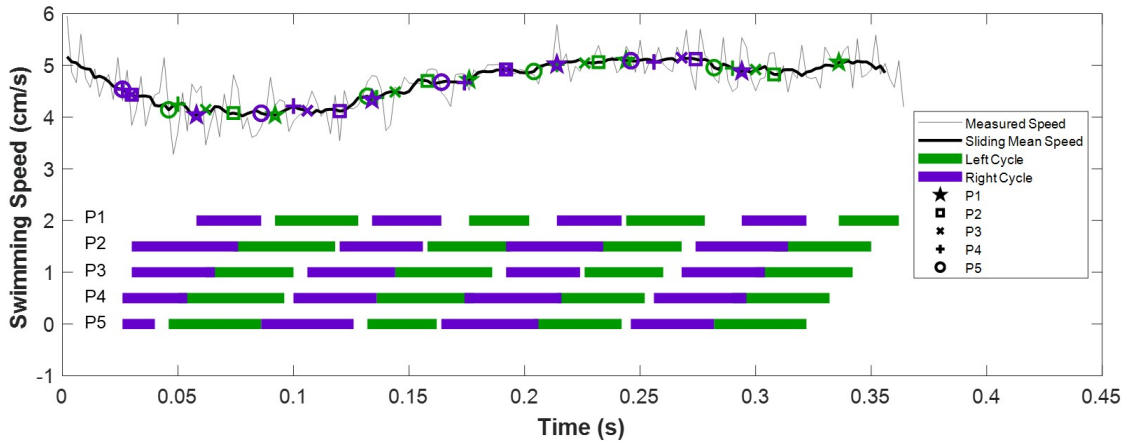


Figure 4.8: Sample swimming speed and power stroke synchrony. Data were collected from one pass containing four complete metachronal cycles in *A. bahia*. Swimming speed data consist of the measured speed in light grey, and a sliding mean value, taken over 0.02s, in black. The bottom portion of the figure depicts the timing and duration of the power strokes for each pleopod, and the bars are color-coded by cycle. Marker points are depicted on the sliding mean swimming speed curve that correspond to the initiation of respective pleopod power strokes. The color of these points correspond to the cycle, and the shape of the points correspond to the pleopod.

The more constant speed may be a result of *A. bahia* having more paddles in its metachronal stroke than *E. superba*. Though metachrony in *A. bahia* is comprised of two, 5-paddle cycles, the entire stroke consists of 10 paddles operating independently of each other, twice as many paddles compared to *E. superba*. Each power stroke contributes some amount of thrust to the resulting motion. As the number of paddles in a stroke increases, the time between each power stroke decreases, allowing for a more constant input of thrust and less impulse from any specific paddle. Organisms with only one set of paddles, like daphniids (Skipper et al., 2019) and juvenile *Artemia sp.* (Williams, 1994), have sharp periodic

speed graphs, corresponding to their power stroke. As the number of paddles in a stroke increases, these impulses occur more frequently, and should result in smoother swimming. *Americamysis bahia*'s more constant speed may be a result of not having a significantly long appendage, or having a greater number of paddles used in its metachronal stroke than euphausiids.

4.4.2 Nondimensional Characterization

The challenge of comparing variables across different metachronal designs highlights the need for nondimensional comparisons, which allow for generalizations about relationships to be made across different length scales. Table 4.2 summarizes important nondimensional parameters in crustaceans with different numbers of cycles per stroke, numbers of paddles per cycle, and Reynolds numbers.

There are two variants of the Reynolds number to consider when looking at metachronal motion. The first is the whole-body Reynolds number (Re_{BL}), calculated using the body length and the resulting swimming speed of the organism. The second variant is the Reynolds number of the pleopod (Re_{pleo}), calculated using the length of the pleopod (L_{pleo}) and the maximum speed of the pleopod tip during the power stroke (U_{pleo}), which can be estimated as

$$U_{pleo} = \pi f \theta_{rad} L_{pleo} \quad (4.2)$$

where f is the stroke frequency, and θ_{rad} is the stroke amplitude in radians. The whole-body Reynolds number for *A. bahia* is 170 ± 20 ($n = 13$), and the Reynolds number of the pleopods is 40 ± 3 ($n = 13$). There is a factor of roughly four difference between the pleopods and the body, firmly putting the pleopods in a drag-based regime. This nearly order-of-magnitude difference between pleopod and whole-body Reynolds number is consistent across other species.

The Strouhal number, defined as

$$St = \frac{f A_{\text{pleo}}}{V_{\text{BL}}} \quad (4.3)$$

where f is frequency, A_{pleo} is arc length of the flapping appendage estimated as $2L_{\text{pleo}}\sin(\text{amplitude}/2)$, and V_{BL} is the whole-body velocity, is a fluid dynamics parameter used to describe flow with an oscillating component. It represents the ratio of unsteady effects to inertial effects. At higher St , oscillations dominate in the flow, and at low St , the oscillations are swept by the moving fluid. Strouhal numbers between 0.2 and 0.4 result in the highest propulsive efficiency of a flapping airfoil (Triantafyllou et al., 1993), and this efficient Strouhal number range is observed in many organisms that flap or paddle (Taylor et al., 2003). The mean St for *A. bahia* is 0.5 ± 0.04 ($n = 13$, Table 4.2), which falls just outside of this efficient range.

In swimming fish, St varies with speed. At low speeds ($< 1BL/s$), Strouhal numbers are highly variable, and have been recorded as low as 0.1 and as high as 0.9. As speed increases, these values converge to the more efficient value of $St = 0.3$ (Saadat et al., 2017). This trend also exists in *A. bahia* (Figure 4.9). Although *A. bahia*'s mean St is greater than the optimal range 0.2-0.4, as its speed increases, its St decreases and falls into the efficient range at speeds above approximately $9BL/s$. *Americamysis bahia* pleopod motion appears tuned to achieve fast speeds.

The advance ratio, defined as

$$J = \frac{V_{\text{BL}}}{2\theta_{\text{rad}} f L_{\text{pleo}}} \quad (4.4)$$

where θ_{rad} is the stroke amplitude in radians, is another nondimensional measure of efficiency (Walker, 2002; Murphy et al., 2011). It is the ratio of the resulting body speed to appendage speed. For large advance ratios ($J > 1$), the organism moves at the same speed, or faster than its appendages. For small advance ratios, the appendages move quicker than

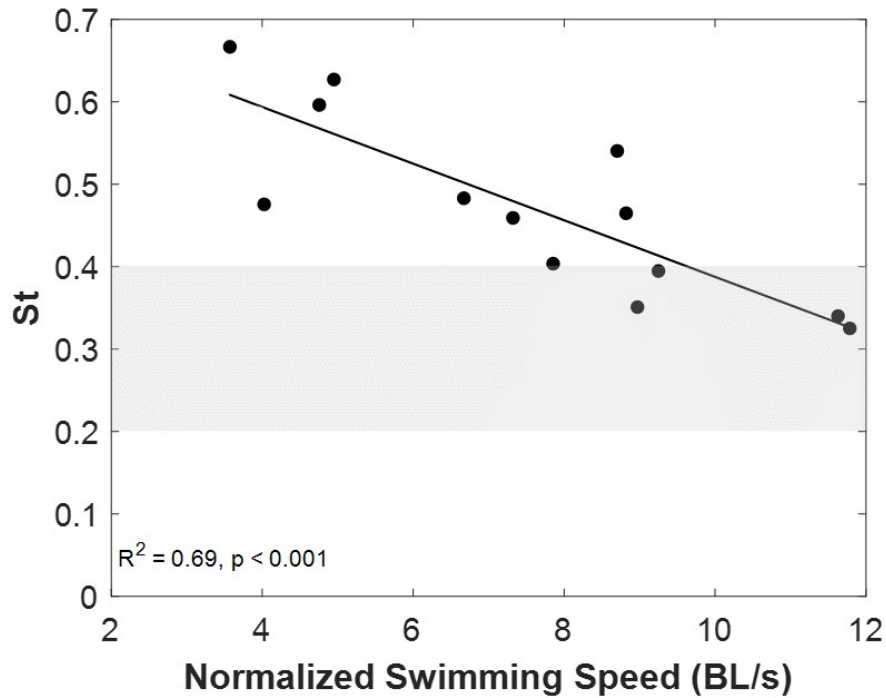


Figure 4.9: Strouhal number (St) decreases with normalized swimming speed for *A. bahia*. The shaded grey region highlights the efficient Strouhal number range of 0.2-0.4 as documented by Taylor et al. (2003)

the body.

Many organisms with one set of appendages have an advance ratio between 0.1 and 0.6 (Walker, 2002), indicating that the resulting speed of the body is less than that of the appendages. However, with multi-appendage swimmers, J is often greater than 1, indicating that the legs are moving at the same speed or slower than the body. If it is assumed that each paddle in a stroke equally contributes to the total thrust, advance ratios for multi-appendage swimmers can be normalized by the number of paddles in a metachronal stroke,

$$J_n = \frac{V_{BL}}{2\theta f L_{pleo} n_{pad}} \quad (4.5)$$

where n_{pad} = number of paddles, then J_n values for multi-appendage species are similar to the 0.1-0.6 range observed in organisms with one appendage (Walker, 2002; Murphy et al., 2011).

For *A. bahia*, J_n (0.09 ± 0.01 , $n = 13$) falls just outside the expected range of 0.1-0.6 (Table 4.2). The appendage tip is moving faster than the resulting body speed. However, J_n increases with swimming speed, and it reaches J_n of 0.1 at approximately 9BL/s (Figure 4.10). The other two-cycle mysid, *G. ingens*, also has an extremely low J_n of 0.02, and it swims at speeds less than 2BL/s (Table 4.2). Small J_n ratios at low speeds in mysids indicate that employing multiple metachronal cycles is relatively ineffective at low speeds. Together, trends with St , J_n , and swimming speed suggest that dual ipsilateral metachrony is effective at speeds greater than 9BL/s in *A. bahia*.

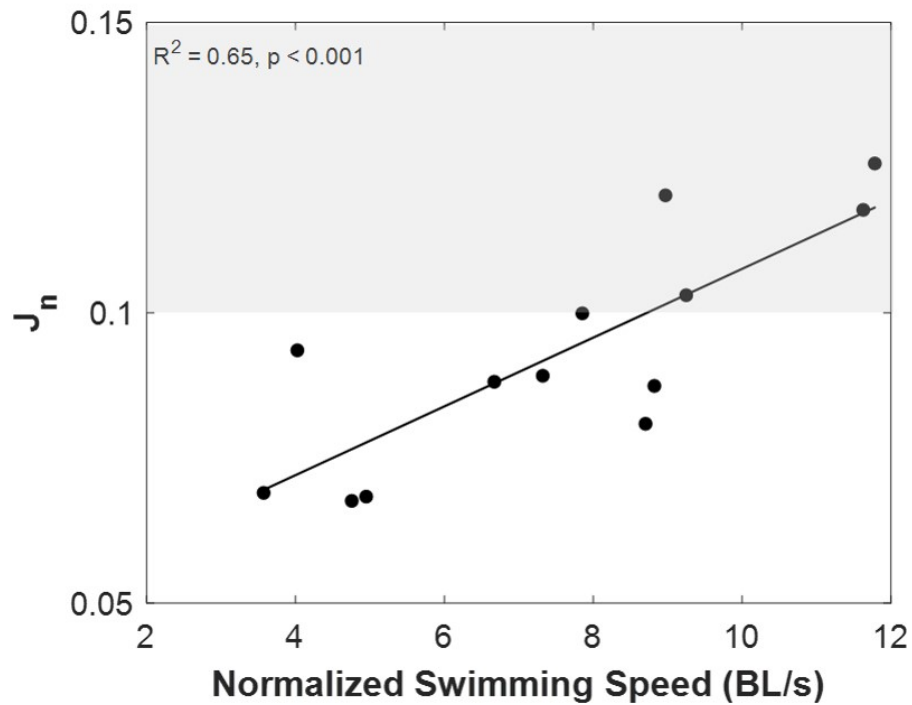


Figure 4.10: Normalized advance ratio (J_n) increases with normalized swimming speed for *A. bahia*. The shaded grey region highlights the expected range of J_n values for one-paddle swimmers of 0.1-0.6 as documented in Walker (2002).

4.4.3 When to Use Pleopods

Pleopod stroking results in fast forward swimming and in speeds greater than when the organism uses its thoracopods alone to swim. However, it remains unclear what acts as a cue for *A. bahia* to swim using its pleopods. All experiments were performed such that

Table 4.2: Metachronal characterization of four crustaceans. Re_{BL} and Re_{pleo} are variants of Equation 4.1, St is calculated from Equation 4.3, J is calculated from Equation 4.4, J_n from Equation 4.5. *Euphausia superba* data only includes fast forward swimming

Species	Contralateral Appendage Symmetry	Paddles per Cycle	BL (cm)	Swimming Speed (BL/s)	Stroke Frequency (Hz)	Re_{BL}	Re_{pleo}	St	J	J_n	Reference
<i>Americamysis bahia</i>	-	5	0.47±0.02	7.60±0.74	13.98±0.48	170±20	40±3	0.50±0.04	0.90±0.05	0.09±0.01	This paper
<i>Gnathopausia ingens</i>	-	13	6-12	0.7	3.12	2000	900	0.82	0.50	0.02	Hessler (1985) Cowles et al. (1986)
<i>Euphausia superba</i>	+	5	3.5±1.3	4.0	6.2±2.0	2000	800	0.50	1.1-1.5	0.2-0.3	Murphy et al. (2011)
<i>Odontodactylus havanensis</i>	+	5	3.5-6.4	20-40	17.00	50000	5000	0.2	2.1	0.4	Campos et al. (2012)

there was no stimulus exerted on the tank from the experimenter. It is possible that heating in the laboratory or ventilation may have provoked pleopod swimming, but this was not noticed. This study also cannot say how infrequent this behavior is. The estimate of 10% does not take into account the sex of the individuals recorded. In 2020, the experimental design was set up such that only recordings of pleopod utilization were captured. Additionally, *A. bahia* does not necessarily streamline itself to go faster, as has been observed in *E. superba* (Murphy et al., 2011), the body angles for thoracopod swimming and pleopod swimming do not differ. Pleopod swimming allows the organism to travel in the same direction that thoracopod swimming does, though it shows an insignificant bias to using its pleopods while diving.

CHAPTER 5
TRENDS IN STROKE KINEMATICS, REYNOLDS NUMBER, AND SWIMMING
MODE IN SHRIMP-LIKE ORGANISMS

5.1 Introduction

Motion within multi-appendage systems requires coordination between appendages to ensure they operate in optimal combinations to prevent collisions between limbs and minimize energy expenditure. Organization of the coordinated motion comes from different patterns of appendage sequencing. Metachrony is one such sequencing, where appendages beat in a time-delayed manner, resulting in a wave-like motion. Metachronal motion occurs at various length scales and can serve diverse functions in biological systems. For example, in lungs, cilia beat in a metachronal stroke, creating fluid transport along a membrane (Sanderson and Sleight, 1981; Chateau et al., 2018). Metachrony can also be used for propulsion in both terrestrial (millipedes: Garcia et al., 2021) and aquatic (ctenophores: Goebel et al., 2020, euphausiids: Kils, 1981, remipedes: Kohlhage and Yager, 2011, tomopteris: Daniels et al., 2021) organisms.

Metachronal propulsion is well-documented in shrimp-like organisms, owing to their abundance and relatively large size. These organisms share a similar body plan known as the caridoid facies (Hessler, 1983). Prominent features of the caridoid facies include a carapace around the thorax with thoracopods used for generating feeding currents and propulsion, and an elongated flexible abdomen with biramous pleopods (Hessler, 1983). Thoracopods and pleopods, depending on the species, can both be used for metachronal propulsion. Thoracic metachrony occurs in several mysid species (Hessler, 1983; Laverack et al., 1977; Schabes and Hamner, 1992), and pleopod metachrony has been documented in stomatopods (Campos et al., 2012; Ford et al., 2021; Garayev and Murphy, 2021), eu-

phausiids (Murphy et al., 2011; Murphy et al., 2013), and some mysids (Ruszczyk et al., 2021).

An organism's physical environment typically imposes design constraints on propulsion. Metachronal stroke kinematics are no exception and are subject to varying force balances in their environment. To represent the physical environment of an organism, the Reynolds number (Re) quantifies the relative strength of inertial to viscous forcing. The Reynolds number is defined as,

$$Re = \frac{UL}{\nu} \quad (5.1)$$

where U is the characteristic velocity, L is the characteristic length scale, and ν is the kinematic viscosity of the fluid. There is some evidence that Re affects the functioning of metachrony. Metachronal propulsion creates counter-rotating vortices resulting in a downward jet, and when similar stroke kinematics are performed at a smaller Re , the resulting jet is weaker with reduced vertical momentum compared to larger Re environments (Ford et al., 2019; Zhang et al., 2014; Granzier-Nakajima et al., 2020). Reynolds number can also affect morphological aspects of the metachronal stroke. For a given Re , there exists an optimal number of appendages and spacing between appendages that results in the greatest time-averaged fluid flux (Granzier-Nakajima et al., 2020; Ford and Santhanakrishnan, 2021a).

Euphausia superba kinematic analysis reveals how stroke kinematics, including stroke amplitude, pleopod beat frequency, and phase lag can vary to achieve different swimming modes including fast forward swimming (FF), hovering (HOV), and upside down swimming (USD) (Murphy et al., 2011). Phase lag in metachrony is defined as the time between sequential pleopod power strokes, normalized by the duration of the entire set of appendages to undergo one complete metachronal stroke. Swimming modes are visually differentiated first by krill orientation. USD occurs when the organism's body angle with the horizontal is greater than 90° , whereas HOV and FF both occur when the organism is in an upright orientation. HOV and FF are differentiable by the magnitude of their nor-

malized swim speed. HOV occurs at speeds less than 1 body length per second (BL/s) and FF occurs at speeds greater than 2 BL/s, with a transitional mode occurring between 1-2 BL/s. At speeds less than 2 BL/s, *E. superba*'s primary means of acceleration occurs by increasing stroke amplitude and at speeds greater than 2BL/s, after pleopods reach their maximum stroke amplitude, speed increases as a result of increasing beat frequency. For *E. superba*, FF requires a greater beat frequency and stroke amplitude than HOV, and while FF and USD utilize equal phase lags between sets of adjacent pleopods, HOV has unequal phase lag between pleopods (Murphy et al., 2011).

Analysis of swimming in shrimp-like organisms is multifaceted, requiring three different components to be evaluated when considering system design: stroke kinematics, Re , and the resulting swimming mode. To begin to describe this relationship, the current study undertakes two tasks. First, *E. pacifica* stroke kinematics are quantified. Using these data, a novel way to differentiate between HOV and FF is implemented, where the fitted inflection points of a Gompertz function to amplitude and beat frequency against normalized swimming speed are considered when determining the speed where the krill changes its means of increasing speed from increasing stroke amplitude to increasing beat frequency. Trends originally observed in *E. superba* will be applicable to *E. pacifica* when differentiating swimming modes. FF will have a greater beat frequency and stroke amplitude than HOV, and phase lag will vary between swimming modes. Second, *E. pacifica* stroke kinematics are used in tandem with several other 5-paddle, shrimp-like, metachronal swimmers to identify any large-scale trends between stroke kinematics, swimming mode, and Re . Regardless of species, similar swimming modes will have similar trends in stroke kinematics. FF will require greater beat frequency and stroke amplitudes than HOV, and phase lag will vary between swimming modes. Additionally, regardless of species, increasing stroke kinematics should increase Re , as beat frequency, stroke amplitude, and phase lag all affect the swimming speed of the organism.

5.2 Methodology

5.2.1 Animal Collection and Maintenance

Euphausia pacifica were collected off the coast of Newport, OR in July and September of 2019. Organisms were collected, stored in 2L Nalgene bottles at a density of approximately 5ind/L, and shipped overnight in a cooler filled with ice packs to maintain a cooler temperature to Georgia Institute of Technology (Atlanta, GA). Upon arrival, bottles were opened and allowed to aerate. Bottles were 15°C upon arrival. Recording began immediately upon arrival.

5.2.2 Recording

Ten randomly selected *E. pacifica* were transferred to a 12cm x 12cm x 13cm tank filled with 1L of water. Water obtained from the krill shipment containers was passed through a Pall A/E glass fiber filter (1 μ -pore size) before being used in the experiments, which allowed experimental water to match the organism's habitat.

Two high speed digital cameras (AOS PRI-X and AOS PRI-S; AOS Technologies AG, Baden-Daettwil, Switzerland) were orthogonally-positioned to view free-swimming krill in the experimental tank. Cameras were each equipped with an AF Micro-Nikkor 60mm f/2.8D lens, and recorded at 500fps. Each camera was illuminated with an 850nm dual voltage IR light (Super Circuits, Austin TX) positioned directly in front of each camera on the opposite side of the tank, backlighting the organisms. Illumination in the near-IR wavelengths is critical to minimize the phototactic response of the krill while providing enough light for image capture. Prior to the organisms' recording, a 1mm calibration wand was placed in the center of the tank and imaged to allow for pixel to mm conversion in the digital images. Both cameras were focused on the location of the calibration wand to ensure they recorded the same region, which resulted in an active volume of 3.5cm × 3.5cm × 2.5cm. The calibration wand was removed and organisms were allowed a 30min

acclimation period in an undisturbed tank before recording began.

During recording, events were captured by manually triggering the cameras to record when an organism swam within the field of view of both cameras. The triggering action resulted in capturing the previous 1000 buffered frames and recording the next 1000 frames. Recording sessions lasted 2hrs or until *E. pacifica* specimens became lethargic and passes between the cameras were more than 30min apart. Lethargy was attributed to temperature increase in the experimental tank, as the cameras recorded in a 20°C environment, rather than the 15°C water krill were previously housed in. Each block yielded approximately 15 passes to choose one recording of each swimming mode for further analysis, ensuring independent sampling within swimming mode. Image sequences were chosen such that there were roughly 10 qualitative examples of each of the three types of swimming mode specified in Murphy et al. (2011) observed in *E. superba* (i.e., FF, HOV, and USD), resulting in 30 total passes analyzed (Table 5.1).

5.2.3 Image Analysis

Krill body positions in the recordings were quantified using the DLTdv5 software for MATLAB (Hedrick, 2008). The organism's head, 6th abdominal segment, and telson were tracked on both cameras. The organism's body length (BL) was measured from the eye to the base of the telson. Pleopods were labelled such that P1 was the anterior-most and P5 was the posterior-most. For each set of pleopods, three key locations were tracked: where the pleopod attached to the body, the joint between the protopodite and the exo- and endopodites, and the tip of the pleopod. From this data set, body angle (BA) is defined as the angle of the organism relative to horizontal, α is the angle of the pleopod orientation relative to the body (which varied throughout the stroke period), and β is the bending angle of the pleopod joint (which varied throughout the stroke period). The complete digital quantification of the krill, including 18 points, BL, α , and β is shown in Figure 5.1.

Stroke angles α and β were calculated for each pleopod for each recording following the

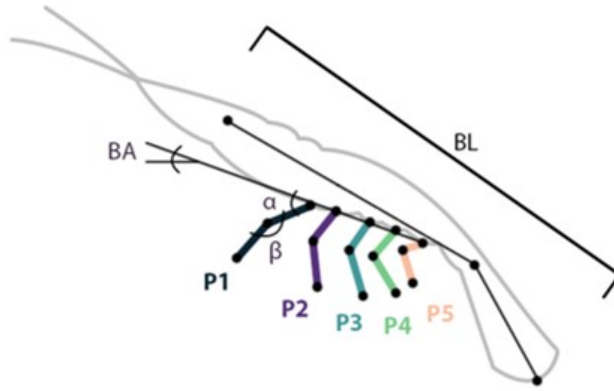


Figure 5.1: Digitization and angle definitions for *E. pacifica*. Pleopods are numbered from anterior (P1) to posterior (P5). Body length (BL) is measured from the head to the base of the telson. Solid black points represent the 18 points identified during digitization of krill position. The angle between the pleopod and the body (α), the angle between the protopodite and the exopodite (β), and the body angle of the organism relative to the horizontal (BA), are depicted on the schematic. Angles α and β , calculated for all five pleopods, are depicted only on P1 for simplicity.

method outlined in Murphy et al. (2011). A stroke began with the initiation of a downward P5 power stroke, and ended when P5 began its next stroke. The time series of stroke angles were transformed such that the initiation of the P5 power stroke occurred at $t = 0$ s. A cubic spline function was fit to each pleopod stroke angle and 100 equally spaced points were calculated based on the fitted function. Occasionally, there were multiple metachronal strokes within a recording. In these instances, strokes were analyzed separately before being combined. The mean stroke period was calculated for that recording, and α and β curves for each stroke were transformed to match the duration of that mean stroke period. Stroke angles within a recording were then averaged at each time point resulting in one representative α and β curve for each pleopod.

Swimming modes of *E. pacifica* were identified based on BA and normalized swimming speed. An observation was categorized as USD if BA was greater than 90° , regardless of swimming speed. HOV and FF were differentiated for upright organism observations based on normalized swimming speed. To determine the swimming speed where *E. pacifica*

transitions between HOV and FF, a 4-point Gompertz function,

$$y = a + (b - a) * -exp[-c(x - d)] \quad (5.2)$$

where a = lower asymptote, b = upper asymptote, c = growth rate, and d = inflection point (Gompertz, 1825), was fit to amplitude as a function of normalized swim speed and beat frequency as a function of normalized swim speed. The Gompertz fit has been used in ecology to model population growth (Yu et al., 2007) and survivorship (Sas et al., 2012), and recently in chemical engineering to model breakthrough curves (Chu, 2020), highlighting the versatility of the function. In the current study, the inflection point for each fitted function were considered when determining the speed to differentiate between HOV and FF.

5.2.4 Across-Species Data Formatting

Stroke kinematics for shrimp-like organisms were analyzed to determine any large-scale trends in swimming mode and whole-body Re (Re_{BL}). Data included in the analysis were required to be for free-swimming organisms featuring the caridoid facies body plan using 5 pleopods in their metachronal stroke. Publications featuring stroke kinematics of metachony in shrimp-like organisms were reviewed for beat frequency, stroke amplitude, phase lag, and basic morphology. If raw data were available in supplementary information, independent samples were analyzed separately. If raw data were unavailable, then kinematic data were extracted from figures displaying stroke amplitude curves for each pleopod by employing the graphreader.com (2021) application, resulting in one representative data point for that publication. Data for frequency, BL , and swimming speed were taken as mean values reported in the literature. Whole-body Re was calculated using the organism's BL and average swimming speed. Swimming mode was determined to be FF, HOV, or USD based on the published kinematics for each species. The final data set consisted of 73

observations across 6 species (Table 5.1).

Table 5.1: Sample count and source data included in the across-species comparison

Species	n			Reference
	FF	HOV	USD	
<i>Americamysis bahia</i>	13	0	0	Ruszczuk et al. (2021)
<i>Euphausia pacifica</i>	12	8	10	Current paper
<i>Euphausia superba</i>	8	6	5	Murphy et al. (2011)
<i>Neogonodactylus bredini</i>	4	0	0	Ford et al. (2021)
<i>Odontodactylus havanensis</i>	4	1	0	Campos et al. (2012), Campos unpublished
<i>Odontodactylus scyllarus</i>	1	1	0	Garayev and Murphy (2021)

5.2.5 Statistical Analysis

Beat frequency and phase lag were compared between *E. pacifica* swimming modes using parametric ANOVAs and Tukey’s honestly significant different tests and nonparametric Kruskal-Wallis (KW) and Steel-Dwass all-pairs (SDAP) tests when applicable. Normality was assessed using Anderson-Darling tests and equal variance using Levene’s tests. Comparisons of pleopod length and phase lag were blocked by individual for ANOVAs and KWs. Stroke amplitude, measured in degrees, is subject to periodicity, favoring analysis via circular statistics, rather than traditional linear statistics (Fisher, 1993). Data were subject to a Watson goodness of fit test to verify they followed a von Mises distribution, and concentration parameters (κ) were compared between groups to verify κ s were greater than 1 and approximately equal between groups. With these assumptions met, Watson-Williams test of homogeneity of means was used to compare pleopod stroke angles within and between each swimming mode. Two-sample Watson-Williams tests were used during posthoc analysis of stroke amplitude to identify significant differences.

Principle component analysis (PCA) was performed on the across-species dataset to investigate how stroke kinematics and Re_{BL} vary across species resulting in similar swimming modes. PCA is an exploratory data reduction technique for multivariate data sets, used to visualize relationships between variables that might otherwise go unnoticed. Stroke kinematics quantifying metachrony, including frequency, amplitude, and phase lag, and re-

sulting Re_{BL} were used to determine how these factors vary with swimming mode. PCA requires all variables have linear relationships. For this reason, $\log(Re_{BL})$ was used rather than the untransformed Re_{BL} , which varied over several orders of magnitude. Frequency, amplitude, phase lag, and $\log(Re_{BL})$ were all mean-centered and standardized prior to PCA analysis. A Kaiser-Meyer-Olkin (KMO) measure of sampling adequacy was used to verify that the size of the data set was large enough for reduction, Bartlett's test of sphericity was performed to verify the data set was suitable for data reduction, and robust PCA outliers analysis was performed to identify any outliers in the dataset. KMO represents the amount of variance within a data set that may be attributed to other variables. KMO ranges from 0 to 1 with a greater KMO value representing fewer partial correlations in the data set, and a minimum value of 0.5 being deemed usable (Kaiser, 1974). To assess how stroke kinematics vary with Re_{BL} , kinematic variables for each behavior were regressed against $\log(Re_{BL})$.

Statistical analysis for *E. pacifica*, multivariate correlations, outlier analysis, PCA, and linear regressions were performed in JMP Pro 16.0.0 (SAS Institute, Inc., Cary, NC). KMO, Bartlett's test, and *E. pacifica* stroke amplitude analysis were performed in R 4.1.1 and RStudio 1.4.1717 (RStudio Team, Boston, MA). Circular statistics were performed using the package "circular" for R (Agostinelli and Lund, 2022). All data are presented as mean \pm standard error.

5.3 Results

5.3.1 *Euphausia pacifica* Kinematics

Euphausia pacifica morphological design, including pleopod length, protopodite, and exo- and endopodite length is reported in Table 5.2. Pleopod length varies with pleopod position, with P2 being greater than P4, and P5 being significantly shorter than all other appendages [ANOVA, $n = 150$, $F(4,145) = 5.16$, $p < 0.001$, Table A.3]. The mean gap length between pleopods normalized by pleopod length (G/L) is 0.59 ± 0.01 .

Table 5.2: *Euphausia pacifica* pleopod segment lengths (mean±SE); n = 30

	P1	P2	P3	P4	P5
Protopodite (mm)	0.95±0.03	0.95±0.03	0.90±0.03	0.86±0.03	0.70±0.03
Exopodite (mm)	0.83±0.04	0.86±0.04	0.88±0.04	0.86±0.04	0.75±0.03
Total (mm)	1.78±0.07	1.80±0.07	1.78±0.07	1.72±0.07	1.44±0.06

A 4-point Gompertz function (Equation 5.2) was fit to frequency and amplitude against normalized swimming speed (Figure 5.2) for the inflection point to be considered as a metric of differentiating between HOV and FF. The inflection point for the fitted function for frequency occurs at 3.04BL/s ($p < 0.0001$, $R^2 = 0.67$), and the inflection point for the fitted function for pleopod amplitude occurs at 1.48BL/s ($p < 0.01$, $R^2 = 0.69$). Based on these data, the value of 2BL/s was used to differentiate between FF and HOV as a representative value between the identified inflection points, and to match the value used in Murphy et al. (2011) for *E. superba*, resulting in a final distribution of $n_{\text{HOV}} = 8$, $n_{\text{FF}} = 12$, and $n_{\text{USD}} = 10$.

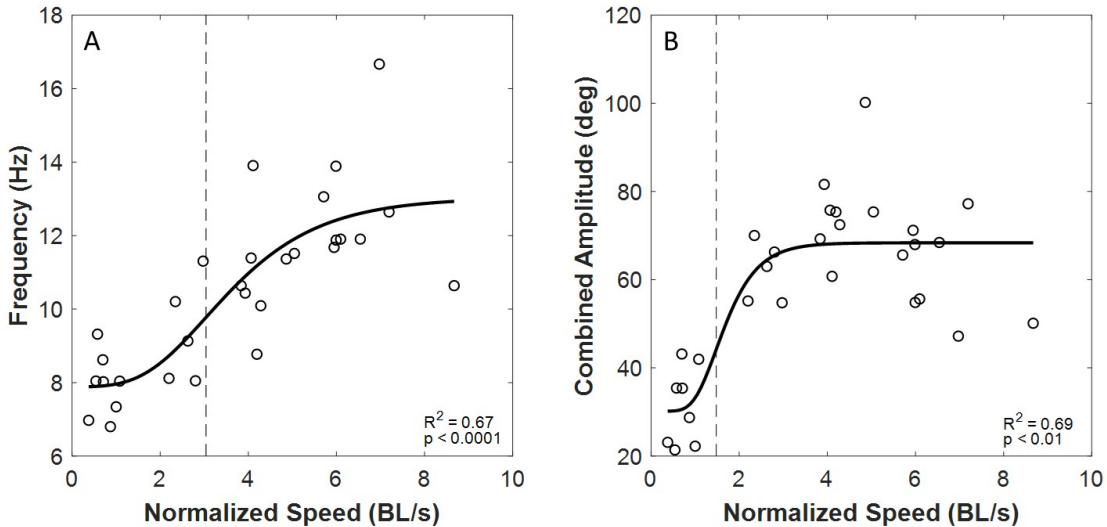


Figure 5.2: Four-point logistic fit of *E. pacifica* kinematics to normalized swimming speed. Logistic fit of (A) frequency and (B) combined amplitude, α , to normalized swim speed. The dashed vertical line in each panel is located at the inflection point for the fitted curve. The inflection point occurs at 3.04BL/s for the frequency curve and at 1.48BL/s for the amplitude curve.

The stroke angle time series for each pleopod is delayed in time relative to its neigh-

bor, forming a metachronal stroke for each swimming mode (Figure 5.3). Each complete stroke begins with the initiation of a P5 power stroke, followed by P4, and continues anteriorly along the organism’s body. Power strokes for any pleopod occur when α increases. Beat frequency varies with swimming mode [$F(2,27) = 13.20$, $p < 0.001$], with HOV ($7.9 \pm 0.3 \text{ Hz}$) having a significantly smaller beat frequency than FF ($11.9 \pm 0.6 \text{ Hz}$) and USD ($10.6 \pm 0.6 \text{ Hz}$) ($p_{\text{FF-HOV}} < 0.0001$, $p_{\text{USD-HOV}} = 0.01$, $p_{\text{FF-USD}} = 0.20$).

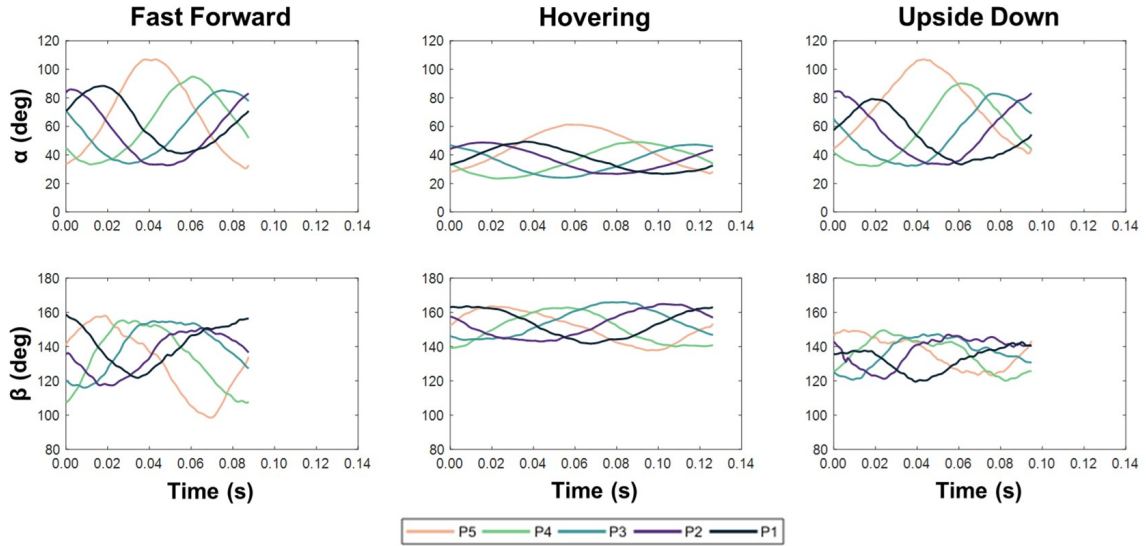


Figure 5.3: Stroke angles for three swimming modes. Stroke angles α and β for fast forward swimming ($n = 12$), hovering ($n = 8$), and upside down swimming ($n = 10$) for one time-standardized stroke. Individual samples were combined for each pleopod (following the method in Murphy et al. (2011)). The angle time records are colored by pleopod.

Pleopod stroke amplitude varies within swimming mode (Figure 5.4). Within FF, P5 has the greatest amplitude out of all appendages [$F(4,55) = 5.24$, $p < 0.01$, Table A.4]. All pleopod amplitudes are statistically similar within HOV and USD [$F_{\text{HOV}}(4,35) = 2.44$, $p_{\text{HOV}} = 0.06$, $F_{\text{USD}}(4,45) = 1.23$, $p_{\text{USD}} = 0.31$]. Pleopod stroke amplitude also varies between swimming modes. FF and USD stroke amplitudes are consistently greater than HOV [$F_{\text{P1}}(2,27) = 12.81$, $p_{\text{P1}} < 0.001$, $F_{\text{P2}}(2,27) = 18.96$, $p_{\text{P2}} < 0.001$, $F_{\text{P3}}(2,27) = 34.70$, $p_{\text{P3}} < 0.001$, $F_{\text{P4}}(2,27) = 21.02$, $p_{\text{P4}} < 0.001$, $F_{\text{P5}}(2,27) = 17.92$, $p_{\text{P5}} < 0.001$, Table A.5].

Phase lag varies among pleopod pairs and differs between swimming modes (Figure 5.5). For FF, P1-P5 phase lag is greater than P5-P4 lag, P4-P3 lag, and P2-P1 lag ($F =$

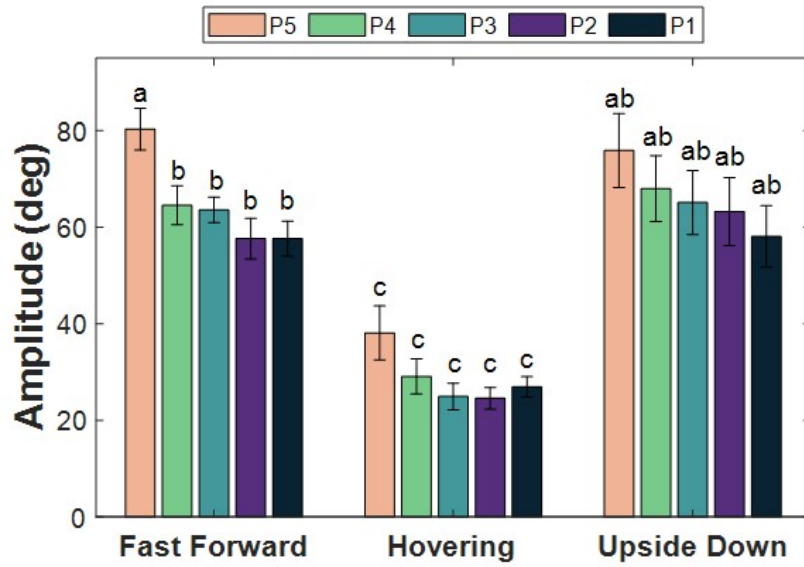


Figure 5.4: Stroke amplitude for three swimming modes (Mean±SE). Significantly similar stroke amplitudes are denoted with letters. The only swimming mode with significantly different stroke amplitudes between pleopods is FF. USD has similar stroke amplitudes to FF across all five pleopods. HOV stroke amplitudes are significantly lower than both FF and USD.

6.23, $p < 0.001$, Table A.6). For HOV and USD, there are no differences between phase lags within each mode ($F_{\text{HOV}} = 0.29$, $p_{\text{HOV}} = 0.89$, $F_{\text{USD}} = 1.85$, $p_{\text{USD}} = 0.14$). Additionally, for HOV and USD, the mean phase lag for each interlimb combination is not significantly different than the ideal 0.2 phase lag for perfect metachrony in a 5-paddle system [$t_{\text{HOV}(39)} = -0.47$, $p_{\text{HOV}} = 0.64$, $t_{\text{USD}(49)} = -0.69$, $p_{\text{USD}} = 0.49$].

5.3.2 Metachrony in Caridoid Facies

Analysis of metachrony in caridoid facies organisms spanned 6 species, 4 orders of Re_{BL} magnitude, and 3 swimming modes. Of the 73 points, $n_{\text{FF}} = 42$, $n_{\text{HOV}} = 16$, and $n_{\text{USD}} = 15$ (Table 5.1). To reduce dimensionality for the PCA, phase lag data in these organisms were further consolidated. Phase lag variables were divided into two classifications. Within-cycle phase lag comprises all appendages that are immediately adjacent to each other (i.e., P5-P4, P4-P3, P3-P2, and P2-P1), and between-cycle phase lag represents the lag

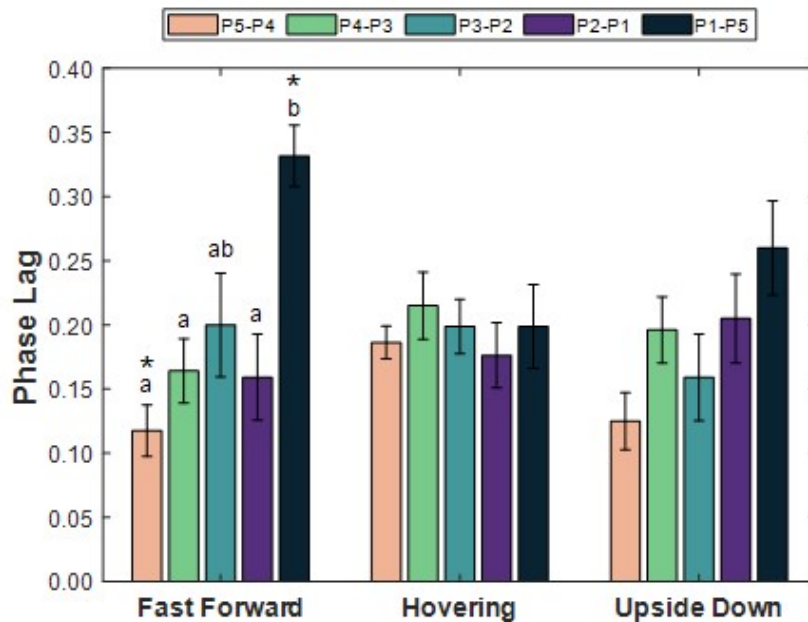


Figure 5.5: Phase lag for three swimming modes (Mean \pm SE). The only swimming mode with significantly different inter-limb phase lags is fast forward swimming. Significant groupings are denoted with letters. All inter-limb phase lags for hovering and upside down swimming are not different from each other. For all three modes, inter-limb phase lags that are significantly different than the expected 0.20 are denoted with an asterisk.

between consecutive cycles (i.e., P1-P5). The KMO on frequency, amplitude, $\log(\text{Re}_{\text{BL}})$, and between-cycle lag (KMO = 0.56) was greater than the KMO on frequency, amplitude, $\log(\text{Re}_{\text{BL}})$ and within-cycle lag (KMO = 0.49), directing the use of between-cycle lag in the PCA. Bartlett's test confirmed this data set was suitable for data reduction [$\chi^2(6) = 93.73$, $p < 0.0001$], and there were no outliers.

PCA performed on frequency, amplitude, between-cycle phase lag, and $\log(\text{Re}_{\text{BL}})$ explained 82.4% of the variance in the data set (Figure 5.6). The PCA found minor separation between the three swimming modes. Separation occurred primarily along principle component 1 (PC1), with similar positive loadings for all four variables. FF and HOV are clustered on opposite sides of PC1, while USD overlaps both regions. There is no discernable clustering by mode along PC2.

To further explain PCA results, the kinematics variables demonstrated differences across

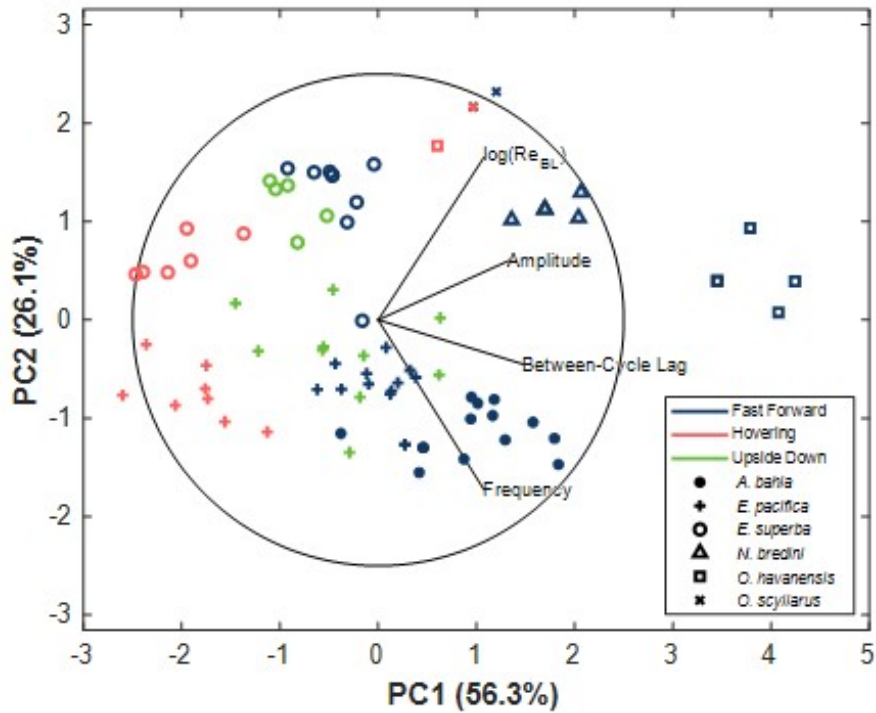


Figure 5.6: PCA of stroke kinematics in free-swimming shrimp-like crustaceans. Eigenvectors of the PCA are superimposed on the figure. Symbol color indicates the recorded swimming mode and symbol shape indicates the species. The first two PCs capture 82.4% of the overall variance in the data set. All variables were mean-centered and standardized by SD prior to analysis.

swimming mode. Frequency is the greatest in FF, is less in USD, and is lowest in HOV (SDAP; $p_{FF-USD} = 0.05$, $p_{FF-HOV} < 0.0001$, $p_{HOV-USD} = 0.03$). Amplitude is greater in FF in USD and HOV (SDAP; $p_{FF-HOV} < 0.0001$, $p_{FF-USD} = 0.01$, $p_{HOV-USD} = 0.05$). Between-cycle phase lag is greater in FF than in USD and HOV (SDAP; $p_{FF-HOV} < 0.001$, $p_{FF-USD} < 0.01$, $p_{HOV-USD} = 0.47$). $\log(\text{Re}_{BL})$ is greater in FF and USD than in HOV (SDAP; $p_{FF-HOV} < 0.01$, $p_{FF-USD} = 1.00$, $p_{HOV-USD} < 0.01$) (Figure 5.7).

The resulting PCA was also grouped according to species, which resulted in more clear clustering than swimming mode (Figure 5.6). Euphausiids, *E. pacifica* and *E. superba*, had negative loadings on PC1 compared to stomatopods, *N. bredini*, *O. havanensis*, and *O. scyllarus*, indicating smaller frequencies, amplitudes, $\log(\text{Re}_{BL})$, and between-cycle phase lags in euphausiids than stomatopods (Figure 5.8). *Euphausia pacifica* and *E. superba*

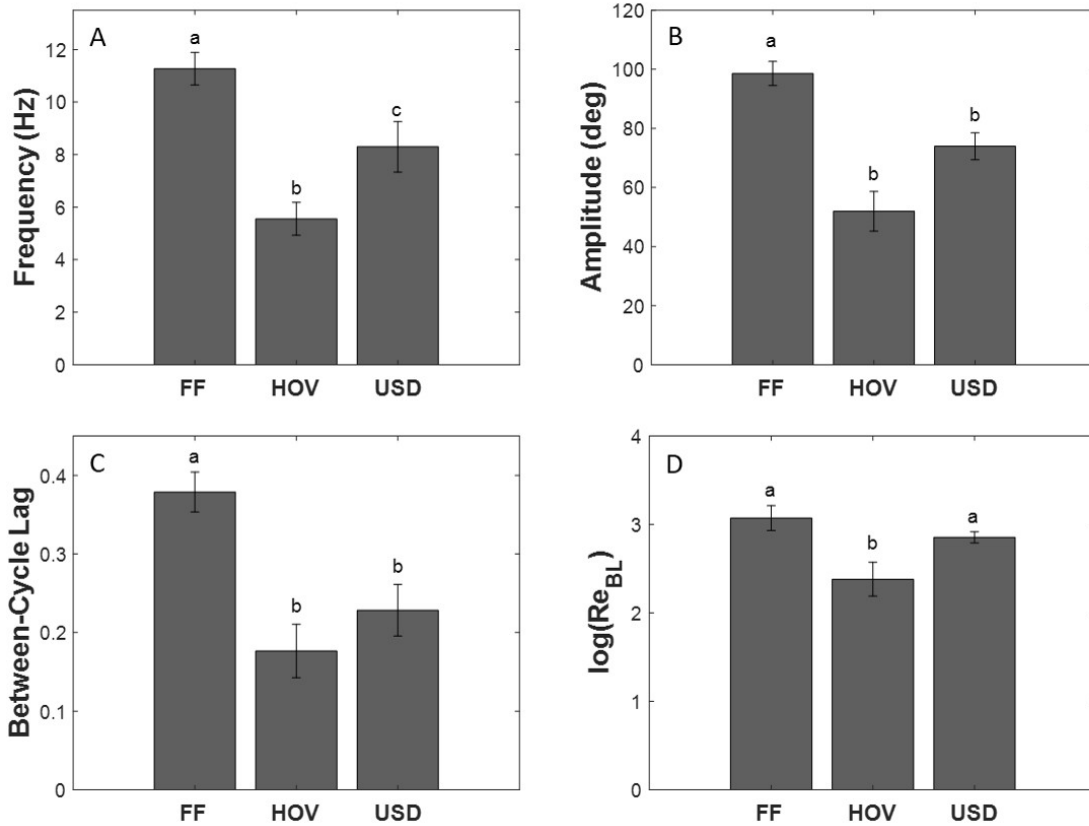


Figure 5.7: Metachronal stroke kinematics and Re_{BL} in swimming modes (Mean \pm SE). (A) Frequency, (B) amplitude, (C) between-cycle phase lag, and (D) the logarithm of the whole-body Reynolds number (Re_{BL}) for FF, HOV, and USD. Significantly similar groups within each figure are noted with letters. Between-cycle phase lag is defined as the time period lag between consecutive cycles (P1-P5) divided by the total cycle period.

also separate out over PC2, where variability is mainly driven by $\log(Re_{BL})$ and frequency, indicating that *E. pacifica* operates with a greater beat frequency and a smaller Re_{BL} than *E. superba* (Figure 5.8).

5.4 Discussion

5.4.1 Metachrony in *E. pacifica*

Organisms adapt different gaits, or patterns of limb movement, to minimize energy expenditure (Hoyt and Taylor, 1981) and limb stress (Biewener, 1990; Fusuoka et al., 2015) while increasing speed (Alexander, 1989). The term “gait” is often used for terrestrial

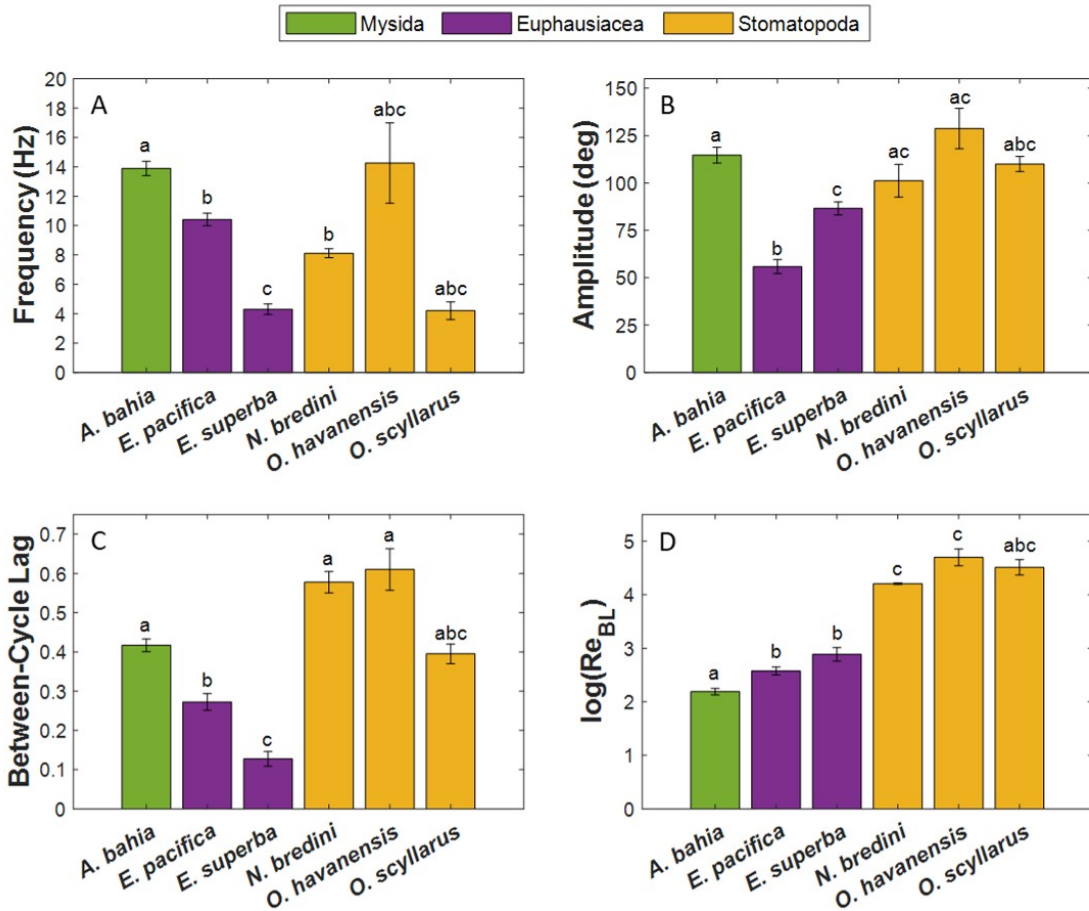


Figure 5.8: Metachronal stroke kinematics and Re_{BL} in shrimp-like organisms (Mean \pm SE). (A) Frequency, (B) amplitude, (C) between-cycle phase lag, and (D) the logarithm of the whole-body Reynolds number (Re_{BL}) for *A. bahia*, *E. pacifica*, *E. superba*, *N. bredini*, *O. havanensis*, and *O. scyllarus*. Bars are colored based on lowest taxonomic order. Between-cycle phase lag is defined as the time period lag between consecutive cycles (P1-P5) divided by the total cycle period.

organisms but sees inconsistent usage when discussing aquatic propulsion. This may be because aquatic propulsion studies are dominated by fish, which primarily swim by undulating their bodies rather than altering limb synchrony. “Gait” and “swimming mode” are used interchangeably when describing aquatic propulsion, although “gait” more often refers to differentiation based on a change in the relative usage of pectoral and caudal fins, while swimming mode refers to differentiation based on resulting swimming speed (Blake, 2004). Because swimming speed is used to differentiate between HOV and FF instead of phase lag patterns, “swimming mode” is more applicable to describe the different swim-

ming patterns in euphausiids.

To quantitatively determine the transition speed where *E. pacifica* sees greater influence on speed from increasing amplitude to increasing frequency, the inflection point from a 4-point Gompertz function fitted to amplitude versus normalized swimming speed and frequency versus normalized swimming speed was considered. The inflection point occurs where the respective kinematic increases most rapidly, visible as the steepest portion of the curve. Following the hypothesis that speed increases by increasing stroke amplitude for HOV and by increasing beat frequency for FF, then the function should be steepest for amplitude when the organism is performing HOV and steepest for frequency when the organism is performing FF. Indeed, the inflection point when fitting amplitude to normalized swimming speed occurs at 1.48BL/s, which matches the range of speed quantifying HOV in *E. superba*, and the inflection point when fitting frequency to normalized swim speed occurs at 3.04BL/s, which matches FF in *E. superba* (Murphy et al., 2011). Therefore, 2BL/s was chosen in *E. pacifica* to differentiate between HOV and FF, consistent with *E. superba*.

The three swimming modes in euphausiids serve different ecological functions. HOV allows negatively buoyant organisms to maintain their position in the water column. FF enables an organism to chase prey, find mates, and escape predation. Faster swimming results in a more energetic wake disturbance with greater fluid velocity (Ford and Santhanakrishnan, 2021b), which can be costly for the krill, making them more visible to predators that sense hydrodynamic features. USD can be a means of feeding, repositioning the organism so it can obtain phytoplankton located above it. This can be seen in *E. superba* feeding on sea ice macroalgae (Stretch et al., 1988). Additionally, some krill species mat, where dense aggregations of krill will lay upside down as a phototactic response to a greater light intensity reflected off substrate particles compared to direct sunlight (O'Brien et al., 1986).

Euphausia pacifica and *E. superba* achieve similar normalized swimming speeds. *Euphausia pacifica* reach speeds up to 7.2BL/s, and *E. superba* reach speeds up to 6.9BL/s

(Murphy et al., 2011). However, these top speeds are reached through a different combination of kinematic parameters. For FF, *E. pacifica* has a greater beat frequency (11.9 ± 0.6 Hz vs. 5.7 ± 0.5 Hz, respectively) and a smaller stroke amplitude ($65.5 \pm 2.9^\circ$ vs. $99.0 \pm 2.5^\circ$, respectively) than *E. superba*. In fact, *E. pacifica* consistently have a greater frequency and smaller stroke amplitude than *E. superba* for all three swimming modes (HOV: 7.9 ± 0.3 Hz vs. 3.0 ± 0.1 Hz, and $28.7 \pm 3.0^\circ$ vs. $67.3 \pm 2.1^\circ$. USD: 10.6 ± 0.6 Hz vs. 3.7 ± 0.4 Hz, and $66.1 \pm 5.2^\circ$ vs. $89.6 \pm 2.5^\circ$).

Differences in kinematic parameters may be attributed to different morphological designs between these two species. *E. pacifica* has a greater G/L than *E. superba* (0.6 ± 0.01 vs. 0.3 ± 0.04 , respectively), indicating that *E. pacifica*'s pleopods are spaced farther apart than *E. superba*'s. Traditionally, an organism with more closely-spaced appendages and a smaller G/L should have a smaller stroke amplitude due to the potential for appendages to collide in a metachronal stroke (Ford and Santhanakrishnan, 2021a). *Euphausia superba* has a smaller G/L than *E. pacifica* yet uses greater stroke amplitudes. *Euphausia superba* may achieve this by beating their pleopods in slightly different stroke planes allowing for spatial separation between appendages. This technique is observed in mysid shrimp, where 8 thoracic appendages comprise a metachronal stroke (Schabes and Hamner, 1992).

5.4.2 Metachrony in Caridoid Facies

Kinematics and Swimming Mode

Swimming modes separated out primarily along PC1 in the PCA, with no visible separation along PC2. Frequency, amplitude, between-cycle lag, and $\log(\text{Re}_{\text{BL}})$ had similar weights in the calculation of PC1. Therefore, all four variables can be used to predict the resulting swimming mode of the organism. This is because swimming modes are differentiated using the resulting swimming speed of the organism. Whole-body Re is calculated using the swimming speed, and swimming speed is dependent on beat frequency (Murphy et al., 2011), stroke amplitude (Murphy et al., 2011; Ford et al., 2021), and phase lag (Ford and

Santhanakrishnan, 2021a; Ford and Santhanakrishnan, 2021b). Increasing or optimizing these factors results in increased swimming speed, and while not directly included in the PCA, the importance of swim speed in characterizing swimming mode is evident.

Kinematics and Order

In addition to clustering by swimming mode, the PCA shows strong clustering based on taxonomic order. There is separation along PC1, primarily between euphausiids and stomatopods. The stomatopods form the main clustering on the positive PC1 axis and have greater swimming speeds than euphausiids. *Americamysis bahia* also lies on the positive PC1 axis with stomatopods. This results from the between-cycle lag in *A. bahia* being more similar to stomatopods than euphausiids.

Increased between-cycle phase lag can take two forms, which can have opposite effects on the smoothness of swimming. It can represent a 5-paddle metachronal stroke becoming more synchronous, as observed in stomatopods, or a time delay between multiple concurrent metachronal cycles, as observed in *A. bahia*. Stomatopods employ a fast start swimming motion, reaching speeds up to 40BL/s (Campos et al., 2012). This technique favors hybrid metachrony, allowing for greater stroke amplitudes that generate more thrust (Ford et al., 2021). Fast start swimming mimics a synchronous stroke, in that it allows for a large increase in speed. However, much of the speed gained during the power strokes is lost during the recovery strokes, resulting in an unsteady speed profile (Alben et al., 2010). In contrast, *A. bahia*'s pleopods on the same abdominal segment operate independently of each other, resulting in two concurrent metachronal cycles (Ruszczyk et al., 2021). Although *A. bahia* has 10 paddles in its metachronal stroke, its stroke is comprised of two, 5-paddle metachronal cycles, one on the left side and one on the right side of the body. The extended P1-P5 phase lag in *A. bahia* occurs in each cycle at the time when the opposite cycle is initiating its set of power strokes. Because there is always one pleopod undergoing a power stroke, rather than a large delay where the pleopods are all undergoing recovery

strokes, *A. bahia* has a smoother speed profile than a hybrid metachronal stroke (Ruszczyk et al., 2021).

The species distribution shows clear separation along PC2 in the PCA, which contrasts with swimming mode discussed above. Separation along PC2 comes from two main factors. A negative value indicates greater beat frequency and a positive value indicates a greater $\log(\text{Re}_{\text{BL}})$. The difference between *A. bahia* and the stomatopods is evident along PC2. Although they have similar trends with phase lag, *A. bahia* has a much smaller Re_{BL} than stomatopods. The primary separation between the two euphausiid species also occurs along PC2, and indeed, *E. superba* has both greater Re_{BL} and smaller beat frequency than *E. pacifica*.

Stroke Kinematics and Re_{BL}

By neglecting the fact that species plays a role in the stroke kinematics required to achieve different swimming modes, it is possible to compare how Re_{BL} changes with stroke kinematics to achieve similar swimming modes. For all three swimming modes, Re_{BL} does not change with increasing beat frequency (Figure 5.9A). This result at first appears surprising, as increasing beat frequency increases swimming speed (Murphy et al., 2011; Goebel et al., 2020; Ruszczyk et al., 2021), which should result in a greater Re_{BL} . However, Re_{BL} remains constant across species because beat frequency is inversely related to size (Figure 5.10), which indicates scalability constraints to metachronal stroke kinematics.

Whole-body Re increases with stroke amplitude for HOV, but does not for FF or USD (Figure 5.9B). In FF, organisms are already operating near their maximum stroke amplitude, which is naturally restricted to 180° . HOV features a wide range of obtainable amplitudes, and as stroke amplitude increases, Re_{BL} increases. Increasing stroke amplitude results in a more powerful fluid jet to support an organism in the water column. A larger organism requires a stronger fluid jet flow to produce thrust to counterbalance their weight. Stomatopods require a stronger jet to maintain their position, and therefore a greater HOV

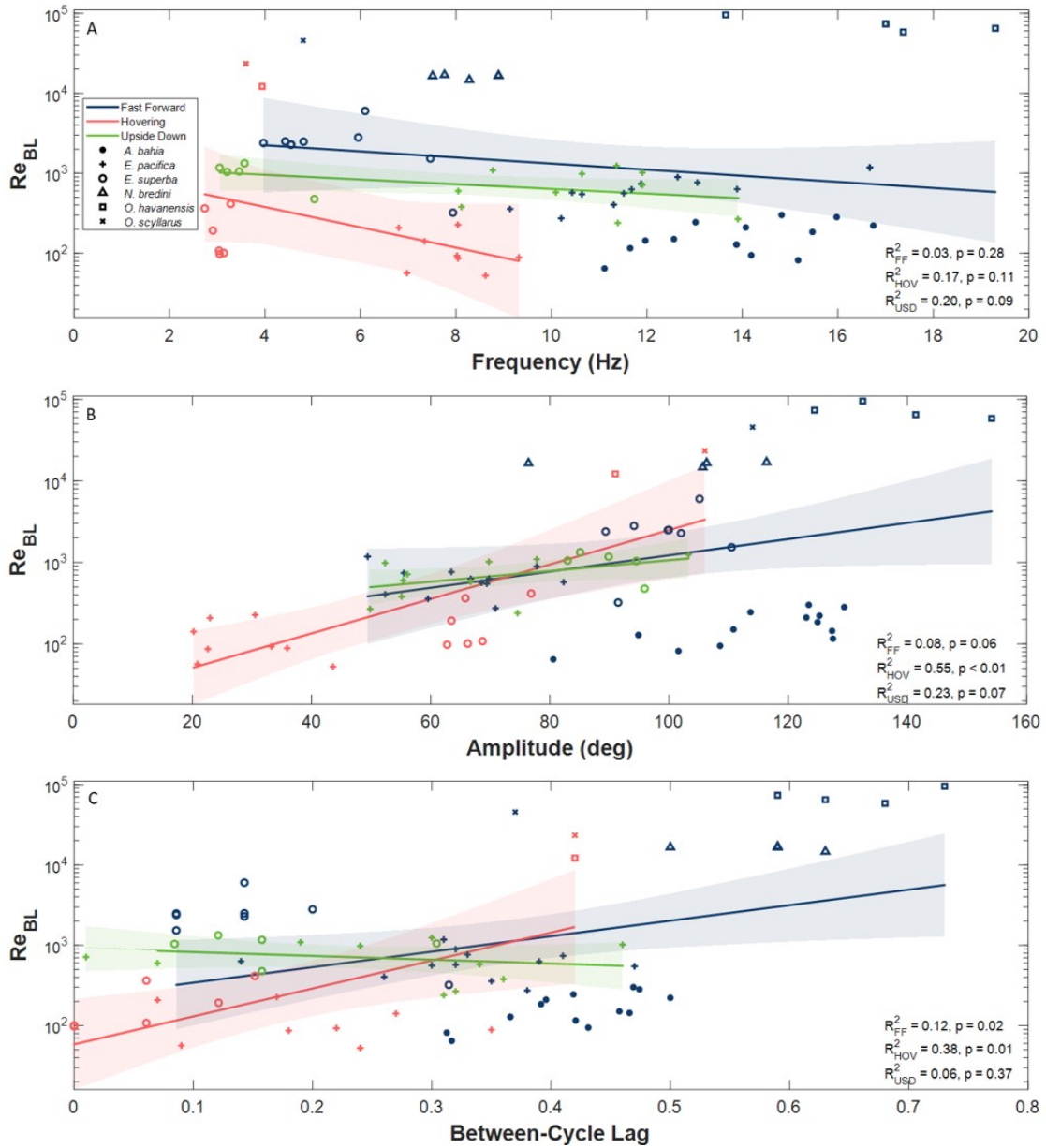


Figure 5.9: Re_{BL} response to stroke kinematics. Linear regressions of Re_{BL} against (A) frequency, (B) amplitude, and (C) between-cycle phase lag with 95% CI indicated by the shaded region. Symbol color indicates swimming mode and symbol shape indicates the species. There are no significant relationships between Re_{BL} and frequency for any mode, Re_{BL} increases with stroke amplitude for HOV, and Re_{BL} increases with between-cycle phase lag for FF and HOV.

stroke amplitude than smaller organisms, resulting in a greater Re_{BL} .

Whole-body Re increases with between-cycle phase lag for FF and HOV, but not for USD (Figure 5.9C). Increasing between-cycle phase lag increases speed by shifting a

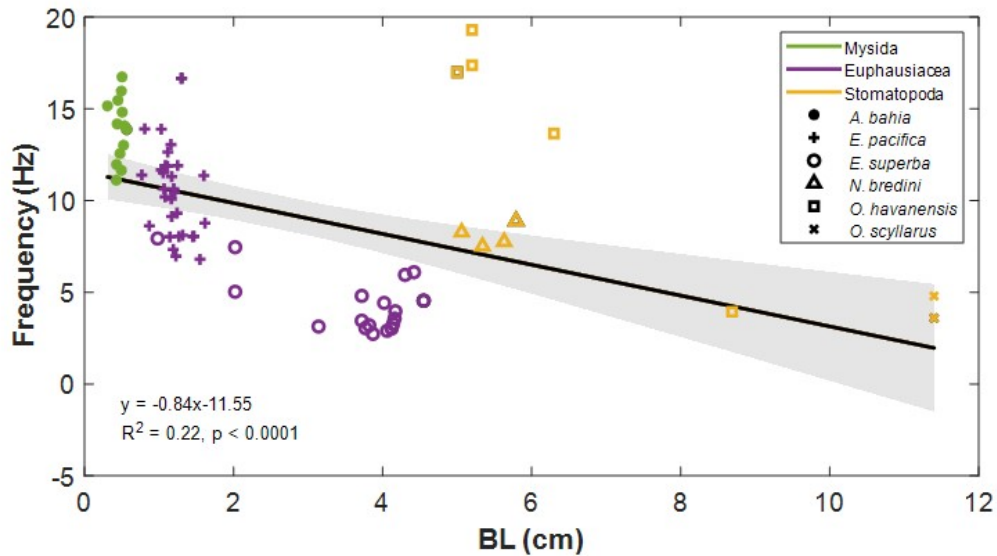


Figure 5.10: Linear regression of frequency to BL. Linear regression of frequency against BL (cm) for shrimp-like organisms with 95% CI indicated by shaded region. Symbol color indicates lowest taxonomic order, and symbol shape indicates species.

metachronal stroke to become more hybrid, with a metachronal power stroke and a more synchronous recovery stroke. This allows organisms to reach greater speeds, which increases their Re_{BL} . For HOV, increasing the between-cycle phase lag allows for greater stroke amplitudes to contribute to the fluid jet and thrust generation that counterbalances the weight of larger organisms.

Efficient versus Uniform Phase Lag

In physical and numerical simulations, 0.15-0.25 has been documented to be the range of phase lag that results in the best propulsion, either defined by greatest average body speed (Alben et al., 2010) or greatest volumetric fluid flux (Zhang et al., 2014; Granzier-Nakajima et al., 2020). However, these simulations are focused on the within-cycle phase lag between immediately adjacent appendages, and not the between-cycle phase lag between the last appendage and the first appendage. Most organisms included in this study have a within-cycle phase lag in the optimal range, indicating that they are swimming efficiently (Figure 5.11A).

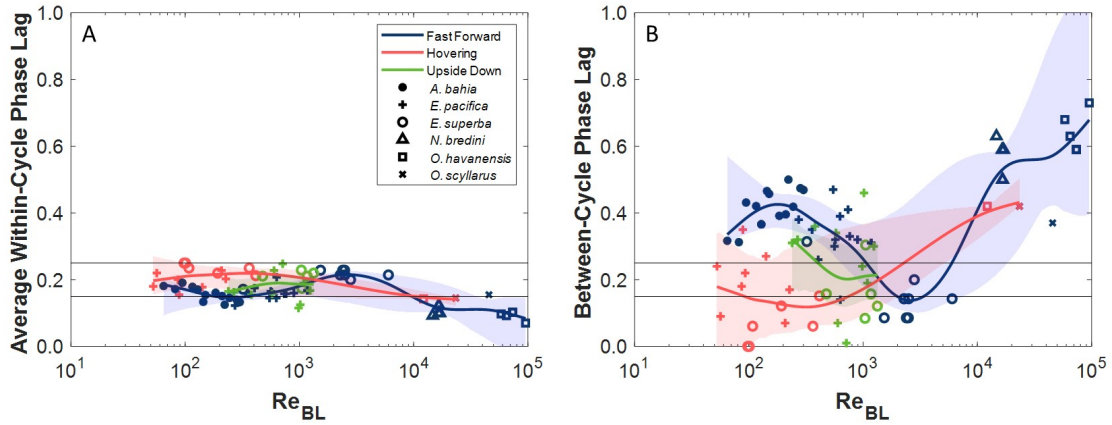


Figure 5.11: Phase lag across Re_{BL} . Spline-fitted smoothing curves (smoothing parameter = 0.99) for fast forward swimming (blue), hovering (red), and upside down swimming (green) for (A) within-cycle phase lag and (B) between-cycle phase lag. Symbol shapes represent species. CIs were stratified by taxonomic order to include at least one mysid, euphausiid, and stomatopod in the bootstrapped calculation. Metachrony range of 0.15-0.25 is bracketed via the horizontal lines showing the efficient range in (A) and the uniform range in (B).

However, uniform metachrony occurs when all phase lags are equal, not just the within-cycle phase lags. In these 5-paddle metachronal swimmers, a within-cycle phase lag of 0.15 between each pair of adjacent appendages results in a P1-P5 lag of 0.40, and a within-cycle phase lag of 0.25 results in a P1-P5 phase lag of zero. To achieve uniform metachrony in 5-paddle swimmers, P1-P5 phase lag should be restricted to a range of 0.15-0.25, which constrains the within-cycle phase lag to be between 0.19 and 0.21. Among the swimming modes, the appearance of a between-cycle lag of 0.15-0.25 occurs at different Re_{BL} (Figure 5.11B). For $Re_{BL} < 10^3$, uniform metachrony results in HOV, whereas for $10^3 < Re_{BL} < 10^4$, uniform metachrony results in FF. For $Re_{BL} > 10^4$, a hybrid metachronal stroke becomes favored as indicated by the increasing P1-P5 phase lag.

Because uniform metachrony in shrimp-like organisms results in different swimming modes at different Re_{BL} , it is important to take length scale into consideration when using biology as inspiration for robotic design. FF, which is often related to the more commonly described “cruising” swimming mode, does not need to be uniformly metachronal to be considered efficient in terms of fluid displacement. These results indicate that variations

in metachrony provide efficient propulsion within these systems, and the special case of uniform metachrony will result in different swimming modes at different length scales.

CHAPTER 6

CONCLUSIONS AND CLOSING REMARKS

This study undertook two unique projects to better understand crustacean behavior and morphology in low and intermediate Reynolds number environments. The first section in this chapter discusses the conclusions and presents study limitations and future directions for the first project, which set out to quantify a freshwater copepod's behavioral response to microscale turbulence. The second section in this chapter is dedicated to the second project undertaken in this study- to discover trends in shrimp-like organisms' propulsive designs. This project achieved two specific goals. First, it quantified metachrony in a 10-paddle, shrimp-like system, and second, it discovered overarching kinematic trends in metachronal systems across different length scales and swimming modes.

6.1 A Freshwater Copepod's Behavioral Response to Microscale Turbulence

Turbulence affects all aspects of copepod lives, ranging from large-scale population structure to individual-level interactions. Species respond to these environmental perturbations differently based on ecological factors. The marine copepod, *A. tonsa* uses a Burgers vortex, a microscale flow feature meant to model dissipative-scale turbulent eddies, as an aggregation cue. *Hesperodiptomus shoshone* is a freshwater copepod also known to aggregate. Male and female *H. shoshone* were exposed to four different intensities of a Burgers vortex as well as a stagnant negative control in two different orientations to determine the universality of a Burgers vortex as an aggregation cue in copepods.

6.1.1 Conclusions

Hesperodiptomus shoshone showed minimal response to a Burgers vortex. Only male *H. shoshone* show any change in a kinematic parameter relative to vortex intensity level,

decreasing their NGDR in response to vortex intensity, quantified by axial strain rate. Differences in body-vortex alignment could also be attributed to sex. This is in stark contrast to *A. tonsa*, who notably elicit spiral trajectories that follow the flow of the Burgers vortex at vortex intensity levels of 2 and greater (Elmi et al., 2021). This phenomenon is absent in *H. shoshone*, as they swim relatively perpendicular through the vortex, seemingly non-responsive to the fluid flow. If a Burgers vortex were an aggregation cue in copepods, *H. shoshone* may not be under as much ecological pressure to aggregate with conspecifics for mating.

Rather than *H. shoshone* changing its behavior in response to the intensity of the Burgers vortex, swimming behavior varied primarily with vortex orientation (i.e., horizontally-aligned vortex axis vs. vertically-aligned vortex axis)- or more appropriately, the physical restrictions of the configuration of the Burgers vortex apparatus. The observed differences may be attributed to physical restrictions on the natural trajectories of the copepods, with paddles in a horizontally-aligned vortex favoring vertical trajectories, and paddles in a vertically-aligned vortex favoring horizontal trajectories. This also was distinctly different than the observations for *A. tonsa*, which demonstrated spiral-like trajectories around the vortex core that were less influenced by the presence of the apparatus's paddles.

6.1.2 Limitations and Future Directions

In this study, *H. shoshone* showed minimal response to vortex intensity, and instead, greater response to the orientation of the Burgers vortex. The orientation of the horizontal and vertical Burgers vortex apparatuses served to confine *H. shoshone*'s motion, resulting instead in changes in swimming based on body orientation and trajectory. Kinematic variables that initially appeared significant in response to vortex orientation (i.e., relative velocity and NGDR) should be analyzed in terms of *H. shoshone*'s body orientation angle or trajectory with respect to gravity, rather than vortex orientation.

It would also be beneficial to determine how often *H. shoshone* was actively swimming

in the Burgers vortex apparatus, instead of passively sinking through the space between the two paddles. The experimental design assumed that *H. shoshone* would actively swim in the vortex. Knowing that *H. shoshone* show minimal response to the presence of a vortex, it is possible that several tracked instances of *H. shoshone* between the paddles were of the copepod sinking, rather than actively swimming through the observation region. Tracks from the horizontal apparatus would be particularly susceptible to this artefact, as paddle location did not vertically restrict passive sinking through the observation region, whereas in the vertical apparatus, paddle placement made sinking through the observation region – unless the copepod began sinking while within the region – next to impossible.

Finally, expanding this study to include more comparisons between the physical environment of *H. shoshone* and *A. tonsa* may provide more insight as to the different responses to a Burgers vortex between these two species. Turbulence levels of *H. shoshone*'s home lake would verify that this copepod experiences the range of vortex intensity levels included in this study. Second, a more thorough analysis of physical drivers of aggregation in alpine lakes may be related to *H. shoshone* aggregation. Alpine lakes are highly seasonal, and rather than aggregation being initiated by hydrodynamic features, cues originating from seasonal changes, such as decreasing lake temperature, shorter daylight periods, or seasonal changes in turbulence may be linked to *H. shoshone* aggregation rather than microscale turbulent features.

Outside of *H. shoshone*, quantifications of other plankton, including phytoplankton or fish and crustacean larvae, will provide a more thorough understanding of the relationship between plankton and dissipative eddies.

6.2 Trends in Shrimp-like Organisms' Propulsive Design

Metachronal propulsion in shrimp-like organisms is useful in multi-appendage bio-inspired design. Metachrony occurs in these organisms across many length scales, making shrimp-like organisms an ideal group to look at for alternative approaches to multi-appendage de-

signs. In this study, the stroke kinematics for two different shrimp-like species were quantified, to be used in tandem with previously published data on other shrimp-like metachronal swimmers to describe the relationship between stroke kinematics, swimming mode, and whole-body Reynolds number.

6.2.1 Conclusions

Americamysis bahia beat their 10 pleopods independently, resulting in two concurrent ipsilateral metachronal cycles. Pleopod usage in *A. bahia* results in faster swimming than thoracopodal swimming and greater normalized swimming speeds than the one-cycle euphausiid, *E. superba*. There is no apparent relationship between cyclic increases in swimming speed with the power stroke of any particular limb, suggesting that employing more appendages results in smoother swimming. Additionally, *A. bahia* does not use its pleopods to swim at speeds less than 2BL/s, and analysis of nondimensional parameters suggests that multiple cycles are less efficient at speeds slower than 9BL/s.

Euphausia pacifica beat their pleopods in a metachronal stroke to achieve three distinct swimming modes – hovering (HOV), fast forward swimming (FF), and upside down swimming (USD). The inflection point and shape of a fitted Gompertz function to amplitude and frequency against normalized swimming speed help identify a speed threshold between HOV and FF. Additionally, *E. pacifica* achieves different swimming modes by using similar trends in stroke kinematics as the larger *E. superba*. Beat frequency and stroke amplitude are larger in FF than in HOV, and phase lag varies between the three swimming modes. Despite similarities between the two euphausiids, *E. pacifica* consistently operates with a greater beat frequency and smaller stroke amplitude than *E. superba*, indicating that body length scale affects the stroke kinematics.

Across several shrimp-like organisms, similar trends in stroke kinematics achieve similar swimming modes. FF generally has a greater beat frequency, stroke amplitude, between-cycle phase lag, and whole-body Reynolds number (Re_{BL}) than HOV, with USD acting as

an intermediate mode between HOV and FF. Increasing stroke kinematics can have different effects on the Re_{BL} . Increasing beat frequency across all three swimming modes does not increase Re_{BL} , indicating scalability constraints to metachrony. Increasing amplitude only increases Re_{BL} in HOV because larger organisms like stomatopods require the greater thrust that occurs from increased stroke amplitude to maintain their position in the water column. Between-cycle phase lag increases Re_{BL} for FF and HOV due to a corresponding increase in swimming speed. Finally, uniform metachrony in a 5-paddle system, revealed by the between-cycle phase lag being in the range 0.15-0.25, results in different swimming modes reaching optimal uniformity at different Re_{BL} .

6.2.2 Limitations and Future Directions

In this study, *A. bahia* beat their pleopods for short amounts of time, only completing 2.46 ± 0.42 ($n = 13$) strokes per recording. Because of the limited number of strokes, pleopod beating in *A. bahia* results in quick bursts of speed. However, if more strokes were to occur, the mysid may show greater maneuverability. For example, if the cycle frequencies on opposite sides of the body were different within a stroke, pleopod usage could result in an imbalance of force that turns the animal in the direction of the slower cycle. Differences in cycle beat frequencies corresponding to a turn were not observed, although the duration of most of these recordings was short, only 0.27 ± 0.04 s, making it difficult to accurately quantify the organisms' trajectory. Additionally, similar ipsilateral phase lags differed between concurrent cycles, but due to the short time series, these data were pooled per abdominal segment. Changing the phase lag between ipsilateral paddles affects the swimming speed of the organism, but no attempts have been made to relate phase lag to measurements of trajectory.

This study focused on the kinematics of metachrony, and due to the relative complexity of *A. bahia*, some measurements were not possible. Images show that *A. bahia* pleopods have an exopodite and endopodite on the distal segment of their pleopod, but the fanning

of these segments was not visible in the recordings. Increasing paddle surface area during the power stroke increases the amount of thrust resulting in forward propulsion (Cheer and Koehl, 1987; Kim and Gharib, 2011a). The extent to which *A. bahia* fan their distal segment to increase the surface area of the stroke, and how this potential fanning compares to *E. superba* that are not space-limited by the presence of a contralateral appendage in a separate cycle (Murphy et al., 2011) remains unclear.

Additionally, although the fluid mechanics of *A. bahia* are speculated about, no flow measurements were taken. Further research into the hydrodynamics of dual ipsilateral metachrony would provide more insight as to why this is effective at faster speeds, and why pleopodal swimming in mysid shrimp is uncommon.

Finally, the overarching trends in metachrony identified in Chapter 5 were focused on stroke kinematics and neglected morphological adaptations for metachrony, which may have contributed to the strong separation by species in the PCA. Factors such as appendage rigidity (Kim and Gharib, 2011b), paddle surface area (Cheer and Koehl, 1987; Kim and Gharib, 2011a), and spacing between appendages (Ford and Santhanakrishnan, 2021a) can affect the characteristics of a metachronal stroke. Additionally, this analysis only accounted for the phase lag between power strokes and did not consider the recovery stroke. Temporal asymmetry (i.e., the difference in duration of the power and recovery strokes) and spatial asymmetry (i.e., the difference in appendage trajectory between the power and recovery strokes) can both affect metachrony (Herrera-Amaya et al., 2021). Inclusion of these factors may allow for future analysis of how parameter values contribute to metachrony and different swimming modes, rather than how metachrony varies among individual species.

As interest in metachronal propulsion increases due to increased interest in bio-inspired design, it would be beneficial to expand a meta-analysis from shrimp-like organisms to include other metachronal swimmers. Metachronal propulsion also occurs in copepods, ciliates, ctenophores, tomopterids, and remipedes (Byron et al., 2021b). Inclusion of these diverse body plans and approaches to metachrony could result in more comprehensive ob-

servations of metachronal propulsion.

Appendices

APPENDIX A
SUPPLEMENTARY TABLES

Table A.1: Correlation function of *A. bahia* pleopod stroke amplitude across pleopod combinations

	P5		P4		P3		P2	
	Pearson r	p	Pearson r	p	Pearson r	p	Pearson r	p
P1	0.54	0.06	0.60	0.03	0.87	<0.01	0.88	<0.01
P2	0.66	0.01	0.77	<0.01	0.95	<0.01		
P3	0.81	<0.01	0.84	<0.01				
P4	0.91	<0.01						

Table A.2: Correlation function of *A. bahia* pleopod phase lag across pleopod-pair combinations

	P1-P5 Lag		P2-P1 Lag		P3-P2 Lag		P4-P3 Lag	
	Pearson r	p	Pearson r	p	Pearson r	p	Pearson r	p
P5-P4 Lag	-0.80	<0.01	-0.47	0.10	0.60	0.03	0.19	0.54
P4-P3 Lag	-0.66	0.48	-0.58	0.04	-0.02	0.94		
P3-P2 Lag	-0.35	0.25	-0.63	0.02				
P2-P1 Lag	0.28	0.35						

Table A.3: Tukey HSD p-values for *E. pacifica* pleopod length comparisons

	P5	P4	P3	P2
P1	<0.0001	0.07	1.00	0.94
P2	<0.0001	<0.01	0.88	
P3	<0.0001	0.11		
P4	<0.0001			

Significant differences are bolded

Table A.4: Two-sample Watson-Williams p-values *E. pacifica* FF stroke amplitude comparisons

	P5	P4	P3	P2
P1	< 0.001	0.21	0.20	0.52
P2	< 0.01	0.57	0.65	
P3	< 0.01	0.83		
P4	0.01			

Significant differences are bolded

Table A.5: Two-sample Watson-Williams p-values for *E. pacifica* stroke amplitude comparisons between swimming modes

	P5		P4		P3		P2		P1	
	HOV	USD	HOV	USD	HOV	USD	HOV	USD	HOV	USD
FF	< 0.0001	0.52	< 0.0001	0.64	< 0.0001	0.79	< 0.0001	0.82	< 0.0001	0.96
USD	< 0.001		< 0.0001		< 0.0001		< 0.0001		< 0.001	

Significant differences are bolded

Table A.6: Tukey HSD p-values for *E. pacifica* FF phase lag comparisons

	P5-P4	P4-P3	P3-P2	P2-P1
P1-P5	< 0.001	< 0.01	< 0.01	< 0.01
P2-P1	0.90	1.00	0.90	
P3-P2	0.40	0.94		
P4-P3	0.85			

Significant differences are bolded

REFERENCES

- Agostinelli, C and U Lund (2022). *R package circular: Circular Statistics (version 0.4-94)*. CA: Department of Environmental Sciences, Informatics and Statistics, Ca' Foscari University, Venice, Italy. UL: Department of Statistics, California Polytechnic State University, San Luis Obispo, California, USA.
- Alben, S, K Spears, S Garth, D Murphy, and J Yen (2010). “Coordination of multiple appendages in drag-based swimming”. In: *Journal of the Royal Society Interface* 7, pp. 1545–1557.
- Alcaraz, M, E Saiz, and A Calbet (1994). “Small-scale turbulence and zooplankton metabolism: Effects of turbulence on heartbeat rates of planktonic crustaceans”. In: *Limnology and Oceanography* 39.6, pp. 1465–1470.
- Alexander, D E (1988). “Kinematics of swimming in two species of *Idotea* (Isopoda: Valvifera)”. In: *Journal of Experimental Biology* 138.1, p. 37.
- Alexander, D E, J Blodig, and S Hsieh (1995). “Relationship between function and mechanical properties of the pleopods of isopod crustaceans”. In: *Invertebrate Biology* 114.2, pp. 169–179.
- Alexander, R N (1989). “Optimization and gaits in the locomotion of vertebrates”. In: *Physiological Reviews* 69.4, pp. 1199–1227.
- Anagnostopoulou, L and G N Thomopoulos (2013). “Comparative study of the functional morphology of antennae, pleopods and exoskeleton among five species of Amphipoda (Crustacea) living in different ecological zones: A gradual transition from marine to terrestrial environment”. In: *Journal of Biological Research* 16, p. 19.
- Anderson, E J and M A Grosenbaugh (2005). “Jet flow in steadily swimming adult squid”. In: *Journal of Experimental Biology* 208, pp. 1125–1146.
- Ayancik, F, F E Fish, and K W Moored (2020). “Three-dimensional scaling laws of cetacean propulsion characterize the hydrodynamic interplay of flukes’ shape and kinematics”. In: *Journal of the Royal Society Interface* 17.20190655.
- Bagøien, E and T Kiørboe (2005). “Blind dating- mate finding in planktonic copepods. III. Hydromechanical communication in *Acartia tonsa*”. In: *Marine Ecology Progress Series* 300, pp. 129–133.
- Barrera-Moreno, O A, J Ciros-Perez, E Ortega-Mayagoitia, J A Alcantara-Rodriguez, and E Piedra-Ibarra (2015). “From local adaptation to ecological speciation in copepod populations from neighboring lakes”. In: *PLoS One* 10.4, e0125524.

- Bickel, S L, J D M Hammond, and K W Tang (2011). “Boat-generated turbulence as a potential source of mortality among copepods”. In: *Journal of Experimental Marine Biology and Ecology* 401.1, pp. 105–109.
- Biewener, A A (1990). “Biomechanics of mammalian terrestrial locomotion”. In: *Science* 250.4984, pp. 1097–1103.
- Blake, R W (2004). “Fish functional design and swimming performance”. In: *Journal of Fish Biology* 65, pp. 1193–1222.
- Bliss, D E (1968). “Transition from water to land in decapod crustaceans”. In: *American Zoologist* 8, pp. 355–392.
- Boudrias, M A (2002). “Are pleopods more than “just legs”? The functional morphology of swimming limbs in *Eurythenes gryllus* (Amphipoda)”. In: *Journal of Crustacean Biology* 22.3, pp. 581–594.
- Boxshall, G A and R Huys (1998). “The ontogeny and phylogeny of copepod antennules”. In: *Philosophical Transactions of the Royal Society of London B* 353, pp. 765–786.
- Byron, M L, D W Murphy, K Katija, A P Hoover, J Daniels, K Garayev, D Takagi, E Kanso, B J Gemmell, M Ruzsczyk, and A Santhanakrishnan (2021a). “Metachronal motion across scales: Current challenges and future directions”. In: *Integrative and Comparative Biology* 61.5, pp. 1674–1688.
- Byron, M L, A Santhanakrishnan, and D W Murphy (2021b). “Metachronal coordination of multiple appendages for swimming and pumping”. In: *Integrative and Comparative Biology* 61.5, pp. 1561–1566.
- Campos, E O, D Vilhena, and R L Caldwell (2012). “Pleopod rowing is used to achieve high fast forward swimming speeds during the escape response of *Odontodactylus havanensis* (Stomatopoda)”. In: *Journal of Crustacean Biology* 32, pp. 171–179.
- Caparroy, P, M T Perez, and F Carlotti (1998). “Feeding behavior of *Centropages typicus* in calm and turbulent conditions”. In: *Marine Ecology Progress Series* 168, pp. 109–118.
- Chateau, S, U D’Ortona, S Poncet, and J Favier (2018). “Transport and mixing induced by beating cilia in human airways”. In: *Frontiers in Physiology* 9.161, pp. 1–16.
- Cheer, A Y L and M A R Koehl (1987). “Paddles and rakes: Fluid flow through bristled appendages of small organisms”. In: *Journal of Theoretical Biology* 129, pp. 17–39.
- Chu, K H (2020). “Fitting the Gompertz equation to asymmetric breakthrough curves”. In: *Journal of Environmental and Chemical Engineering* 8.103713.

- Colin, S P, K R Costello Sutherland, B J Gemmell, J O Dabiri, and K T Du Clos (2020). “The role of suction thrust in the metachronal paddles of swimming invertebrates”. In: *Scientific Reports* 10.17790.
- Comeau, M and K Benhalima (2018). “Functional anatomy of the male reproductive system of the American lobster (*Homarus americanus*)”. In: *Journal of Morphology* 279.10, pp. 1431–1443.
- Costello, J H, S P Colin, B J Gemmell, J O Dabiri, and K R Sutherland (2015). “Multi-jet propulsion organized by clonal development in a colonial siphonophore”. In: *Nature Communications* 6, pp. 1–6.
- Cowles, D L, Childress J J, and Gluck D L (1986). “New method reveals unexpected relationship between velocity and drag in the bathypelagic mysid *Gnathophausia ingens*”. In: *Deep Sea Research* 33, pp. 865–880.
- Daniels, J, N Aoki, J Havassy, K Katija, and K J Osborn (2021). “Metachronal swimming with flexible legs: A kinematic analysis of the midwater polychaete *Tomopteris*”. In: *Integrative and Comparative Biology* 61.5, pp. 1658–1673.
- DeMont, M E and J M Gosline (1998). “Mechanics of jet propulsion in the hydromedusan jellyfish, *Polyorchis penicillatis* II. Energetics of the jet cycle”. In: *Journal of Experimental Biology* 135, pp. 333–345.
- Doall, M H, J R Strickler, D R Fields, and J Yen (2002). “Mapping the free-swimming attack volume of a planktonic copepod, *Euchaeta rimana*”. In: *Marine Biology* 140, pp. 871–879.
- Drucker, E G and J S Jensen (1996). “Pectoral fin locomotion in the striped surfperch I. Kinematic effects of swimming speed and body size”. In: *Journal of Experimental Biology* 199, pp. 2235–2242.
- Eckman, V W (1905). “On the influence of the earth’s rotation on ocean-currents”. In: *Ann Arbor, London: University Microfilms Inc.*
- Elmi, D, D R Webster, and D M Fields (2021). “Response of the copepod *Acartia tonsa* to the hydrodynamic cues of small-scale, dissipative eddies in turbulence”. In: *Journal of Experimental Biology* 224.
- Epifanio, C E and J H Cohen (2016). “Behavioral adaptations in larvae of brachyuran crabs: A review”. In: *Journal of Experimental Marine Biology and Ecology* 482, pp. 85–105.
- Fields, D M (2010). “Orientation affects the sensitivity of *Acartia tonsa* to fluid mechanical signals”. In: *Marine Biology* 157, pp. 505–514.

- Fields, D M and J Yen (1993). “Outer limits and inner structure: The 3-dimensional flow field of *Plauromamma xiphias* (Calanoida: Metridinidae)”. In: *Bulletin of Marine Science* 53.1, pp. 84–95.
- (1997). “The escape behavior of marine copepods in response to a quantifiable fluid mechanical disturbance”. In: *Journal of Plankton Research* 19.9, pp. 1289–1304.
- (2002). “Fluid mechanosensory stimulation of behavior from a planktonic marine copepod, *Euchaeta rimana* Bradford”. In: *Journal of Plankton Research* 24.8, pp. 747–755.
- Fininko, G A, A E Kideys, B E Anninsky, T A Shiganova, A Roohi, M R Tabiri, H Rostami, and S Bagheri (2006). “Invasive ctenophore *Mnemiopsis leidyi* in the Caspian Sea: Feeding, respiration, reproduction and predatory impact on the zooplankton community”. In: *Marine Ecology Progress Series* 314, pp. 171–185.
- Fish, F E and G V Lauder (2006). “Passive and active flow control by swimming fishes and mammals”. In: *Annual Review of Fluid Mechanics* 38, pp. 193–224.
- Fisher, N I (1993). *Statistical Analysis of Circular Data*. Cambridge University Press.
- Ford, M P, H K Lai, M Samaee, and A Santhanakrishnan (2019). “Hydrodynamics of metachronal paddling: Effects of varying Reynolds number and phase lag”. In: *Royal Society Open Science* 6.191387.
- Ford, M P, W J Ray, E M DiLuca, S N Patek, and A Santhanakrishnan (2021). “Hybrid metachronal rowing augments swimming speed and acceleration via increased stroke amplitude”. In: *Integrative and Comparative Biology* 61.5, pp. 1619–1630.
- Ford, M P and A Santhanakrishnan (2021a). “Closer appendage spacing augments metachronal swimming speed by promoting tip vortex interactions”. In: *Integrative and Comparative Biology* 61.5.
- (2021b). “On the role of phase lag in multi-appendage metachronal swimming of euphausiids”. In: *Bioinspiration & Biomimetics* 16.066007.
- Franks, P J S, B G Inman, J A MacKinnon, M H Alford, and A F Waterhouse (2022). “Oceanic turbulence from a planktonic perspective”. In: *Limnology and Oceanography* 67, pp. 348–363.
- Friend, J A and A M M Richardson (1986). “Biology of terrestrial amphipods”. In: *Annual Review Entomology* 31, pp. 25–48.
- Fulton, C J, J L Johansen, and J F Steffensen (2013). “Energetic extremes in aquatic locomotion by coral reef fishes”. In: *PLoS ONE* 8.e54033.

- Fusuoka, Y, Y Habu, and T Fukui (2015). “A simple rule for quadrupedal gait generation determined by leg loading feedback: A modeling study”. In: *Scientific Reports* 5.8169, pp. 1–11.
- Garayev, K and D W Murphy (2021). “Metachronal swimming of mantis shrimp: Kinematics and interpleopod vortex interactions”. In: *Integrative and Comparative Biology* 61.5, pp. 1631–1643.
- Garcia, A, G Krummel, and S Priya (2021). “Fundamental understanding of millipede morphology and locomotion dynamics”. In: *Bioinspiration & Biomimetics* 16.023003.
- Gilbert, O. M. and E. J. Buskey (2005). “Turbulence decreases the hydrodynamic predator sensing ability of the calanoid copepod *Acartia tonsa*”. In: *Journal of Plankton Research* 27.10, pp. 1067–1071.
- Goebel, W L H, S P Colin, J H Costello, B J Gemmell, and K R Sutherland (2020). “Scaling of ctenes and consequences for swimming performance in the ctenophore *Pleurobrachia bachei*”. In: *Invertebrate Biology* 139, pp. 1–9.
- Gompertz, B (1825). “On the nature of the function expressive of the law of human mortality, and on a new mode of determining the value of life contingencies”. In: *Proceedings of the Royal Society of London* 2, pp. 252–253.
- Grams, M and S Richter (2021). “Locomotion in *Anaspides* (Anaspidacea, Malacostraca)-insights from a morpho-functional study of thoracopods with some observations on swimming and walking”. In: *Zoology* 144.125883.
- Granzier-Nakajima, S, R D Guy, and C Zhang-Molina (2020). “A numerical study of metachronal propulsion at low to intermediate Reynolds numbers”. In: *Fluids* 5, pp. 1–15.
- Hartnoll, R G (1969). “Mating in the Brachyura”. In: *Crustaceana* 16.2, pp. 161–181.
- Hedrick, T L (2008). “Software techniques for two- and three-dimensional kinematic measurements of biological and biomimetic systems”. In: *Bioinspiration & Biomimetics* 3.034001.
- Herrera-Amaya, A, E K Seber, D W Murphy, W L Patry, T S Knowles, M M Bubel, A E Maas, and M L Byron (2021). “Spatiotemporal asymmetry in metachronal rowing at intermediate Reynolds numbers”. In: *Integrative and Comparative Biology* 61.5, pp. 1579–1593.
- Herrick, F H (1911). *Natural History of the American Lobster*. Arno Pr. ISBN: 0405103980.

- Hessler, R R (1983). “A defense of the caridoid facies; wherein the early evolution of the Eumalacostraca is discussed”. In: *Crustacean Phylogeny, Crustacean Issues*, pp. 145–164.
- (1985). “Swimming in Crustacea”. In: *Earth and Environmental Science Transactions of The Royal Society of Edinburgh* 76, pp. 115–122.
- Hjelmeland, K, B H Pedersen, and E M Nilssen (1988). “Trypsin content in intestines of herring larvae, *Clupea harengus*, ingesting inert polystyrene spheres or live crustacea prey”. In: *Marine Biology* 98, pp. 331–335.
- Hoskin, C J, C Moritz, K R McDonald, and M Higgie (2005). “Reinforcement drives rapid allopatric speciation”. In: *Nature* 437.7063, pp. 1353–1356.
- Hoyt, D F and C R Taylor (1981). “Gait and the energetics of locomotion in horses”. In: *Nature* 292, pp. 239–240.
- Huntley, M E, Zhou M, and Nordhausen W (1995). “Mesoscale distribution of zooplankton in the California current in late spring, observed by optical plankton counter”. In: *Journal of Marine Research* 53, pp. 647–674.
- Hwang, J and R Strickler (2001). “Can copepods differentiate prey from predator hydromechanically?” In: *Zoological Studies* 40.1, pp. 1–6.
- Jimenez, J (1997). “Oceanic turbulence at millimeter scales”. In: *Scientia Marina* 61.Supl. 1, pp. 47–56.
- Jumars, P A, J H Trowbridge, E Boss, and L Karp-Boss (2009). “Turbulence-plankton interactions: A new cartoon”. In: *Marine Ecology* 30, pp. 133–150.
- Kaiser, H F (1974). “An index of factorial simplicity”. In: *Psychometrika* 39.1, pp. 31–36.
- Keiler, J, C S Wirkner, and S Richter (2017). “One hundred years of carcinization - the evolution of the crab-like habitus in Anomura (Arthropoda: Crustacea)”. In: *Biological Journal of the Linnean Society* 121.1, pp. 200–222.
- Kils, U (1981). “Swimming behavior, swimming performance and energy balance in Antarctic krill, *Euphausia superba*”. In: *BIOMASS Scientific Series No. 3*, pp. 1–122.
- Kim, D and M Gharib (2011a). “Characteristics of vortex formation and thrust performance in drag-based paddling propulsion”. In: *Journal of Experimental Biology* 214, pp. 2283–2291.
- (2011b). “Flexibility effects on vortex formation of translating plates”. In: *Journal of Fluid Mechanics* 677, pp. 255–271.

- Kjørboe, T and E Saiz (1995a). “Planktivorous feeding in calm and turbulent environments, with emphasis on copepods”. In: *Marine Ecology Progress Series* 122, pp. 135–145.
- (1995b). “Turbulence-enhanced prey encounter rates in larval fish: Effects of spatial scale, larval behaviour and size”. In: *Journal of Plankton Research* 17.12, pp. 2319–2331.
- Kjørboe, T, E Saiz, and A Visser (1999). “Hydrodynamic signal perception in the copepod *Acartia tonsa*”. In: *Marine Ecology Progress Series* 179, pp. 97–111.
- Klein, P and G Lapeyre (2009). “The oceanic vertical pump induced by mesoscale and submesoscale turbulence”. In: *Annual Review of Marine Science* 1.1, pp. 351–375.
- Kohlhage, K and J Yager (2011). “An analysis of swimming in remipede crustaceans”. In: *Philosophical Transactions of the Royal Society B* 346, pp. 213–221.
- Kohnk, S, S N Gorb, S Boretius, and D Brandis (2018). “Not only for males: The pleonholding mechanism in female calappids (Crustacea: Decapoda: Brachyura)”. In: *Invertebrate Biology* 137.2, pp. 93–104.
- Kohnk, S, T Kleinteich, D Brandis, and S N Gorb (2017). “Biomechanics of pleon attachment in the European shore crab *Carcinus maenas* (Linnaeus, 1758) (Brachyura: Portunoidea: Carcinidae)”. In: *The Journal of Crustacean Biology* 37.2, pp. 142–150.
- Kolmogorov, A N (1941). “The local structure of turbulence in incompressible viscous fluids for very large Reynolds numbers”. In: *Dokl. Akad. Nauk. SSSR* 31, pp. 538–540.
- Labat, J, P Mayzaud, D Dallot, A Errhif, S Razouls, and S Sabini (2002). “Mesoscale distribution of zooplankton in the sub-Antarctic frontal system in the Indian part of the Southern ocean: A comparison between optical plankton counter and net sampling”. In: *Deep-Sea Research I* 49, pp. 735–749.
- Landsberger, M, G von der Emde, D Haverkate, S Schuster, J Gentsch, E Ulbricht, A Reichenbach, F Makarov, and H Wagner (2008). “Dim light vision - Morphological and functional adaptations of the eye of the mormyrid fish, *Gnathonemus petersii*”. In: *Journal of Physiology - Paris* 102, pp. 291–303.
- Laverack, M S, D M Neil, and R M Robertson (1977). “Metachronal exopodite beating in the mysid *Praunus flexuosus*: A quantitative analysis”. In: *Proceedings of the Royal Society of London B* 198, pp. 139–154.
- Lee, C, H Dahms, S Cheng, S Souissi, F G Schmitt, R Kumar, and J Hwang (2011). “Mating behavior of *Pseudodiaptomus annandalei* (Copepoda, Calanoida) at calm and hydrodynamically disturbed waters”. In: *Marine Biology* 158, pp. 1085–1094.

- Lenz, P H and J Yen (1993). “Distal setal mechanoreceptors of the first antennae of marine copepods”. In: *Bulletin of Marine Science* 51.1, pp. 170–179.
- Lim, J L and M E DeMont (2009). “Kinematics, hydrodynamics and force production of pleopods suggest jet-assisted walking in the American lobster *Homarus americanus*”. In: *The Journal of Experimental Biology* 212, pp. 2731–2745.
- Loria, K A, K R Christianson, and P T Johnson (2020). “Phenology of alpine zooplankton populations and the importance of lake ice-out”. In: *Journal of Plankton Research* 0.0, pp. 1–15.
- Lussier, S M, A Kuhn, M J Chammas, and J Sewall (1988). “Techniques for the laboratory culture of *Mysidopsis* species (Crustacea: Mysidacea)”. In: *Environmental Toxicology and Chemistry* 7, pp. 969–977.
- Lussier, S M, A Kuhn, and R Comeleo (1999). “An evaluation of the seven-day toxicity test with *Americamysis bahia* (formerly *Mysidopsis bahia*)”. In: *Environmental Toxicology and Chemistry* 18.12, pp. 2888–2893.
- Luteharms, J R E and D J Baker (1980). “A statistical analysis of the meso-scale dynamics of the Southern ocean”. In: *Deep Sea Research Part A, Oceanographic Research Papers* 27.2, pp. 156–159.
- Maar, M, T G Nielsen, A Stips, and A W Visser (2003). “Microscale distribution of zooplankton in relation to turbulent diffusion”. In: *Limnology and Oceanography* 48.3, pp. 1312–1325.
- Mackas, D L, M Tsurumi, M D Galbraith, and D R Yelland (2005). “Zooplankton distribution and dynamics in a north Pacific eddy of coastal origin: II. Mechanisms of eddy colonization by and retention of offshore species”. In: *Deep-Sea Research II* 52, pp. 1011–1035.
- MacKenzie, B R and T Kiørboe (1995). “Encounter rates and swimming behavior of pause-travel and cruise larval fish predators in calm and turbulent laboratory environments”. In: *Limnology and Oceanography* 40.7, pp. 1278–1289.
- Mariani, P, V Botte, and M R d’Alcala (2005). “An object-oriented model for the prediction of turbulence effects on copepods”. In: *Deep-Sea Research II* 52, pp. 1287–1307.
- Marszalek, M (2002). “Proximate factors influencing the spatial distribution of a high altitude copepod: *Hesperodiptomus shoshone*”. MA thesis. Concordia University.
- Martinez, R, A Calbet, and E Saiz (2018). “Effects of small-scale turbulence on growth and grazing of marine microzooplankton”. In: *Aquatic Sciences* 80.1, pp. 1–11.

- McWilliams, J C (2016). “Submesoscale currents in the ocean”. In: *Proceedings of the Royal Society A* 472, p. 20160117.
- Meland, K, J Mees, M Porter, and K J Wittmann (2015). “Taxonomic review of the orders Mysida and Stygiomysida (Crustacea, Pericarida)”. In: *PLoS ONE* 10.e0124656.
- Melo, P A M C, M DeMelo Junior, S J De Macedo, M Araujo, and S Neumann-Leitao (2014). “Copepod distribution and production in a mid-Atlantic ridge archipelago”. In: *Anais Da Academia Brasileira De Ciencias* 86.4, pp. 1719–1733.
- Michalec, F, I Fouxon, S Souissi, and M Holzner (2020). “Efficient mate finding in planktonic copepods swimming in turbulence”. In: *eLife* 9, e62014.
- Michalec, F, O Praud, S Cazin, and E Climent (2022). “Experimental investigation of preferential concentration in zooplankton swimming in turbulence”. In: *The European Physical Journal E* 45.12, pp. 1–13.
- Michalec, F, S Souissi, and M Holzner (2015). “Turbulence triggers vigorous swimming but hinders motion strategy in planktonic copepods”. In: *Journal of the Royal Society Interface* 12.20150158.
- Molenock, J (1969). “*Mysidopsis bahia*, a new species of mysid (Crustacea: Mysida) from Galveston Bay, Texas”. In: *Tulane Studies in Zoology and Botany* 15, pp. 113–116.
- Murphy, D W, D R Webster, S Kawaguchi, R King, and J Yen (2011). “Metachronal swimming in Antarctic krill: Gait kinematics and system design”. In: *Marine Biology* 158, pp. 2541–2554.
- Murphy, D W, D R Webster, and J Yen (2013). “The hydrodynamics of hovering in Antarctic krill”. In: *Limnology and Oceanography: Fluids & Environments* 3, pp. 240–255.
- Narendra, A, J F Kamhi, and Y Ogawa (2017). “Moving in dim light: Behavioral and visual adaptations in nocturnal ants”. In: *Integrative and Comparative Biology* 57.5, pp. 1104–1116.
- O’Brien, D P, D A Ritz, and R J Kirkwood (1986). “Stranding and matting behavior in *Nyctiphanes australis* (Euphausiidae: Crustacea)”. In: *Marine Biology* 93, pp. 465–473.
- Peichl, L (2005). “Diversity of mammalian photoreceptor properties: Adaptations to habitat and lifestyle?” In: *The Anatomical Record Part A* 287A, pp. 1001–1012.
- Pender-Healy, L (2014). “Tracking response of the freshwater copepod *Hesperodiaptomus shoshone*: Importance of hydrodynamic features”. MA thesis. Georgia Institute of Technology.

- Peters, F and C Marrasse (2000). “Effects of turbulence on plankton: An overview of experimental evidence and some theoretical considerations”. In: *Marine Ecology Progress Series* 205, pp. 291–306.
- Quetin, L B and J J Childress (1980). “Observation on the swimming activity of two bathypelagic mysid species maintained at high hydrostatic pressures”. In: *Deep Sea Research* 27A, pp. 383–391.
- Rhines, P B (2015). “Mesoscale Eddies”. In: *Encyclopedia of ocean sciences*, pp. 1717–1730.
- Ross, R M and L Quetin (2000). “Reproduction in Euphausiacea”. In: *Krill: Biology, ecology, and fisheries*, pp. 150–181.
- Ruszczyk, M, D R Webster, and J Yen (2021). “Dual phase-shifted ipsilateral metachrony in *Americamysis bahia*”. In: *Integrative and Comparative Biology* 61.5, pp. 1644–1657.
- Saadat, M, F E Fish, A G Domel, V Di Santo, G V Lauder, and H Haj-Hairiri (2017). “On the rules for aquatic locomotion”. In: *Physical Review Fluids* 2, pp. 1–12.
- Saiz, E and M Alcaraz (1992a). “Enhanced excretion rates induced by small-scale turbulence in *Acartia* (Copepoda: Calanoida)”. In: *Journal of Plankton Research* 14.5, pp. 681–689.
- (1992b). “Free-swimming behavior of *Acartia clausi* (Copepoda: Calanoida) under turbulent water movement”. In: *Marine Ecology Progress Series* 80, pp. 229–236.
- Saiz, E, M Alcaraz, and G Paffenhofer (1992). “Effects of small-scale turbulence on feeding rate and gross-growth efficiency of three *Acartia* species (Copepoda: Calanoida)”. In: *Journal of Plankton Research* 14.8, pp. 1085–1097.
- Saiz, E, A Calbet, and E Broglio (2003). “Effects of small-scale turbulence on copepods: The case of *Oithona davisae*”. In: *Limnology and Oceanography* 48.3, pp. 1304–1311.
- Saiz, E and T Kiørboe (1995). “Predatory and suspension feeding of the copepod *Acartia tonsa* in turbulent environments”. In: *Marine Ecology Progress Series* 122, pp. 147–158.
- Salas, M P A (2002). “Distribution pattern of *Hesperodiaptomus shoshone* and *Leptodiaptomus coloradensis* and its effects on their mating and reproductive potential”. MA thesis. Concordia University.
- Sanderson, M J and M A Sleight (1981). “Ciliary activity of cultured rabbit tracheal epithelium: Beat pattern and metachrony”. In: *Journal of Cell Science* 47, pp. 331–347.

- Sas, A A, H Snieder, and J Korf (2012). “Gompertz law as an intrinsic principle of aging”. In: *Medical Hypotheses* 78, pp. 659–663.
- Schabes, M and W Hamner (1992). “Mysid locomotion and feeding: Kinematics and water-flow patterns of *Antarctomysis sp.*, *Acanthomysis sculpta*, and *Neomysis rayii*”. In: *Journal of Crustacean Biology* 12, pp. 1–10.
- Schmidt, C and J W Wagele (2001). “Morphology and evolution of respiratory structures in the pleopod exopodites of terrestrial Isopoda (Crustacea, Isopoda, Oniscidea)”. In: *Acta Zoologica* 82.4, pp. 315–330.
- Seridjii, R and A Hafferssas (2000). “Copepod diversity and community structure in the Algerian basin”. In: *Crustaceana* 73.1, pp. 1–23.
- Seuront, L (2013). “Chemical and hydromechanical components of mate-seeking behavior in the calanoid copepod *Eurytemora affinis*”. In: *Journal of Plankton Research* 35.4, pp. 724–743.
- Shen, X, Marcos, and H C Fu (2020). “How the bending mechanics of setae modulate hydrodynamic sensing in copepods”. In: *Limnology and Oceanography* 65, pp. 749–761.
- Shimeta, J, P A Jumars, and E J Lessard (1995). “Influences of turbulence on suspension feeding by planktonic protozoa; experiments in laminar shear fields”. In: *Limnology and Oceanography* 40.5, pp. 845–859.
- Skipper, A N (2016). “Behavior response of an alpine lake copepod to think layer structure”. MA thesis. Georgia Institute of Technology.
- Skipper, A N, D W Murphy, and D R Webster (2019). “Characterization of hop-and-sink daphniid locomotion”. In: *Journal of Plankton Research* 41, pp. 142–153.
- Sprules, W G (1972). “Effects of size-selective predation and food competition on high altitude zooplankton communities”. In: *Ecology* 53.3, pp. 375–386.
- Stockl, A L, K Kihlstrom, S Chandler, and S Sponberg (2017). “Comparative system identification of flower tracking performance in three hawkmoth species reveals adaptations for dim light vision”. In: *Philosophical Transactions of the Royal Society of London B* 372, p. 20130078.
- Stretch, J J, P P Hamner, W M Hamner, W C Michel, J Cook, and C S Sullican (1988). “Foraging behavior of Antarctic krill *Euphausia superba* on sea ice macroalgae”. In: *Marine Ecology Progress Series* 44.2, pp. 131–139.

- Suchman, C. L. and B. K. Sullivan (1998). “Vulnerability of the copepod *Acartia tonsa* to predation by the scyphomedusa *Chrysaora quinquecirrha*: Effect of prey size and behavior”. In: *Marine Biology* 132, pp. 237–245.
- Sudo, S, K Hoshika, T Yano, and Y Shimazaki (2010). “The dynamic behavior of opossum shrimps”. In: *Journal of Aero Aqua Bio-Mechanisms* 1.1, pp. 80–85.
- Sudo, S, K Sekine, M Shimizu, S Shida, T Yano, and Y Tanaka (2009). “Basic study on swimming of small aquatic creatures”. In: *Journal of Biomedical Science and Engineering* 4.1, pp. 23–36.
- Tattersall, W M and O S Tattersall (1951). *The British Mysidacea*. Ray Society. ISBN: 978-1-904690-09-2.
- Taylor, G K, R L Nudds, and A L R Thomas (2003). “Flying and swimming animals at Strouhal number tuned for high power efficiency”. In: *Nature* 45, pp. 707–711.
- Tiselius, P (1992). “Behavior of *Acartia tonsa* in patchy food environments”. In: *Limnology and Oceanography* 37.8, pp. 1640–1651.
- Triantafyllou, G S, M S Triantafyllou, and M A Grosenbaugh (1993). “Optimal thrust development in oscillating foils with application to fish propulsion”. In: *Journal of Fluids and Structures* 7, pp. 205–224.
- True, A, D R Webster, M Weissburg, J Yen, and A Genin (2015). “Patchiness and depth-keeping of copepods in response to simulated frontal flows”. In: *Marine Ecology Progress Series* 539, pp. 65–76.
- Tsuda, A, H Sugusaki, and S Kimura (2000). “Mosaic horizontal distributions of three species of copepods in the subarctic Pacific during spring”. In: *Marine Biology* 137, pp. 683–689.
- Visser, A W, P Mariani, and S Pigolotti (2009). “Swimming in turbulence: Zooplankton fitness in terms of foraging efficiency and predation risk”. In: *Journal of Plankton Research* 31.2, pp. 121–133.
- Vogel, S (2013). “Thrust for Flying and Swimming”. In: *Comparative Biomechanics: Life’s Physical World*, pp. 251–270.
- Walker, J A (2002). “Functional morphology and virtual models: Physical constraints on the design of oscillating wings, fins, legs, and feet at intermediate Reynolds numbers”. In: *Integrative and Comparative Biology* 42, pp. 232–242.

- Webster, D R, A Brathwaite, and J Yen (2004). “A novel apparatus for simulating isotropic oceanic turbulence at a low Reynolds number”. In: *Limnology and Oceanography: Methods* 2, pp. 1–12.
- Webster, D R and D L Young (2015). “A laboratory realization of the Burgers’ vortex cartoon of turbulence-plankton interactions”. In: *Limnology and Oceanography: Methods* 13, pp. 92–102.
- Webster, D R, D L Young, and J Yen (2015). “Copepods’ response to Burgers’ vortex: Deconstructing interactions of copepods with turbulence”. In: *Integrative and Comparative Biology* 55.4, pp. 706–718.
- Williams, E H (2012). “Long term effects of climate on two pond predators”. In: *The American Midland Naturalist* 167, pp. 366–343.
- Williams, T A (1994). “A model of rowing propulsion and the ontogeny of locomotion in *Artemia* larvae”. In: *Biological Bulletin* 187, pp. 164–173.
- Wittmann, K (2013). “Comparative morphology of the external male genitalia in Lophogastrida, Stygiomysida, and Mysida (Crustacea, Eumalacostraca)”. In: *Zoomorphology* 132.4, pp. 389–401.
- Yen, J (2000). “Life in transition: Balancing inertial and viscous forces by planktonic copepods”. In: *Biological Bulletin* 198, pp. 213–224.
- Yen, J, P H Lenz, D V Gassie, and D K Hartline (1992). “Mechanoreception in marine copepods: Electrophysiological studies on the first antennae”. In: *Journal of Plankton Research* 14.4, pp. 495–512.
- Yen, J, D W Murphy, L Fan, and D R Webster (2015). “Sensory-motor systems of copepods involved in their escape from suction feeding”. In: *Integrative and Comparative Biology* 55.1, pp. 121–133.
- Yen, J and N T Nicoll (1990). “Setal array on the first antennae of a carnivorous marine copepod, *Euchaeta norvegica*”. In: *Journal of Crustacean Biology* 10.2, pp. 218–224.
- Yen, J, K D Rasberry, and D R Webster (2008). “Quantifying copepod kinematics in a laboratory turbulence apparatus”. In: *Journal of Marine Systems* 69, pp. 283–294.
- Yen, J, J K Sehn, K Catton, A Kramer, and O Sarnelle (2011). “Pheromone trail following in three dimensions by the freshwater copepod, *Hesperodiptomus shoshone*”. In: *Journal of Plankton Research* 33.6, pp. 907–916.

- Yen, J and J R Strickler (1996). “Advertisement and concealment in the plankton: What makes a copepod hydromechanically conspicuous?” In: *Invertebrate Biology* 115.3, pp. 191–205.
- Yen, J, M J Weissburg, and M H Doall (1998). “The fluid physics of signal perception by mate-tracking copepods”. In: *Philosophical Transactions of the Royal Society B* 353, pp. 787–804.
- Yu, Y, W Wang, and Z Lu (2007). “Global stability of Gompertz model of three competing populations”. In: *Journal of Analysis and Applied Mathematics* 334, pp. 333–348.
- Zhang, C, R D Guy, B Mulloney, Q Zhang, and T J Lewis (2014). “Neural mechanism of optimal limb coordination in crustacean swimming”. In: *PNAS* 11, pp. 13840–13845.
- Zhang, D and J Lin (2004). “Fertilization success without anterior pleopods in *Lysmata wurdemanni* (Decapoda: Caridea), A protoandric simultaneous hermaphrodite”. In: *Journal of Crustacean Biology* 24.3, pp. 470–434.